PAVOL JOZEF ŠAFÁRIK UNIVERSITY IN KOŠICE
FACULTY OF SCIENCE
DEPARTMENT OF BIOPHYSICS

UNIVERSIDAD AUTÓNOMA DE MADRID
FACULTAD DE CIENCIAS QUÍMICAS
DEPARTAMENTO DE QUÍMICA-FÍSICA APLICADA

INSTITUTO DE ESTRUCTURA DE LA MATERIA
CONSEJO SUPERIOR DE INVESTIGACIONES CIENTÍFICAS

DOCTORAL THESIS

DETECTION OF ORGANOCHLORINE PESTICIDES BY SURFACE-ENHANCED RAMAN SCATTERING ON DITHIOL-FUNCTIONALIZED PLASMON NANOPARTICLES

Jana Kubacková

SUPERVISORS:

Dr. Santiago Sánchez-Cortés

Dr. Daniel Jancura

MADRID, 2014

PAVOL JOZEF ŠAFÁRIK UNIVERSITY IN KOŠICE
FACULTY OF SCIENCE
DEPARTMENT OF BIOPHYSICS

UNIVERSIDAD AUTÓNOMA DE MADRID
FACULTAD DE CIENCIAS QUÍMICAS
DEPARTAMENTO DE QUÍMICA-FÍSICA APLICADA

INSTITUTO DE ESTRUCTURA DE LA MATERIA
CONSEJO SUPERIOR DE INVESTIGACIONES CIENTÍFICAS

DOCTORAL THESIS

DETECTION OF ORGANOCHLORINE PESTICIDES BY SURFACE-ENHANCED RAMAN SCATTERING ON DITHIOL-FUNCTIONALIZED PLASMON NANOPARTICLES

Jana Kubacková

SUPERVISORS:

Dr. Santiago Sánchez-Cortés

Dr. Daniel Jancura

MADRID, 2014

Statutory Declaration

I do solemnly and sincerely declare that this Doctoral Thesis has been written by me under the guidance of my supervisors Dr. Santiago Sánchez-Cortés and Dr. Daniel Jancura, and with the use of the referenced literature.

Košice, 25th August 2014

Abstract

Surface-enhanced Raman spectroscopy (SERS) is one of the most powerful analytical techniques for detection of trace amount of chemicals. It is due to the coupling of the Raman scattering of a molecular system to a localized plasmon resonance of silver or gold nanostructures. However, many molecules of great interest lack affinity for metal surfaces and their SERS detection is not possible. On the other hand, the affinity of an analyte towards metal surface can be increased by modifying or functionalizing the surface with the organic molecules. In this thesis we have used linkers, aliphatic dithiols, to functionalize silver and gold nanoparticles for the SERS detection of low concentrations of organochlorine pesticides (aldrin, α-endosulfan, lindane and dieldrin). Using various types of metal colloids and aliphatic α,ω-dithiols as bifunctional linkers it was found that the most suitable substrate for SERS detection of these pesticides are citrate silver colloid nanoparticles covered by 1,8-octanedithiol (10^{-5} M). It should be also noted that functionalization of the metal surface by aromatic dithiols does not lead to a SERS substrate suitable for the detection of the pesticides. Furthermore, the fingerprint region (300–400 cm^{-1}) for the SERS detection of the pesticides was determined. The studied pesticides follow a Langmuir adsorption model from which the adsorption constant and the limit of detection for individual pesticides were determined. The obtained results confirm the high sensitivity of SERS for the detection of low quantities (~10^{-8}M) of organochlorine pesticides which provide solid basis for the construction of suitable nano-sensors for the identification and quantitative analysis of this type of chemicals.

Moreover, the adsorption mechanism of aromatic and linear aliphatic α,ω-dithiols on silver and gold nanoparticles has been studied in this thesis by UV-VIS absorption spectroscopy, SERS and transmission electron microscopy. All these experimental techniques were employed to obtain information about the adsorption and coordination mechanism, the orientation, conformational order, and packing of the dithiols on the metal nanoparticle surface.

Table of Content

List of figures and tables

List of abbreviation

AD	Alkyl Dithiols
AgC	Cittrate-reduced silver colloid
AgH	HydroXylamine-reduced silver colloid
ArD	Aromatic Dithiols
ATSDR	Agency for Toxic Substances and Disease Registry
AuC	Citrate-reduced gold colloid
BDT	1,4-BenzeneDiThiol
BPDT	BiPhenyl-4,4'-DiThiol
CCD	Charge-Coupled Device
CDC	Centers for Disease Control and Prevention
CRD	Chemicals Regulation Directorate
CSIC	Consejo Superior de Investigaciones Científicas
DT6	1,6-HexaneDiThiol
DT8	1,8-OctaneDiThiol
DT10	1,10-DecaneDiThiol
ECD	Electron Capture Detection
EM	ElectroMagnetic
EPA	Environmental Protection Agency
FAO	Food and Agriculture Organization
FID	Flame Ionization Detector
FTIR	Fourier Transform InfraRed spectroscopy
GC	Gas Chromatography
HPLC	High-Performance Liquid Chromatography
HS	Hot Spot
ICC	Indian Chemical Council

i.e.	means 'that is', from the Latin 'id est'
InGaAs	Indium Gallium Arsenide
IR	InfraRed
LSP	Localized Surface Plasmon
LSPR	Localized Surface Plasmon Resonance
MALDI	Matrix-Assisted Laser Desorption/Ionization
MS	Mass Spectrometry
NIR	Near InfraRed
NMR	Nuclear Magnetic Resonance
NP	NanoParticle
OP	Organochlorine Pesticide
PAH	Polycyclic Aromatic Hydrocarbon
PbS	Lead Sulfide
PCP	PolyChlorinated Pesticide
PMT	PhotoMultiplier Tube
POP	Persistent Organic Pollutant
QC	Quality Control
RS	Raman Spectroscopy
SAM	Self-Assembled Monolayer
SERS	Surface-Enhanced Raman Spectroscopy
SMD	Single Molecular Detection
TEM	Transmission Electron Microscopy
TOF	Time-Of-Flight
US	United States
UV	UltraViolet
VIS	Visible
WHO	World Health Organization

1 Introduction

Surface-enhanced Raman spectroscopy (SERS) is a very powerful spectroscopic technique because the Raman signal contains detailed information about the vibrational characteristics of an analyzed molecule, that represent an actual fingerprint of the molecule, and because the high sensitivity of this method provides a promising utility for chemical detection even at low concentrations. The high sensitivity of SERS is mainly due to the giant electromagnetic (EM) enhancement induced by nanostructured noble metal surfaces and is associated to localized surface plasmon resonance (LSPR) [Moskovits, M. 1985; Aroca, R. 2006]. Since the intensity of SERS depends on the 4^{th} power of the intensity of the electric field, SERS enhancements factors greater than 10^6 can be achieved and these enhancements have been reported by numerous research groups [Halas, N.J. *et al.* 2011; Shafer-Peltier, K.E. *et al.* 2003; Grubisha, D.S. *et al.* 2003; Nam, J.M. *et al.* 2004; Lyandres, O. *et al.* 2005; Kneipp, J. *et al.* 2005; Premasiri, W.R. *et al.* 2005]. Such great enhancement is, under certain conditions, sufficient for single or few molecule detection, making SERS an extremely useful technique for chemical and biomolecular detection [Kneipp, K. *et al.* 1997; Nie, S. & Emory, S.R. 1997; Moskovits, M. & Jeong, D.H. 2004; Cao, Y.C. *et al.* 2002].

One of the scientific interests at the Department of Biophysics, Šafárik University in Košice, is focused on the application of SERS technique for the detection of trace amount of chemical compounds with important impact on the environment and the human health (e.g. photodynamically active drugs, pollutants). Under this goal, the team from the Department of Biophysics, Šafárik University in Košice, is engaged in an international cooperation with the group of Dr. Santiago Sánchez-Cortés from the Instituto de Estructura de la Materia, CSIC, Madrid (Spain). This group possesses a large experience in the field of SERS, specially in its application to the study of chemical compounds with medical and environmental interest. This collaboration enabled to start the presented dissertation project which is mainly focused on the application of SERS for the detection of trace quantities of organochlorine pesticides.

Pesticides belong between chemicals which represent substantial risks for human health (cancerogenecity) and pose long-term danger to the environment through their persistence in nature and human body. With respect to this fact, the detection and identification of these chemicals (even at very low concentrations) is very important.

This thesis presents a short review of the principles and mechanisms involved in SERS and the application of this method in the field of the selective analytical detection of pollutants. The main part of the thesis contains our results concerning the SERS detection of selected organochlorine pesticides (aldrin, dieldrin, lindane and α-endosulfan). For this purpose we had to find an "optimal" experimental condition allowing the detection of the studied molecules even at low concentrations. This process involved the characterization of aliphatic and aromatic dithiols as bifunctional linkers to functionalize silver and gold nanoparticles (NPs) for SERS measurements. The dithiols linkers were used for two different goals: i) to induce the nanoparticle linkage and creation of interparticle junctions where sensitive hot spots are hosted, and ii) to functionalize silver and gold nanoparticles for the SERS detection of low concentrations of analyzed organochlorine pesticides. Further, we have found the colloidal system (type of metal colloid, selection of the "optimal" dithiol and concentration of the dithiol) optimal for SERS detection of low concentrations of the selected pesticides. The optimal SERS substrate was consequently utilized for the determination of the quantitative parameters (adsorption constant to the metal surface, limit of detection) characterizing the studied molecules. The obtained results provide a good basis for the following optimization procedure which should lead to a design of nanosensor system, based on the silver and gold nanoparticles functionalized with dithiols, for the detection of the organochlorine pesticides.

2 The main objectives of the thesis

The principal task of this dissertation thesis consists on the application of SERS for the detection of very low concentrations of environmental pollutants. Emphasis is given on the utilization of SERS in the detection of trace amount of selected organochlorine pesticides. To accomplish this task, the thesis has the following specific objectives:

- Presentation of a comprehensive review on the mechanisms and applications of SERS with the emphasis on the detection of trace amounts of chemicals and provide information about properties of selected organochlorine pesticides (aldrin, dieldrin, lindane, α-endosulfan).
- Preparation of dithiol-functionalized silver and gold colloidal nanoparticles for utilization in SERS detection of selected organochlorine pesticides by varying several experimental conditions.
- Characterization of the prepared SERS substrates by analyzing the plasmon resonance of nanoparticles, the SERS spectroscopy of the immobilized dithol layers on metal surface as well as the study of the morphology by transmission electron microscopy.
- Optimization of the dithiol-functionalized substrates for the SERS detection of organochlorine pesticides and proposal for their application in environmental practice.
- Evaluation of the prepared functionalized nanoparticles in the SERS detection of organochlorine pesticides and determination of fingerprint region, binding constants to metal surface and limit of detection for the individual pesticides.

3 Theoretical backgrounds

3.1 Raman spectroscopy

3.1.1 Introduction

Raman spectroscopy is a spectroscopic technique used in condensed matter physics, chemistry and bio-sciences to study vibrational, rotational, and other low-frequency modes in an analyzed system [Gardiner, D.J. 1989]. It is a non–destructive and non–invasive tool that provides detailed information about the molecular composition, structure and interactions within a sample and thus it is also very useful for chemical detection. This analytical technique, together with infrared (IR) spectroscopy, belongs to vibrational spectroscopy, it means that these techniques measure vibrational energy levels which are associated with the motions of the chemical bonds in a studied molecule (Fig. 1). The vibrational spectrum of each molecule is unique, like a fingerprint, molecular and structural information is obtained by careful examination of the spectra taking special note of the band position, line shape and intensity. IR and Raman spectroscopy provide complementary information about the molecular structure of the analyzed molecules [Hendra, P. 1998].

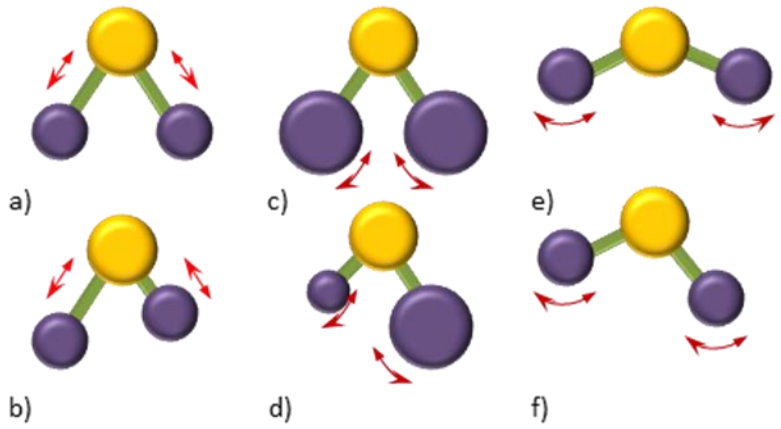

Fig. 1 – Normal modes of molecular vibrations (each of these modes is associated with a characteristic frequency of the vibration): (a) symmetric stretching, (b) antisymmetric stretching, (c) out-of-plane wagging, (d) out-of-plane twisting, (e) in-plane scissoring, (f) in-plane rocking.

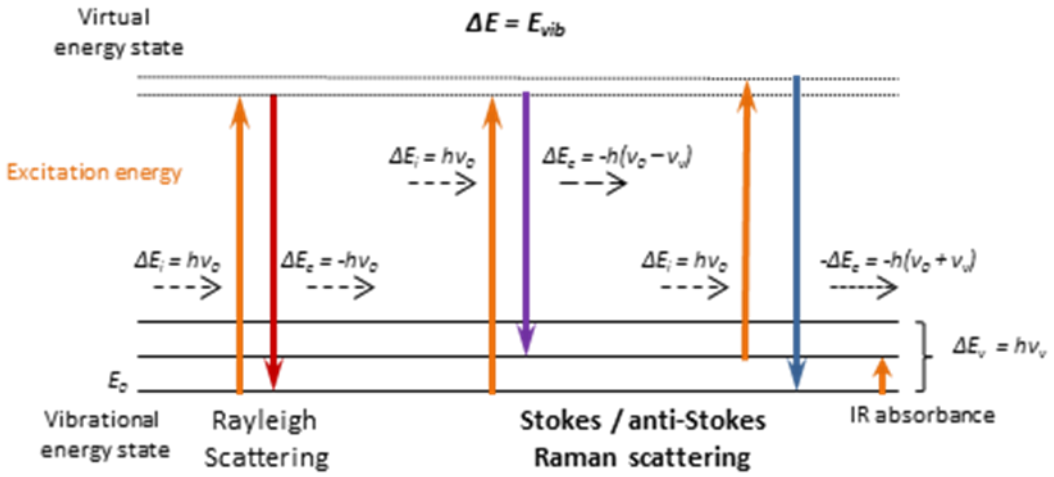

Fig. 2 – Schematic illustration of three types of radiation scattering by a molecule excited to a virtual energy state by a photon with energy $E = h\nu_0$.

The energy changes detected in Raman spectroscopy are those required to cause nuclear motion. If only electron cloud distortion is involved in scattering, the photons will be scattered with very small frequency changes, as the electrons are comparatively light. This scattering process is regarded as elastic scattering and is called Rayleigh scattering [Smith, W.E. & Dent, G. 2005]. The elastically scattered light has the same energy as the incident laser light and it is the dominant scattering process (Fig. 2). However, if nuclear motion is induced during the scattering process, energy will be transferred either from the incident photon to the molecule or from the molecule to the scattered photon. In these cases the process of light scattering is inelastic and the energy of the scattered photon is different from that of the incident photon (Fig. 2). This phenomenon is called Raman scattering. It is inherently a weak process in that only one in every 10^6-10^8 scattered photons is Raman scattered [Smith, W.E. & Dent, G. 2005].

3.1.2 A brief historical note about Raman spectroscopy

Although the inelastic scattering of light was predicted by Smekal in 1923, it was not until 1928 that it was firstly observed experimentally by the Indian physicist Chandrasekhara Venkata Raman. Together with his student K.S. Krishnan they observed the effect of inelastic light scattering by molecule in water and purified

alcohols [Raman, C.V. & Krishnan, K.S. 1928]. Since then, this phenomenon has been referred to as Raman scattering. Because of this observation, Raman earned the of the Nobel Prize award in Physics in 1930 [Smith, W.E. & Dent, G. 2005]. Independently and simultaneously G. Landsberg and L. Mandelstam (from the former Soviet Union) covered the same effect in crystals [Landsberg, G. & Mandelstam, L.A. 1928]. Systematic pioneering theory of the Raman scattering was developed by physicist George Placzek between 1930 and 1934 [Placzek, G. 1934]. This new observed phenomenon of inelastic light scattering allowed the study of molecular vibrations and rotations. It should be noted that studies on this phenomenon were based upon previous work of Rayleigh and his coworkers [Strutt, J.W. 1871; Strutt, J.W. 1881; Strutt, J.W. 1899].

Despite the initial excitement about the discovery of the Raman scattering, its spectroscopic application remains quite limited until 1960s, when the first lasers were developed. In the first years of the Raman spectroscopy, the mercury arc became the principal light source, first with photographic detection and then with spectrophotometric detection. Before the advent of the laser (monochromacity and coherence), Raman spectroscopy suffered from the low intensity of the inelastic scattering and the much larger intensity of the Rayleigh scattering.

3.1.3 Principles of Raman spectroscopy

In Raman spectroscopy, the sample is irradiated with a monochromatic light, usually from a laser in the visible, near infrared, or near ultraviolet regions, and it is the radiation scattered from the molecule what is detected. The origin of the scattered radiation is considered to be the oscillating electric and magnetic multipole moments induced in a molecule by the electromagnetic fields of the incident light waves. During Raman scattering process, the incident photon excites the molecule into a virtual state. For the spontaneous Raman effect the molecule will be excited from the ground vibrational state E_0 to a virtual energy state, and relax into a higher energy vibrational excited state (Fig. 2). This is called Stokes scattering. However, due to thermal energy, some molecules may be present in a vibrational excited state. Scattering from these

states to the ground state is called anti-Stokes scattering and involves transfer of energy to the scattered photon [Smith, W.E. & Dent, G. 2005].

A change in the molecular polarization, corresponding to a change in the shape, size or orientation of the electron cloud that surrounds the molecules [Hendra, P. 1998], with respect to the vibrational coordinate is required for a molecule to exhibit the Raman effect. The amount of the polarizability change will determine the Raman scattering intensity, whereas the Raman shift is equal to the vibrational level that is involved. The most intense Raman scattering occurs from vibrations which cause a large change in the polarizability of the molecule. Usually, symmetric vibrations cause the largest changes and give the most intense Raman scattering.

The phenomenon of light scattering can be described either classically or quantum mechanically by perturbation theory. Either way, the origin of the scattered radiation is considered to be the oscillating electric and magnetic multipole moments induced in a molecule by the electromagnetic fields of the incident light waves. For normal Raman spectroscopy, the important multipole source is the oscillating electric dipole. For that reason we will limit our description to the electric dipole and we will describe it by means of classical physics [Barron, L.D. 2004].

The objective of the classical theory of Raman spectroscopy is to calculate for a molecule the frequency-dependent liner induced electric dipole vectors $\boldsymbol{p}$ making use of the relationship expressed in Eqn.1

$$\boldsymbol{p} = \alpha \boldsymbol{E} \tag{1}$$

where $\boldsymbol{E}$ is the electric field vector of an incident, plane wave and monochromatic radiation ($\boldsymbol{\omega_1}$ *is* frequency of the radiation) and $\boldsymbol{\alpha}$ is the polarizability tensor of the molecule.

The polarizability tensor is, in general, a function of the nuclear coordinates and hence of the molecular vibrational frequencies. Therefore, the frequency dependent induced electric dipole vectors $\boldsymbol{p}$ will be obtained by introducing into Eqn. 1 the frequency dependence of $\boldsymbol{E}$ and $\boldsymbol{\alpha}$. The amplitude of a linear induced electric dipole of a particular frequency enables the scattered intensity to be calculated using Eqn. 2

$$I = k'_{\omega}\omega_s^4 p_0^2 sin^2\theta \tag{2}$$

$$k'_{\omega} = \frac{1}{32\pi^2\varepsilon_0 c_0^3} \tag{3}$$

To simplify, the scattering system is assumed to be a molecule which is free to vibrate but is fixed in space and can not rotate.

The variation of the polarizability with vibrations of the molecule can be expressed by expanding each component of $\boldsymbol{\alpha_{\rho\sigma}}$ in a Taylor series with respect to the normal coordinates around the equilibrium configuration (index 0):

$$\alpha_{\rho\sigma} = (\alpha_{\rho\sigma}) + \Sigma_k \left(\frac{\partial\alpha_{\rho\sigma}}{\partial Q_k}\right)_0 Q_k + \frac{1}{2}\Sigma_{k,l}\left(\frac{\partial^2\alpha_{\rho\sigma}}{\partial Q_k \partial Q_l}\right)_0 Q_k Q_{l\ldots} \tag{4}$$

In good approximation, powers of $\boldsymbol{Q}$ higher than the first can be omitted and if we restrict ourself initially to one normal mode of vibration $\boldsymbol{Q_k}$, Eqn. 4 simplifies to 5 or in vector notation to 6

$$(\alpha_{\rho\sigma})_k = (\alpha_{\rho\sigma})_0 + (\alpha'_{\rho\sigma})_k Q_k \tag{5}$$

$$\alpha_k = \alpha_0 + \alpha'_k Q_k \tag{6}$$

Assuming simple harmonic motion, the time dependence of $\boldsymbol{Q_k}$ is given by

$$Q_k = Q_{k_0} cos(\omega_k t + \delta_k) \tag{7}$$

Combining Eqn. 6 with Eqn. 7 leads to the time dependence of the polarizability tensor resulting form the $\boldsymbol{k}^{th}$ molecular vibration:

$$\alpha_k = \alpha_0 + \alpha'_k Q_{k_0} cos(\omega_k t + \delta_k) \tag{8}$$

If we insert the frequency dependence of α_k (Eqn. 8) and $E = E_0 cos(\omega_1 t)$ into Eqn. 1 we obtain

$$p = \alpha_0 E_0 \cos(\omega_1 t) + \alpha'_k E_0 Q_{k_0} \cos(\omega_1 t) \cos(\omega_k t + \delta) \tag{9}$$

Using the trigonometric identity

$$\cos(A)\cos(B) = \frac{1}{2}\{\cos(A+B) + \cos(A-B)\} \tag{10}$$

we obtain the final result

$$p = p(\omega_1) + p(\omega_1 - \omega_k) + p(\omega_1 + \omega_k) \tag{11}$$

$$p(\omega_1) = p_0^{Ray} \cos(\omega_1 t) \tag{12}$$

$$p_0^{Ray} = \alpha^{Ray} . E_0 = \alpha_0 . E_0 \tag{13}$$

$$p(\omega_1 \pm \omega_k) = p_{k_0}^{Ram} \cos((\omega_1 \pm \omega_k \pm \delta_k)t) \tag{14}$$

$$p_{k_0}^{Ram} = \alpha_k^{Ram} . E_0 \tag{15}$$

$$\alpha_k^{Ram} = \frac{1}{2}\alpha'_k Q_k \tag{16}$$

Eqn. 11 shows that the linear induced dipole has three distinct frequency components: $p(\omega_1)$ which gives rise to radiation at ω_1 and so accounts for Rayleigh scattering; $p(\omega_1 - \omega_k)$ which gives rise to radiation at $\omega_1 - \omega_k$ and so accounts for Stokes Raman scattering and finally $p(\omega_1 + \omega_k)$ which gives rise to radiation at $\omega_1 + \omega_k$ and so accounts for Anti-Stokes Raman scattering. It should be noted here that the induced dipole $p(\omega_1)$ is in phase with the incident radiation, whereas the induced dipoles oscillating at frequencies $\omega_1 \pm \omega_k$ are phase shifted by δ_k relative to the incident field. In practice, this mean that Rayleigh scattering might not scale linearly with the

scatterer density. For Raman scattering every molecule acts as independent source of radiation and the total scattered intensity scales linearly with the number of scatterers, what is important for quantitative analysis.

In practice, utilization of modern Raman spectroscopy is quite simple. Recent advances in instrument technology have simplified the equipment and variable instrument parameters are few. Raman spectroscopy has the ability to examine solid state matter, aqueous solutions and gas samples. A spectral manipulation is minimal and a simple interpretation of the data may be sufficient and useful for chemical detection [Smith, W.E. & Dent, G. 2005].

Raman spectroscopy is at present important in a broad range of scientific and industrial disciplines. Whilst the technique was initially used to examine inorganics, it grew with extensive use in polymer analysis and nowadays is the application of Raman spectroscopy common in many scientific fields including physics, chemistry, biology, medicine, pharmacy and environmental research as well as in industry, art, archaeology, forensic and biotechnological areas.

Compared to many other analytical techniques, Raman spectroscopy, because of its specificity and simple application, is viewed by many as a very efficient technique of the first use. However, there are two relevant disadvantages that must be considered. The first is the weakness of the Raman scattering that makes necessary a sensitive and highly optimized instrumentation. The second significant disadvantage is the eventual fluorescence emission by impurities or the sample itself that can hide the Raman spectrum. To enhance the sensitivity of this method, to improve the spatial resolution, and to acquire very specific information about analyzed molecules, there have been developed several variations of Raman spectroscopy: SERS, Raman microscopy and resonance Raman spectroscopy, respectively. In this thesis we have focused on the application of SERS for the detection of trace amount of chemicals, concretely organochlorine pesticides. For this reason, the next chapter contains information about the theory and practical application of this specific method.

3.2 SERS spectroscopy

3.2.1 Introduction

Surface-enhanced Raman scattering (SERS) represents a great advance in the field of Raman spectroscopy. SERS is an extremely sensitive technique based on the giant enhancement of the intensity of electromagnetic field induced by nanostructured noble metal surfaces and associated to localized surface plasmon resonance [Moskovits, M. 1985; Wokaun, A. 1985; Aroca, R. 2006; Schlücker, S. 2011]. This effect is a main reason of the dramatic enhancement of Raman scattering (10^6, in same cases even 10^{14}-10^{15}) of molecules located near or at the metal substrate. Most currently employed SERS substrates are metal nanoparticles in suspension (colloids) or immobilized and distributed on a solid surface (island films). Metal colloids have demonstrated to be one of the most active SERS substrates in spite of their instability. Many publications and applications of this technique appeared and attracted substantial attention of many research group worldwide [Etchegoin, P.G. & Le Ru, E.C. 2012; Alonzo-Gonzáles, P. *et al.* 2012; Wu, D.Y. *et al.* 2008]. During the previous years, the research activities in this field dramatically increased due to improvement in experimental techniques resulting from advances in nanotechnology and improved instrumental capabilities. Therefore, SERS has now become a very useful tool in various fields including chemistry, physics and biology.

3.2.2 A brief note about SERS discovery

SERS effect was initially observed in 1974 by Fleischman *et al.* [Fleischman, M. *et al.* 1974]. They reported a strong Raman scattering from pyridine adsorbed onto a silver electrode roughened from an aqueous solution by means of successive oxidation–reduction cycles. In 1977, two groups independently noted that the concentration of scattering species could not account for the enhanced signal and each one proposed a mechanism of the observed enhancement. Jeanmaire and Van Duyne [Jeanmaire, D.L. & Van Duyne, R.P. 1977] proposed an electromagnetic effect while Albrecht and Creighton proposed a charge-transfer effect [Albrecht, M. G. & Creighton, J.A. 1977]. The principles of both mechanisms are explained in the next sub-chapters.

3.2.3 Electromagnetic mechanism of SERS

When a light beam interacts with the conduction electrons existing on the surface of metallic surface, they begin to oscillate as a collective group across the surface. These oscillations are termed surface plasmons and have a resonance frequency at which they absorb and scatter light most efficiently [Zeng, S. *et al.* 2014; Ritchie, R.H. 1957; Polman, A. & Atwater, H.A. 2005]. Plasmons oscillate at frequencies in the visible region and therefore they are suitable for use with the visible and near-infrared resonance (NIR) laser systems commonly used in Raman spectroscopy. When the metal is organized in nanoparticles (NPs) of sub-wavelength size, these plasmons are localized giving rise to localized surface plasmon (LSP) which oscillates at a frequency that depends on the electric permitivity, the size and shape of the nanoparticle. The excitation of surface plasmon in nanoparticles by the incident light leads to the so-called localized surface plasmon resonance (LSPR).

The electromagnetic (EM) mechanism of SERS effect considers that the huge intensification of the Raman signal is due to the fact that the EM field enhancement occurs for both the incident (E_I) and the scattered Raman (E_R) radiations (Fig. 3a), in contrast to the classical Raman process, where a simple emission process takes place (Fig. 3b). This twofold enhancement is attributed to the coupling of the incident and scattered radiations with the above mentioned surface plasmons and subsequent LSPR. Firstly, the field enhancement magnifies the intensity of the incident light (E_I) with ω_I. The excitation of the surface plasmons greatly increases the local field leading to intensification of the EM intensity of the incident light reaching the molecule placed at position r, therefore increasing the intensity of the Raman scattering. Then, the Raman signal, connected with the intensity E_{RM} and emitted by the molecule with frequency ω_{RM}, is further magnified by the surface due to the same mechanism that intensify the EM field of the incident light, resulting in a greater increase in the total output represented by the E_R+E_{RS} overall emission (Fig. 3a).

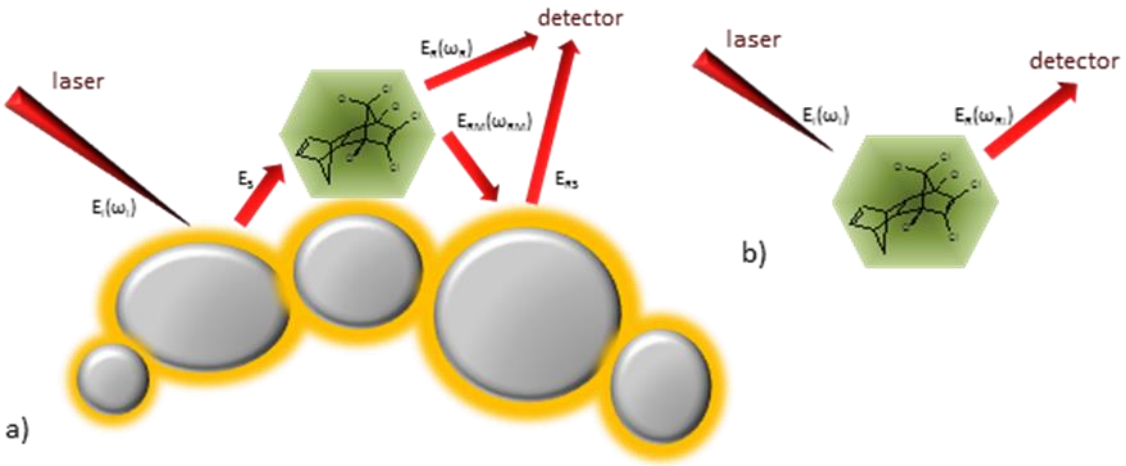

Fig. 3 – Schematic representation of the electromagnetic enhancement mechanism of SERS in the presence (a) and absence (b) of a metal surface.

The intensity of the Raman scattered radiation is proportional to the square of the magnitude of EM fields incident in the position of an analyte. It can be expressed as:

$$I_R \alpha E^2 \tag{17}$$

Where,

I_R is the intensity of the Raman signal,

E is the intensity of EM field coupling with an analyte.

Since at each intensification process the Raman signal is enhanced as E^2, therefore a total enhancement of E^4 will be obtained in the SERS process [Kneipp, K. 2006].

In the special case of a spherical NPs which is subjected to an applied electric field from the laser, the field at the surface can be described as:

$$E_r = E_0 \cos\theta + g\frac{\alpha^3}{r^3} E_0 \cos\theta \tag{18}$$

$\boldsymbol{E_r}$ is the total electric field at a distance *r* from the sphere center,

$\boldsymbol{E_0}$ is the applied electric field,

θ is the angle relative to the direction of the electric field,

a is the radius of the sphere,

g is a term given by the following equation:

$$g = \left(\frac{\varepsilon_1(\omega)-\varepsilon_0}{\varepsilon_1(\omega)+2\varepsilon_0}\right) \quad (19)$$

$\boldsymbol{\varepsilon_0}$ and $\boldsymbol{\varepsilon_1}$ are the dielectric constants of the medium surrounding the sphere and metal sphere, respectively,

ω is the frequency of the incident radiation.

The *g* term governs the SERS intensification and will reach a maximum value when $\mathrm{Re}[\varepsilon_1(\omega)] \approx -2\varepsilon_0(\omega)$ and $\mathrm{Im}[\varepsilon_1(\omega)] \approx 0$. This condition, that corresponds to the maximum LSPR intensification, is found for a reduced group of metals: Au, Ag, Cu, mainly in the visible and NIR regions. Thus, these metals are the most suitable and used for the application in SERS.

According to the electromagnetic mechanism of SERS, the highest enhancement occurs for those vibrational modes which are perpendicularly oriented to the surface. In contrast, the vibrational modes developing parallel to the surface are less intensified. This is due to the polarization of the field on the nanoparticle [Creighton, J.A. 1988].

One interesting consequence of the EM mechanism is the strong gradient of the field intensity on the metal surface. In the case of the metal sphere, the external field depends on the distance as $[R/(R+d)]^{12}$, where ***R*** is the radius of the NP and ***d*** is the distance to the NP surface. This effect means that the vibrational modes placed closer to the metallic surface will appear with a highest intensity in the SERS spectrum. This interesting effect can be used to deduce the interaction mechanism of ananalyte with the metal surface.

Another feature that should be considered is that the EM enhancement is not equal for all frequencies. For those frequencies for which the Raman signal is only slightly shifted from the incident light, both the incident laser light and the Raman signal can be near resonance with the plasmon frequency. When the frequency shift is large, the incident light and the Raman signal cannot both be on the resonance with plasmon frequency, thus the enhancement at both stages cannot be maximal [Langhammer, Ch. 2006].

According to the EM mechanism, SERS gives rise to enhancements factors of 10^6 or more as reported by numerous research groups [Halas, N.J. *et al.* 2011; Shafer-Peltier, K.E. *et al.* 2003; Grubisha, D.S. *et al.* 2003; Nam, J.M. *et al.* 2004; Lyandres, O. *et al.* 2005; Kneipp, J. *et al.* 2005; Premasiri, W.R. *et al.* 2005]. In certain cases, the great enhancement provided by LSPR is sufficient for single or few molecule detection, making SERS an extremely useful technique for chemical and biomolecular detection [Kneipp, K. *et al.* 1997; Nie, S. & Emory, S.R. 1997; Moskovits, M. & Jeong, D.H. 2004; Cao, Y.C. *et al.* 2002].

3.2.4 Chemical mechanism of SERS

For many molecules, often those with alone pair of electrons by which the molecules can bond to the surface, a different SERS enhancement mechanism has been described, that does not involve surface plasmons,. This is called charge transfer or chemical enhancement [Otto, A. *et al.* 1992] and it involves the formation of a bond between an analyte and the metal surface. In this case, a charge-transfer (electrons or holes) is possible from the metal surface to the analyzed molecule and back to the metal again. The formation of this bond will increase the molecular polarizability of the molecule considerably due to interaction with the metal electrons. Basically, the chemical enhancement is thought to proceed via new electronic states which arise from the formation of the bond between the analyte and the metal surface. These new states are believed to be resonant intermediates in the Raman scattering [Schlücker, S. 2011]. The chemical mechanism only applies in specific cases and probably occurs in concert with the electromagnetic mechanism [Lombardi, J.R. *et al.* 1986; Lombardi, J.R. *et al.* 2008].

The phenomenon of SERS chemical enhancement is only possible for the first layer of the analyte attached to the surface, whereas electromagnetic enhancement can occur also from second or subsequent layers. Some enhancement has been claimed up to about 20 Å or more away from the metal surface.

There exists clear evidence for validity of both mechanisms of SERS enhancement. However, it is very difficult to differentiate them. Clearly, chemical enhancement should occur only from molecules directly attached to the surface and consequently should increase only up to monolayer coverage. On the other hand, electromagnetic enhancement, although a longer range effect, drops off with distance from the surface. Thus, most of the electromagnetic enhancement will also arise from adsorbates present on the surface up to monolayer coverage. The vast majority of the evidence points to both effects having a part to play in SERS enhancement, although it is generally believed that electromagnetic enhancement is a more dominant process than charge transfer enhancement [Aroca, R. 2006].

3.2.5 SERS substrates

Typically, the metals that lead to a significant LSPR effect are gold, copper and silver due to their good electric properties and low losses of the energy by the absorption by metallic material. The choice of surface metal is also dictated by the plasmon resonance frequency in an accordance with the available excitation laser. The above mentioned metals have LSPR at frequencies that fall within the visible and NIR regions [Giannini, V. *et al.* 2011].

The SERS effect is a direct consequence of the presence of metal nanostructured features at the metal surface. These features can be developed in a number of ways, for example an oxidation-reduction cycles on electrode surfaces, metal spheroid assemblies produced via lithography, or metal colloids [Jensen, T.R. 2000; Moskovits, M. 1985]. All of these methods produce available nanostructured particles that are capable of serving as metal platforms for SERS [Kneipp, K. 2006].

Each individual particle has a plasmon for which the resonance condition is only satisfied by a small range of wavelengths. However, the electrons are only loosely held and are free to couple to adjacent particles so that the plasmon is actually the plasmon

of more than one particle and has a new frequency range over which resonance can occur [Schlücker, S. 2011]. The actual frequency of the plasmon for single particles decreases as the particle size rises and similarly dimers, trimers, etc., of particles have plasmon resonances at lower frequencies. The aggregation of single nanoparticles leads to nanostructures with better morphological properties to give rise to effective LSPR. Therefore, the activation of metal nanoparticles by a chemical aggregating agent is a usual way to increase the SERS activity of individual NPs.

3.2.6 Hot spots

The LSPR is not homogeneously distributed on the metal surface. There are certain points where the intensification of the electric field derived from the excitation of plasmons reaches a maximum value. These points are usually called hot spots (HS) and are placed in regions of high curvature in anisotropic NPs or in interparticle junctions (Fig. 4). For instance, it is known from many experiments, mainly on small particles adsorbed on a metal surface, that the greatest enhancement does not occur evenly round every isolated particle but at points between some touching particles or clusters of particles [Brasil, A.M. *et al.* 2001].

The formation of size-controlled nanogaps between plasmonic surfaces has given rise to extensive research, both theoretical and experimental [Li, W.Y. *et al.* 2009; Xu, M.M. *et al.* 2009; Du, C.L. *et al.* 2009; Rycenga, M. *et al.* 2009; Camargo, P.H.C. *et al.* 2009; Zuloaga, J. *et al.* 2009]. It has been theoretically predicted that the electromagnetic field in such nanogaps undergoes a huge intensification. This phenomenon is of great importance in SERS, where metal colloids are commonly used to obtain signal intensification even for single molecule detection experiments [Vlckova, B. *et al.* 2008**;** Futamata, M. 2006].

In fact, it is generally accepted that the possibility of single molecule or few molecules detection depends on the existence of interparticle gaps where the main part of the electromagnetic field intensification occurs [Lee Ru, E.C. *et al.* 2006]. Aggregated colloids are the main source for single-molecule detection [Aroca, R.F. *et al.* 2005], but the fabrication of such hot spots became uncontrollable in experiments under macro conditions, and their existence being a matter of luck provided by the

specific aggregation pattern and the morphology induced by the aggregates absorbed NPs. Thus, the molecules adsorbed on the metal surface may effectively play a crucial role in the controllable and reproducible formation of the hot spots [Anderson, D.J. & Moskovits, M. 2006].

3.2.7 Functionalization of metal nanoparticles

When an analyte does not show any tendency to the adsorption on metal NPs, SERS detection depends on an appropriate modification of the properties of metal surfaces, which enables the analyte approach to the surface. The sensitivity and selectivity of metal NPs to analytes can be remarkably enhanced by changing the interfacial properties of the metal surfaces.

There exists a classification of host molecules employed for functionalization of metal surfaces according to the mechanism of interaction with the ligand. Host molecules can be classified into three main groups: inclusion, occlusion and contact hosts. The conditions that these host molecules must fulfill are: good adherence to the metal surface, the existence or formation of intra- or intermolecular cavities able to locate the ligand, high affinity towards the analyte of interest and no overlapping spectroscopic signals. Among the most used functionalizing molecules are considered calixarenes, antibodies or aptamers, which may host or bond to a target molecule, attracting it to the surface [Guerrini, L. *et al.* 2008; Guerrini, L. *et al.* 2008; Cho, E.C. *et al.* 2010; Leyton P. *et al.* 2004**;** Guerrini, L. *et al.* 2006**;** Guerrini, L. *et al.* 2007; Guerrini, L. *et al.* 2009].

One interesting functionalizing method proposed in the present work is the modification of the metal surface with molecules that are able to activate the formation of intra- or intermolecular cavities. These molecules may act as interparticle linkers and host platforms able to accommodate the analyte just at the interparticle junction, where the EM field is enhanced to a huge value (Fig. 4).

In this work we have used as bifunctional linkers several dithiols, linear aliphatic as well as aromatic, for the functionalization of metal NPs to obtain SERS active substrates for the detection of the pollutants studied in this work.

3.2.7.1 Dithiols as bifunctional NPs linkers

An ideal situation for building interparticle HS is the use of bifunctional molecules which act as NPs linkers [Guerrini, L. *et al.* 2009]. Many molecules adsorbed on metal surfaces are not only able to induce the formation of the HS but can also host specific analytes. The molecules that fulfill this double function show two main features: the ability to interact with the metal surface, and affinity to bind the analyte [López-Tocón, I. *et. al.* 2011].

Thiol groups strongly interact with both Ag and Au, the most active metals in SERS. However, monothiols are not suitable linkers for the detection of persistent organic pollutants (POPs) or small aromatic compounds since they form very tight self-assembled monolayers (SAMs) because of the strong intermolecular interactions between aliphatic chains and they avoid a proper NPs linking as they rather act as NPs stabilizers. In these SAMs, there are no cavities or intermolecular spaces where the ligand could be located. In fact, only on-top adsorption was observed in these systems [Domingo, C. *et al.* 2003]. On the contrary, dithiols may act as linkers between metal NPs and induce the formation of nanoclusters of controllable interparticle distance (Fig. 4). The nanogaps thus formed present available binding sites able to host target molecules, therefore these systems can be used as SERS nanosensors.

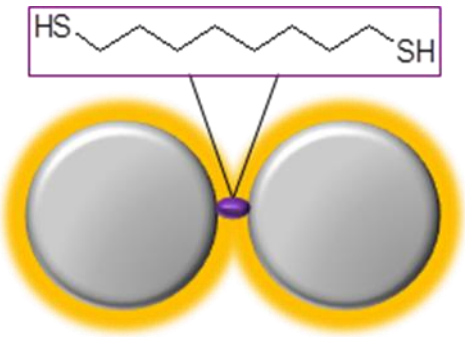

Fig. 4 – An illustration of a modified surface of metal NPs by using aliphatic dithiol as a linker.

In this work, aliphatic and aromatic molecules having two SH groups at both the first and the ending CH_2 groups (α,ω-dithiols) were employed for the functionalization

of metal NPs to prepare SERS active and suitable substrates for the detection of organochlorine pesticides.

3.2.8 SERS as a sensing technique

SERS technique is a suitable technique that can be employed for the analysis of challenging molecules. Typical applications include the *in situ* determination of homogeneity, phase, and crystal orientation, identification of surface contaminats, and measurement of layer thickness [Schlücker, S. 2011]. For this reason SERS performs vital roles in many semiconductor applications, such as measuring stress in silicon microelectronics and helping in the development of novel photovoltaic cells. It characterizes both semiconductor materials and completed devices, and can assess crystalline quality, local stress/strain, dopant/impurity levels and even temperatures in operating devices, on a sub-micrometer scale. Nanotechnology possesses particular challenges because of the novel materials and intrinsically small distance scales involved, and SERS can locate and analyse these nanoscale structures [Smith, W.E. & Dent, G. 2005; Aroca, R. 2006].

The restoration of work of art and historical artefacts is a major concern for conservators, historians, and archeologists, and relies on the accurate identification of the materials involved. SERS is a technique which can be used for the analysis of the composition of paints, pigments, and corrosion products *in situ*, non-destructively. It can study all sizes of item, from small figurines to larger paintings [Huh, Y.S. *et al.* 2009].

Law enforcement agencies need to support prosecutions with reliable and detailed forensic information. High sensitivity and high resolution imaging capabilities enable forensic scientists to find and identify the tiniest traces of evidence, such as microscopic particles of explosive in a fingerprint. The flexibility of SERS makes it valuable in numerous areas, including narcotics, explosives, paints and pigments, fibre-analysis, questioned documents, and gunshot residues [Aroca, R. 2006].

SERS is also a very promising analytical technique in the pharmaceutical industry. The fast, label-free and non-invasive nature of the SERS-based technique together with its high molecular specificity and sensitivity makes SERS highly suitable

for quality control (QC) processes of pharmaceuticals such as QC identification, final goods QC, trace impurity detection and in-line process control. Nowadays, a mayor analytical challenge in this field is the rapid chemical identification of active drug substances with respect to their polymorphic forms, possible contaminants, the distribution and interaction between drug substances and excipients [Schlücker, S. 2011]. The analysis of dosage samples by conventional techniques such as mass spectroscopy (MS), elemental analysis, spectrophotometry or nuclear magnetic resonance (NMR) can be very difficult because of substance inhomogeneity on a similar scale. With the advent of a new instrumentation and intense monochromatic light sources, SERS has become a popular tool analyzing pharmaceutical compounds [Cinta-Pinzaru, S. *et al.* 2004; Williams, A.C. 2001].

SERS technique was also employed in the sensitive and selective detection of trace pollutants by using host cavitants. By properly modifying the chemical properties of the metal surface it is possible to increase drastically the adsorption of environmental pollutants on the substrate [Domingo, C. *et al.* 2007; Sanchez-Cortes, S. *et al.* 2007]. This allowed both the sensitive and selective detection of persistent organic pollutants (POPs), in particular polycyclic aromatic hydrocarbons (PAHs) and polychlorinated pesticides (PCPs) [Schlücker, S. 2011]. These pollutants have been reported to be strong carcinogens [Harvey, R.G. 1997], and therefore their trace detection is a very important goal.

Identification and quantification of POPs (including organochlorine pesticides) in aqueous solutions is usually carried out by high performance liquid chromatography (HPLC) with UV-visible absorption, fluorimetric or amperometric detection or by means of GC-MS (gas chromatography-mass spectrometry) or GC-FID (flame ionization detection). However, most of these techniques include a time consuming pre-concentration steps [Barro, R. *et al.* 2009]. The detection of POPs by means of SERS is of interest because of the ready detection of pollutants directly in multicomponent samples, and because of the direct analysis, many times *in situ*, without the pre-concentration process or solvent extraction usually used in case of chromatography. The detection of PAHs with SERS has been carried out by several groups by using aliphatic organic molecules [Olson, L.G. *et al.* 2004; Schmidt, H. *et al.* 2004]. The main

advantage of SERS applications in the detection of pollutants is that this technique is not only able to detect the existence of the analyte but also provides information on the structural state of the molecule. The choice of the most appropriate host for surface functionalization in SERS nanosensors will obviously depend on the nature and size of the molecule to be detected.

3.3 Pesticides

A pesticide is generally a chemical or biological agent (such as a virus, bacterium, or disinfectant) designed to kill or retard the growth of pests that damage or interfere with the growth of crops, shrubs, trees, timber and other vegetation desired by humans. Target pests can include insects, plant pathogens, weeds, mollusks, nematodes (roundworms), and microbes that cause nuisance, spread disease or are vectors for disease. Although there exists human benefits to the use of the pesticides, there are a lot of drawbacks, such as potential toxicity to humans and other animals. Most of the pesticides are non-specific and may kill life forms that are harmless or useful. Practically all chemical pesticides are poisons and pose long-term danger to the environment and humans through their persistence in nature and body tissue. According to the Stockholm Convention on Persistent Organic Pollutants, 9 of the 12 most dangerous and persistent organic chemicals are pesticides [Gilden, R.C. *et al.* 2010].

3.3.1 Organochlorine pesticides

Organochlorine pesticides (OPs) have extremely strong bonds between the chlorine atom and carbon components, are liposoluble and highly insoluble in water. The widest application for OPs is as insecticides. When used, organochlorine pesticides can leech into our environment via direct application, contaminated waste disposal, incinerator emissions or runoff [CDC 2009; Lorenz, E.S. 2009]. The problem with these substances is that once OPs are used, they can be spread and stay in the environment, a human or animal body, the water supply or the soil for a long time. Therefore, although they are currently banned in many industrial countries, many of these pesticides can be still found in any region of the world and their persistent character

leads to an accumulation in living systems. This is the reason why these compounds can be also detected in persons who were not directly exposed to the pesticides [Jimenez, M. *et al.* 2004].

3.3.1.1 Aldrin and dieldrin

Aldrin (1,2,3,4,10,10-hexachloro1,4,4α,5,8,8α-hexahydro-1,4-endo,exo-5,8-dimethanonaphthalene) and dieldrin (1,2,3,4,10,10-hexachloro-6,7-epoxy1,4,4α,5,6,7,8,8α-octahydro-1,4-endo,exo-5,8-dimethanonaphthalene) (Fig. 5) are structurally similar chemicals that are produced in laboratories and do not occur naturally in the environment. Pure aldrin and dieldrin are white powders, while technical-grade aldrin and dieldrin are tan powders. They slowly evaporate in the air, whereas aldrin evaporates more readily than dieldrin. Both chemicals have mild chemical odors. Like related polychlorinated pesticides, they are highly lipophilic, therefore very low soluble in water, which exacerbates its persistence in the environment [ATSDR 2002].

Aldrin and dieldrin belong between the most important pesticides [Metcalf, R.L. 2002]. They were once used as organochlorine insecticides by contact or ingestion [Hayes, W.J.Jr. 1982]. These two compounds are closely related with respect to their toxicology and mode of action. Aldrin is rapidly converted to dieldrin under most environmental conditions and in a living organism. Dieldrin is a highly persistent compound that has low mobility in soil, can be lost to the atmosphere and bioaccumulates [FAO/WHO 1995; WHO 2003].

Both chemicals were used extensively as a seed dressing for food or soil insecticides on commodity crops such as corn and cotton. They were used as a prophylactic and for treatment of timber against termite infestation [Worthing and Walker 1983]. Dieldrin was also used for mothproofing clothes and carpets. In tropical countries, dieldrin was used as a residual spray in residential dwellings to control vector-borne diseases such as malaria [CDC 2009].

From the point of view of aldrin impact on a human body it should be noted that this compound is a neurotoxin and has caused electroencephalogram abnormalities following short-term or long-term oral, dermal, or inhalation exposure.

After absorption, aldrin is metabolized to dieldrin so rapidly that aldrin is rarely detected. Dieldrin accumulates in fatty tissues, and its metabolites are excreted in bile and feces. It is also excreted in breast milk and can cross the placenta. Aldrin and dieldrin affect human health in similar ways. At high doses, they block inhibitory neurotransmitters in the central nervous system. This blocking action can cause abnormal excitation of the brain, leading to symptoms such as headache, confusion, muscle twitching, nausea, vomiting, and seizures. Based on studies in animals, the Environmental Protection Agency (EPA) has determined that aldrin and dieldrin are probable human carcinogens [ATSDR 2002].

Based on the concern that aldrin and dieldrin could cause severe aquatic environmental change and are potentially carcinogenic, a number of countries have either severely restricted or banned the use of both compounds, particularly in agriculture [US EPA 1990b; CRD 2009]. These two chemicals are no longer produced, but we can still find them in the soil, in water, or in houses where this compound was used and they can be finding also in plants and animals near hazardous waste sites [US EPA 1980].

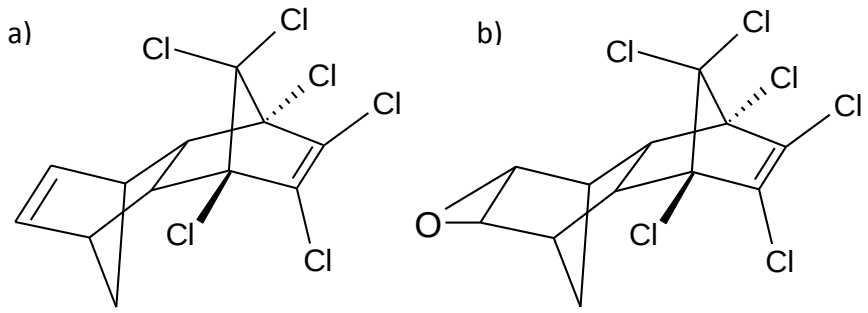

Fig. 5 – Molecular structure of (a) aldrin and (b) dieldrin.

3.3.1.2 Endosulfan

Endosulfan (6,7,8,9,10,10-hexachloro-1,5,5α,6,9,9α-hexahydro-6,9-methano-2,4,3-benzodioxathiepine-3-oxide) (Fig. 6) is other important organochlorine insecticide bearing a bicyclic structure as aldrin and dieldrin and can exist in two isomeric forms: α- and β- endosulfan [Wan, M.T. *et al.* 2005]. This colorless solid compound has emerged as a highly controversial agrichemical due to its acute toxicity,

endocrine effects, and potential for bioaccumulation. Though banned in the European Union and many countries of North and South America, several Asian and West African nations, it is still used extensively in several other countries including India, Brazil, Australia [CRD 2009; US EPA 2010; The Hindu 2011; Weekly Times 2009; The Daily Green 2010; ICC 2009].

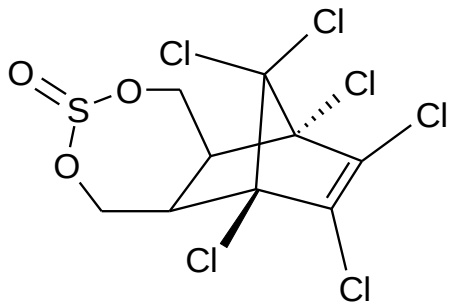

Fig. 6 – Molecular structure of α-endosulfan.

Endosulfan is used in a formulated form as a broad-spectrum contact and stomach insecticide mainly in agriculture. It is a chlorinated hydrocarbon insecticide and acaricide of the cyclodiene subgroup which acts as a poison to a wide variety of insects and mites on contact. Although it may also be used as a wood preservative, it is used primarily on a wide variety of food crops including tea, coffee, grain, fruits, and vegetables, as well as on rice, cereals, maize, sorghum and also on nonfood crops such as tobacco and cotton [ATSDR 1995].

For a human being, endosulfan is highly toxic via the oral, dermal route and may be only slightly toxic via inhalation. Stimulation of the central nervous system is the major characteristic of endosulfan poisoning. Acute endosulfan poisoning can cause convulsions, incoordination, imbalance, difficulty breathing, gagging, vomiting, diarrhea, agitation, and loss of consciousness, psychiatric disturbances, epilepsy, paralysis, brain oedema, impaired memory and death. Long term exposure is linked to immunosuppression, neurological disorders, congenital birth defects, chromosomal abnormalities, mental retardation, impaired learning and memory loss. In addition, several evidences suggest that exposure to endosulfan may cause mutagenic effects in humans if exposure is great enough. Once endosulfan is in the body, it is broken down

in the liver and kidneys into mainly water-soluble products and leaves the body through urine and feces within a few days or a few weeks [ATSDR 2013].

It should be noted that detection limits for the α- and β-isomers of endosulfan usually differ, the α-isomer being easiest to detect. At low concentrations, the identification of endosulfan residues can be hampered by a variety of other pesticides or plant components.

3.3.1.3 Lindane

Lindane (1α,2α,3β,4α,5α,6β-hexachlorocyclohexane) (Fig. 7) is a persistent environmental toxin and a known neurotoxin. It is an organochlorine pesticide compound that is brownish to white crystalline organic powder with a penetrating musty odor.

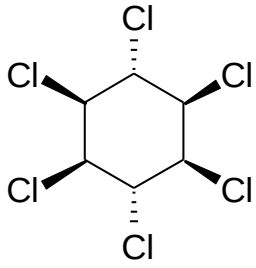

Fig. 7 – Molecular structure of lindane.

The only identified uses for hexachlorocyclohexane-containing products are based on the insecticidal activity of the γ isomer (lindane), which is considered to be the only insecticidally effective component. Lindane is used primarily as an insecticide in the treatment of wood and wooden structures, seed grains, and livestock. Other major uses are as an insecticide for several fruits and vegetable crops, in baits and seed treatments for rodent control, and for treatment of scabies (mites) and lice [Report on Carcinogens 2011].

The routes of potential human exposure to lindane and other hexa-chlorocyclohexane isomers are ingestion, inhalation, and dermal contact. Metabolism of lindane produces several metabolites which are distributed in the body and excreted through various routes like urine, sweats, feces, hairs.

Short-term exposure of lindane to human body may potentially cause high body temperature and pulmonary edema. Long-term exposure of lindane has the potential to cause liver and kidney damage. Many cases of aplastic anemia have also been associated with exposure to lindane, and death from lung cancer was increased among agricultural workers who had used hexachlorocyclohexane (unspecified) and a variety of other pesticides and herbicides. High levels of lindane have been detected in post-mortem human brain from Parkinson's disease patients [ATSDR 2005; WHO 2003].

3.3.2 Detection of organochlorine pesticides

Several analytical tools have been employed so far for detecting the above OPs substances. The most common methods involve separation by gas chromatography coupled with electron capture detection (ECD) [Cerrillo, I. *et al.* 2005; Fernandez, M.F. *et al.* 2007; Guardino, X. *et al.* 1996; Barcarolo, R. *et al.* 1988; Walker, A.I.T. *et al.* 1969], electrolytic conductivity detector [Bennett, D.A. *et al.* 1997], or mass spectrometry [Fernandez, M.F. *et al.* 2007; Mariani, G. *et al.* 1995; Damgaard, I.N. *et al.* 2006; Kobayashi, H. *et al.* 1983; Alford-Stevens, A.L. *et al.* 1986; Richardson, A. & Robinson, J. 1971]. GC has also been used with Fourier transform infrared spectroscopy (FTIR) [Silambarasan, S. and Abraham, J. 2013]. These methods are used for determining aldrin, dieldrin and α- and β-endosulfan in air, water, municipal effluents, sludge, and soil, in human body liquids, food, fish, and feces. The detection of lindane is still imperfectly identified, but there exists a method that determined lindane and its metabolites in urine, serum and faeces samples using HPLC-UV-Vis and mass characterized with matrix-assisted laser desorption/ionization – time-of-flight (MALDI-TOF) [Naidu, N.V. and Yakubu, M.A. 2013]. Despite of some advantages of these analytical methods, like velocity and sensitivity of detection, all of these methods need sample preparation and are rather expensive. Therefore, it is desirable to develope an easy, fast, sensitive, non-destructive and cheap method to detect these pesticides. This is the main reason why we investigate in the present work a detection method of OPs based on the SERS technique.

4 Materials and methods

4.1 Chemicals

Chemical reagents for preparation of SERS substrates

Silver nitrate ($AgNO_3$) and chloroauric acid trihydrate ($HAuCl_4x3H_2O$) were purchased from Merck. Trisodium citrate dihydrate ($Na_3C_6H_5O_7x2H_2O$), hydroxylamine hydrochloride ($NH_2OHxHCl$) and sodium hydroxide (NaOH) were purchased from Sigma-Aldrich. Aggregation reagents, sodium chloride (NaCl) and potassium nitrate (KNO_3), were also obtained from Sigma-Aldrich. All chemicals were of the analytical grade purity.

Dithiols

1,6-Hexanedithiol (DT6) (>97%) was purchased from Sigma Aldrich, while 1,8-octanedithiol (DT8) (>97%) and 1,10-decanedithiol (DT10) (>96%) were obtained from Alfa Aesar. Stock solutions of these substances were prepared in ethanol (>99,5%, Merck) at 10^{-2} M concentration and were further diluted when necessary. 1,4-benzenedithiol (BDT) and biphenyl-4,4'-dithiol (BPDT) (both of >95% purity) were obtained from Sigma-Aldrich. Stock solution of BDT was prepared in ethanol at a concentration 10^{-2} M. Solution of BPDT was dissolved in 1,4-dioxane (>99,8% purity, Sigma-Aldrich) at 10^{-3} M.

Pesticides

The pesticide aldrin was supplied by Riedel-de-Haën with a purity of 99%. The other pesticides, α-endosulfan (>99%), lindane (>97%) and dieldrin (>98%), were purchased from Sigma-Aldrich. These compounds were dissolved in absolute ethanol (>99,5%) at concentrations of 10^{-2} to 10^{-6} M.

4.2 Colloids

4.2.1 Preparation of Ag colloids

Silver nanoparticles were prepared by chemical reduction of an aqueous solution of silver nitrate using two different reduction agents: trisodium citrate dihydrate and hydroxylamine hydrochloride. All aqueous solutions needed for colloids formation were prepared by using Milli-Q water.

Citrate-reduced silver colloid (AgC) was prepared according to a modified Lee and Meisel method [Lee, P.C. & Meisel, D. 1982]. Silver aqueous solution (10^{-3} M) was prepared by dissolving a total of 8,5 mg of $AgNO_3$ in 50 ml of Milli-Q water. Then, a total of 1 ml of a 1% (w/v) trisodium citrate aqueous solution was added to 50 ml of a boiling 10^{-3} M silver nitrate solution. The mixture was kept boiling under reflux for one hour. The obtained colloid showed a turbid gray aspect and had a final pH of 6-7.

Hydroxylamine-reduced silver colloid (AgH) was obtained by the method described by Leopold and Lendl [Leopold, N. & Lendl, B. 2003]. Briefly, solutions of silver nitrate (10^{-2} M) and hydroxylamine hydrochloride ($1,6x10^{-3}$ M) were prepared in Milli-Q water. Then, 10 ml of a 10^{-2} M silver nitrate solution was added dropwise to 90 ml of a $1,6\times10^{-3}$ M solution of hydroxylamine hydrochloride adjusted to pH=9 under vigorous stirring. The resulting solution showed a dark gray coloration with spherical Ag NPs of 35 nm average diameters [Cañamares, M.V. *et al.* 2005].

4.2.2 Preparation of Au colloids

Gold nanoparticles (AuC) were prepared according to a modified Sutherland-Wineforder method [Sutherland, W.S. & Winefordner, J.D. 1992] by a chemical reduction of an aqueous solution of chloroauric acid and as reductant was used trisodium citrate. A total of 46,7 mg of $HAuCl_4x3H_2O$ was firstly dissolved in 1 ml of Milli-Q water (0,118 M). 100 µl of this solution was then diluted in 40 ml of Milli-Q water under intense stirring. Then, 400 µ lof 1% trisodium citrate solution was added dropwise. The obtained yellow solution was heated and maintained for 5 minutes to boiling resulting in a dark claret colloidal suspension. The average diameter of Au nanoparticles prepared by this method was 20 nm.

4.3. Preparation of samples

4.3.1 Preparation of samples for SERS experiments

Samples for SERS measurements of aliphatic and aromatic dithiols were prepared by adding 10 µl of dithiol solutions to 1 ml of the already aggregated colloid. The activation was performed by adding 40 µl of a 0,5 M potassium nitrate solution to 1 ml of silver colloids and the same amount of NaCl was adding to 1 ml of gold colloid. The nitrate activation is related to the removal of the citrate excess existing on the fabricated nanoparticles after their preparation and gives rise to a homogeneous aggregation of nanoparticles in utilized colloids. The final concentrations of dithiols in the samples were 10^{-4} to 10^{-8} M.

Samples for SERS measurements of organochlorine pesticides (aldrin, dieldrin, lindane and α-endosulfan) were prepared as follows. A total of 1 ml of the colloid (silver as well as gold) was activated by the addition of 40 µl of 0,5 M KNO_3. Then 10 µl of a solution of aliphatic dithiol and 10 µl of a solution of organochlorine pesticide, both solutions at appropriate concentrations, were added to the colloid. The final concentrations of the pesticides in the samples were varied in the 10^{-4} to 10^{-8} M range. In all measurements the samples were placed in a 1 cm quartz cuvette.

4.3.2 Preparation of samples for TEM experiments

For TEM measurements, the samples were prepared by the immobilization of the samples on a 3,05 mm diameter copper grid, composed of 200 squares and 100 µm in length. These grids were previously covered by a 0,2 M Formvar chloroform solution in order to obtain a thin transparent film. On this film a small drop of a diluted colloid was deposited and evaporated at a room temperature.

4.4 Instrumental techniques

Ultraviolet-visible absorption spectroscopy

An UV–visible–NIR Shimadzu 3600 spectrometer equipped with a PMT detector (photomultiplier tube) for light detection in the UV–visible range, and InGaAs and PbS

detectors for the NIR, was employed for the measuremenst of the plasmon extinction spectra of colloids. 1 cm optical path quartz cuvettes were used for the measurements.

Raman and SERS spectroscopy

The Raman and surface-enhanced Raman spectra were measured using a Renishaw InVia Raman apparatus equipped with an electrically refrigerated CCD camera and a Leica DM 2500 microsope. The instrument was coupled with various types of laser sources that enable the use of different excitation lines. The line at 532 nm provided by a Nd-YAG laser (Samba model, Cobolt) and the 785 nm line provided from a diode laser (HPNIR 785 model, Renishaw) were used as excitation sources. Raman scattering was filtered by a holographic notch filter system, to eliminate Rayleigh elastic dispersion of photons with adequate diffraction grids, and collected by an electrically air-cooled CCD detector of 400x575 pixels. The colloidal suspensions were placed in a 1 cm optical path quartz cuvette to carry out Raman measurements.

Transmission electron microscopy

Transmission electron microscopy images were taken using a JEOL JEM-2010 with an acceleration voltage of 200 kV

5 Results and discussion

The SERS effect requires as a condition the approach of a studied molecule to the metal. In many cases the molecule is absorbed spontaneously on the metal surface, either by physical mechanisms, either by forming a covalent bond. However, in other cases, the analyte does not show any tendency to an adsorption. This is the case of the OPs pollutants studied in this work, they do not show any affinity to the metal surface of colloidal NPs and require the proper functionalization of the metal surface. For these reasons we needed firstly to prepare, characterize and optimize dithiol-functionalized metal NPs for application in SERS detection of OPs. This first part of the Result section deals with this problematics.

5.1 Adsorption of linear aliphatic α,ω-dithiols onplasmonic metal nanoparticles

5.1.1 UV-Vis and TEM study of the aggregation and formation of interparticle hot spots

The assembly of AgH nanoparticles induced by dithiols was monitored by the extinction spectra of plasmon resonances of the resulting aggregates at a macroscopic level. This study was carried out at different concentrations of aliphatic dithiols to check the effect of the surface coverage on the final aggregate geometry. Extinction spectra of Ag NPs at different dithiol concentrations are shown in Fig. 8 for DT6, DT8, and DT10 dithiols (DTX in general). In the absence of a dithiol linker, the extinction spectrum of the AgH colloid exhibits the usual profile consisting of a narrow Lorentzian curve with a resonance maximum at 406 nm, corresponding to the NPs observed in the TEM micrographs (Fig. 9a).

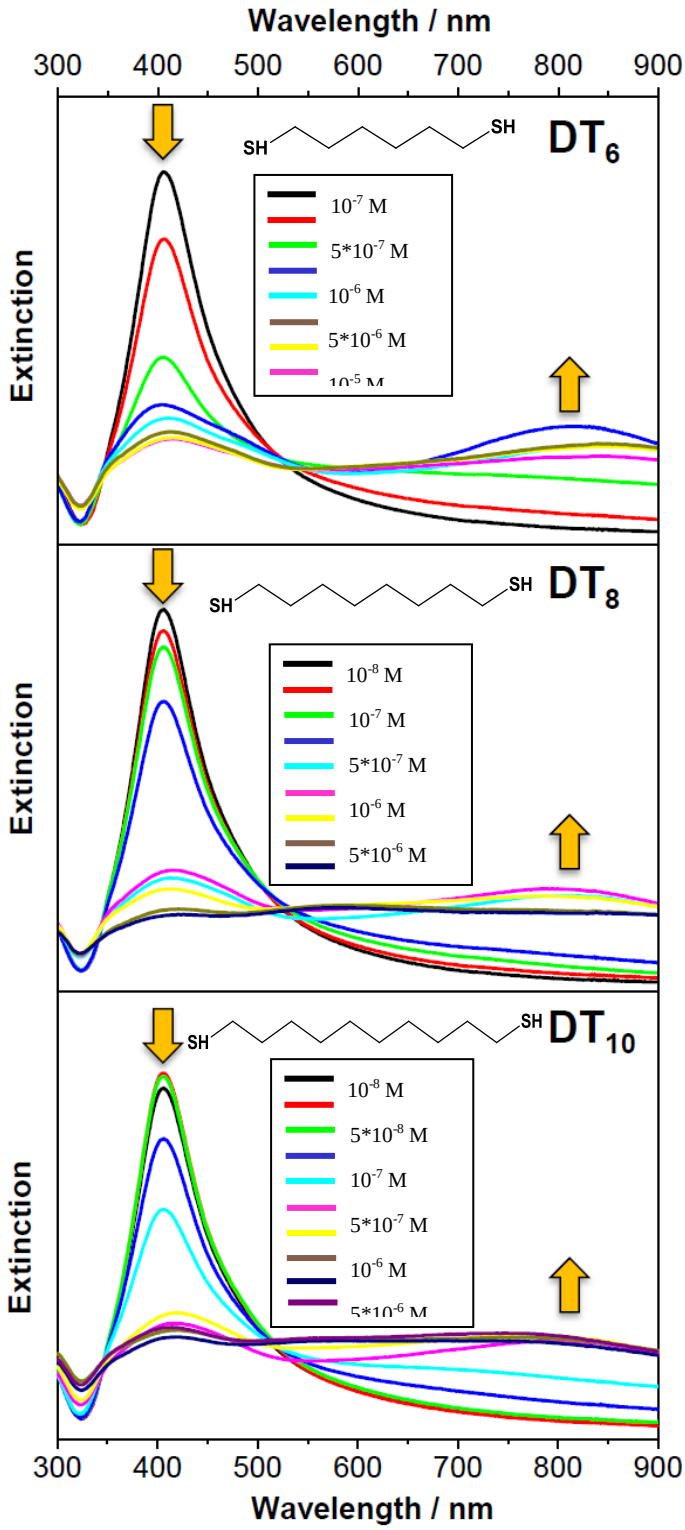

Fig. 8 – Plasmon extinction spectra of AgH colloid aggregated at different concentrations of DT6, DT8, and DT10.

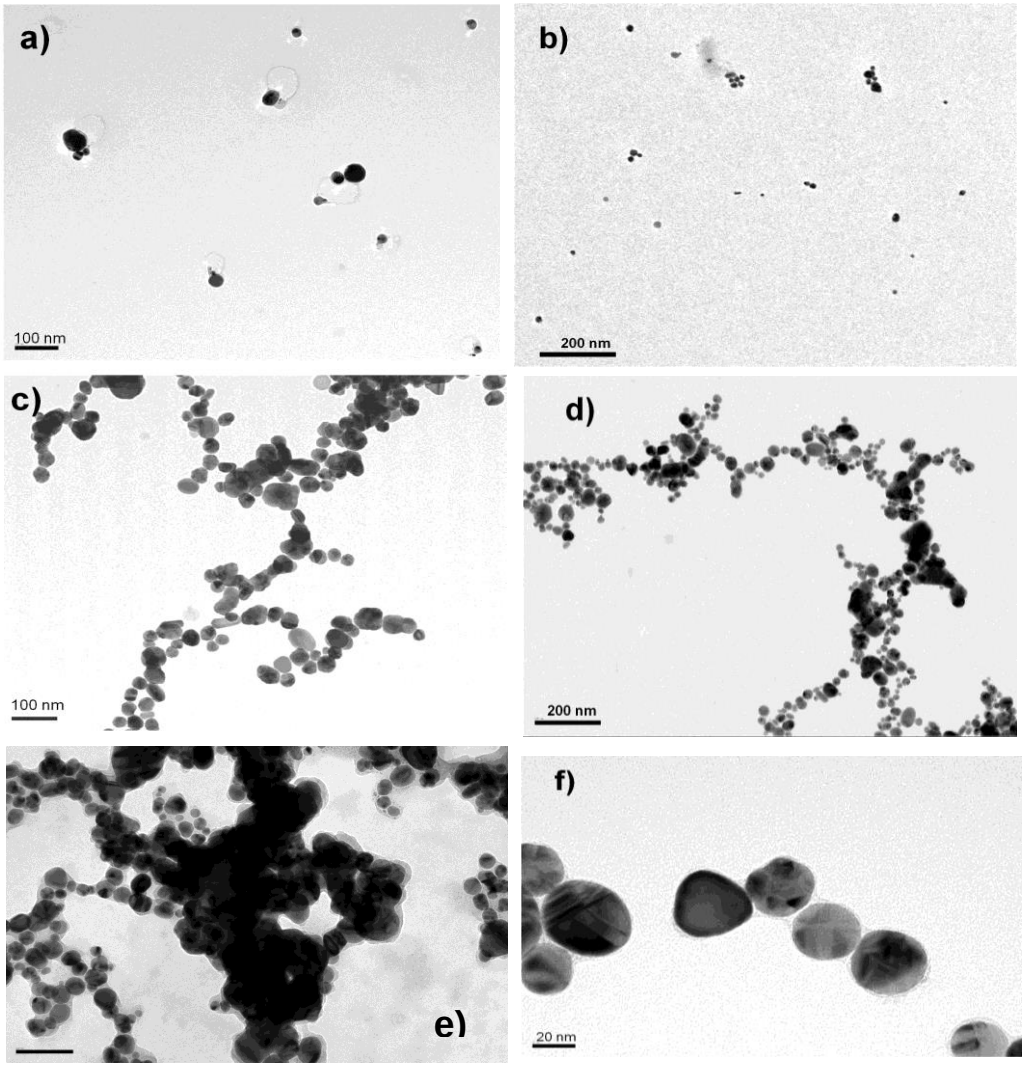

Fig. 9 – TEM images of the silver colloid aggregated by means of DT8, (a) NPs before aggregation and in the presence of the following DT8 concentrations: (b) $5x10^{-7}$ M, (c/d/e) 10^{-6} M, and (f) 10^{-5} M.

At very low dithiol concentrations (10^{-8} to 10^{-6} M), the nanoparticle assembly is weak as deduced from the slight variation occurring in the extinction spectra. This concentration range corresponds to the submonolayer adsorption regime because only at dithiol concentrationsof 10^{-6} to $5x10^{-6}$ M a complete covering of the surface of this kind of nanoparticles occurs [Izquierdo-Lorenzo, I. *et al.* 2012]. The main change observed in the extinction spectra of NPs at these low concentrations of dithiol is the weakening of the band at 406 nm and a slight increase of the extinction at higher wavelengths. To better display the changes occurring in this concentration interval, we

have obtained the difference spectra (as an example spectra of Ag colloid in the presence of DT8 are shown), using as reference the extinction spectrum in the absence of dithiol (Fig. 10). At a DT8 concentration 10^{-7} M, a positive weak band is observed at ca. 500 nm (Fig. 10b), which was also observed in the presence of DT10 and DT6. This band can be attributed to the formation of NPs dimers as this is in the range of the plasmon resonance observed for dimers of AgNPs by other authors [Li, W. Y. *et al.* 2009]. At a concentration of $5x10^{-7}$ M, the dimer band shifts to 506 nm, due to the increasing surface covering, and a new broad band appears at longer wavelengths centered at 633 nm (Fig. 10c). The latter band is attributed to the formation of trimers and small aggregates, also observed in TEM experiments (Fig. 9b).

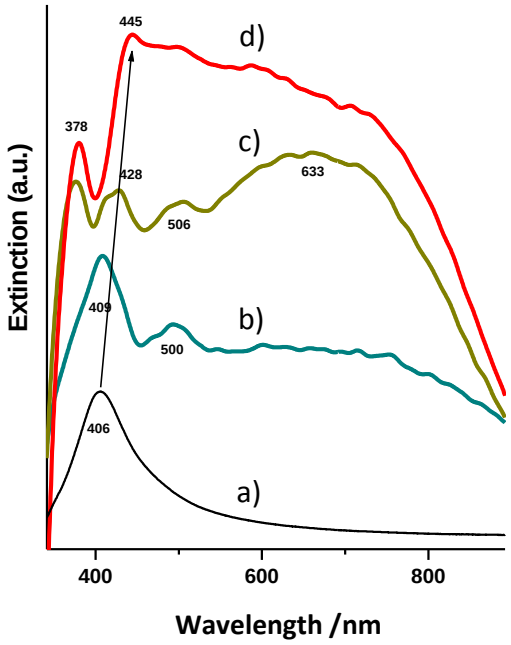

Fig. 10 – Aggregation of AgH colloid at low dithiol concentrations. (a) Extinction spectrum of unaggregated Ag colloid and difference extinction spectra of this colloid aggregated in the presence of DT8 at the following concentrations: (b) 10^{-7} M, (c) $5x10^{-7}$ M, and (d) 10^{-6} M.

Fig. 11 represents the general effect of AgNP aggregation by DTX on the plasmon resonance. In fact, this figure displays the main extinction maxima observed in the high wavelength region for the AgNP suspension upon addition of DTX at different concentrations. As can be seen, the minimum concentration to see dimers in

the difference spectra increases as the length of the linker shortens (Fig. 11a). The higher ability of longer dithiol linkers to start the NPs assembly is attributed to the lower electrical repulsion existing between the linked NPs due to the residual electric charge of these NPs. Under the latter situation, the linking is favored due to the lower electrical barrier that these NPs must overcome.

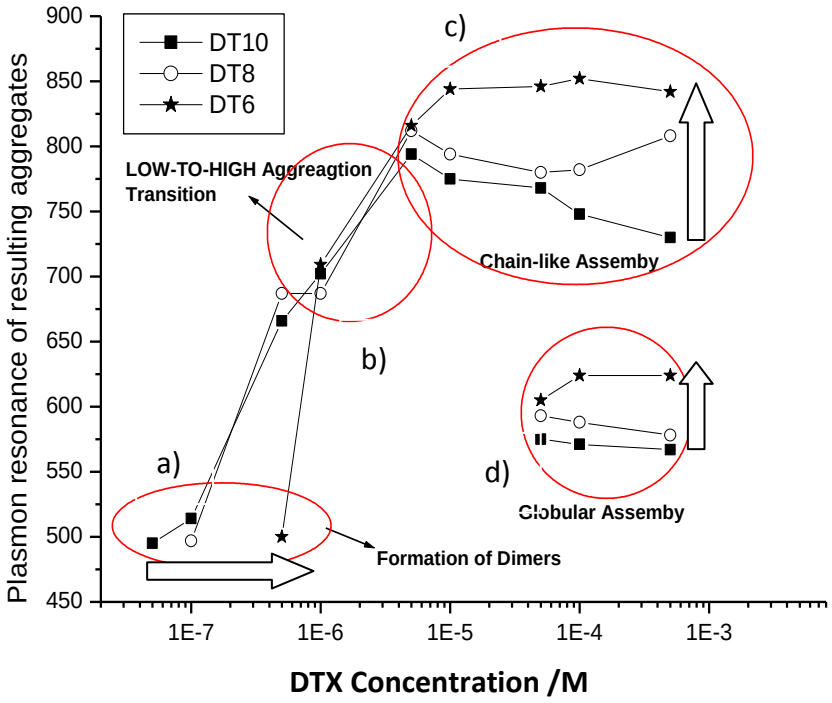

Fig. 11 – Main plasmon resonances measured upon aggregation of AgH colloid at different DTX concentrations. The formation of dimers is observed at concentrations below 10^{-6} (a). The 10^{-6} to $5x10^{-6}$ M interval represents the transition from low-to-high nanoparticle aggregation due to surface saturation (b). Above this threshold, a large aggregation is observed, first under chain-like structures (c), above a second threshold reached at a concentration of $5x10^{-5}$ M, globular structures with largely uncoupled nanoparticles render an additional maximum at lower wavelengths (d).

At concentrations above 10^{-6} M, large changes in the extinction spectra are observed due to the strong NP assembly induced by DTX. The main effect is the intensity decrease of the single particle band (at 410 nm) and the appearing of a second, wider band centered approximately at 800 nm for a concentration $5x10^{-6}$ M.

The threshold concentration to induce a large NPs aggregation is the same for all of the investigated dithiols and corresponds to the concentration at which a full surface coverage is reached, that is 10^{-6} to $5x10^{-6}$ M (Fig. 11b). This indicates that the aggregation is an effect of the surface coverage induced by the linking of DTX, which is practically the same for all of these dithiol linkers, provided that a perpendicular orientation occurs. Thus, the strong change observed in the aggregation of AgNP is attributed to the complete surface coverage expected at the above concentration range. Fig. 9c-e revealed that the aggregates formed upon linking with DTX at a concentration 10^{-6} M have a chain-like morphology. In all cases, the nanoparticles stay within a very close, but not touching, distance ranging between 1 and 2 nm (Fig. 9f). TEM micrographs also evidenced the existence of dithiol films surrounding the nanoparticles.

The position of the plasmon resonance of NPs chains undergoes a clear change upon variation of the DTX concentration. First, a shift to higher wavelengths is seen, due to the increasing DTX chain length, until a maximum value is reached. This value also depends on the linker length. A downward shift of this band is then observed (Fig. 11c-d). This shift of the plasmon resonance can be explained on the basis of the aggregation model already reported by Lin *et al.* [Lin, M.Y. *et al.* 1989]. Because the adsorption of dithiols on the Ag NPs is of a covalent nature, electrostatic repulsion between nanoparticles prevails below a dithiol concentration threshold, and the aggregation is reaction-limited colloid aggregation [Siiman, O. & Feilchenfeld, H. 1988], favored in the form of chain-like super-structures also seen in the TEM micrographs [Cho, E.C. *et al.* 2010]. Above a complete surface coverage by DTX, the dithiols self-assembly inside the hot spots induces a large decrease of the residual electric charge and favors a strong increase in the interparticle distance. At the latter conditions, a different assembly model takes place leading to a diffusion-limited colloid aggregation, which renders globular clusters having plasmon resonances toward shorter wavelengths. This causes the appearance of a new plasmon resonance band, which is blue-shifted in relation to the chains band. In fact, the plasmon resonance at 560−600 nm, observed when the concentration is raised (Fig. 12b), is related to the formation of globular aggregates as seen in TEM micrographs of Fig. 9e. These aggregates can be observed above a threshold concentration of $5x10^{-5}$ M. Moreover, the appearance of

globular aggregates is associated with the formation of multilayers due to an overadsorption of DTX on the metal surface, as deduced from the appearance of a dark shell around the NPs in the TEM images (Fig. 9e).

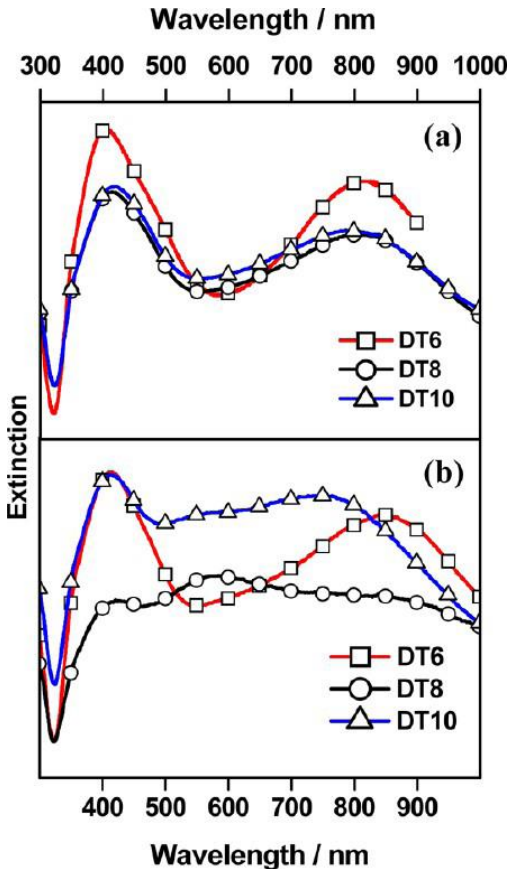

Fig. 12 – Aggregation of Ag colloid at high dithiol concentrations. Extinction spectra of Ag colloid aggregated with DT6, DT8, and DT10 at two concentrations below and above the second threshold ($5x10^{-5}$ M) described in Fig. 11: (a) $5x10^{-6}$ M (linear aggregates) and (b) $5x10^{-4}$ M (linear plus globular aggregates).

Fig. 12 shows in more detail the effect of aggregation on the extinction spectra of Ag NPs below and above the $5x10^{-5}$ M threshold concentration of DTX. The appearance of an intense extinction band at 565-575 nm at high DTX concentration ($5x10^{-4}$ M) is attributed to the formation of globular AgNP aggregates as those displayed in Fig. 9e. This kind of aggregation is more evident in the case of DT8 and DT10 (Fig. 12b), because the distance between NPs leads to a higher uncoupling. On the contrary, DT6 gives rise to a weaker band, which shifts to higher wavelengths

(610-630 nm), as corresponds to a higher interparticle coupling. The position of this peak is also correlated to the dithiol length, in such a way that the shorter is the linking chain, the higher is the extinction wavelength at which it appears (Fig. 11d).

The plasmon resonance values of the resulting chain-like and globular aggregates exhibit a dependence on the linker length in the order: DT6 > DT8 > DT10. This is due to the higher NPs coupling reached as the distance between nanoparticles decreases. As shown in Fig. 9f, the assembly of NPs in chains leads to the formation of a large amount of hot spots in interparticle gaps, whose dimensions can be modified by varying the linker length and concentration. In fact, as the linker concentration increases, so does the interparticle distance, which will be tunable between 1 and 5 nm, from submonolayer to multilayer regimes. As this distribution is extended throughout the colloid, the number of hot spots is expected to be considerable.

A comparison of the aggregating activity of dithiols (DTX) with diamine bifunctional alkenes (DAX), employed in previous esperiments (Guerrini, L. *et al.* 2009), is shown in Tab. 1. As can be seen, the minimum concentration of the linker needed to start the NP assembly is much lower in the case of aliphatic dithiols. This is attributed to the higher affinity of the SH group to the metal in relation to the amino one, which is linked through the formation of an ionic pair [Guerrini, L. *et al.* 2009]. It was also observed, for both diamines and dithiols, that the aggregating activity increases with the linker length. This is again due to the lower electrical repulsion barrier that longer alkene chains must overcome to link two different nanoparticles.

X (N° of C in the chain)	**[DAX]**mol/l	**[DTX]**mol/l
6	$3x10^{-5}$	$5x10^{-7}$
8	$2x10^{-5}$	$\sim10^{-7}$
10	10^{-5}	$\sim10^{-7}$
12	10^{-5}	

Tab. 1 – Comparison between the concentrations of DAX and DTX of different lengths needed to start the Ag NPs assembly in a AgHcolloid.

In conclusion of this part of the work it should be noted that the assembly of Ag NPs by bifunctional alkene chains of variable length allows building size-controlled interparticle spaces. The aggregating activity of aliphatic dithiols is higher than that of diamines and highly correlated to their interacting affinity. The linking activity of dithiols is so high that the dimers formed in the first stage of the assembly process are only detected for very low linker concentrations and in extinction difference spectra. At concentrations above the 10^{-6}-5×10^{-6} M interval, a large NPs aggregation is induced with formation of chain-like structures where Ag NPs are linked through the formation of interparticle gaps. At very high dithiol concentrations, the formation of multilayers leads to the formation of globular structures, where the interparticle gaps are longer.

Chain length and surface coverage are the two factors that will determine the interparticle distance. It can be deduced from the spectroscopic measurements that when the surface coverage by the adsorbed molecules is high, and so is their lateral packing, the linkers adopt straight conformations which will define a fixed interparticle distance depending only on the chain length. When surpassing the linker concentration that induces monolayer formation, dithiols will self-assemble in consecutive layers perpendicular to the surface leading to higher interparticle distances.

This study provided the basis for the applications of linked NPs by aliphatic dithiols in possible analytical applications, since alkene dithiols can act as both linkers of plasmonic nanoparticles and molecular assemblers of pollutants. The next step was to characterize the adsorption mechanism of aliphatic dithiols on silver and gold NPs. The information about the adsorption and coordibnation mechanism, the orientation, conformational order and packing of the aliphatic chains of DTX on metal NPS were obtaimed by means of analysing SERS spectra of DTX at different experimental conditions.

5.1.2 SERS spectra of dithiols: a structural study of the absorption

Fig. 13-15 show the SERS spectra of DT6, DT8 and DT10 obtained on AgH. SERS spectra of dithiols obtained on AgC are very similar to the spectra obtained using AgH colloid, but also display strong citrate features at DTX concentrations below 1 µM (not shown). In contrast, the SERS spectra registered on AuC display different profiles as shown in Fig. 16b and c. Intense SERS spectra were obtained until a very low concentration of dithiols (10^{-8} M), in spite of the low Raman cross section of these compounds. This high sensitivity indicates that dithiols are effectively forming hot spots where the EM field is highly enhanced and consequently the Raman signal of these molecules is substantially enhanced. The SERS enhancement factor for DT8 at a concentration of 10^{-8} M was determined to be $5x10^{6}$, demonstrating that this enhancement is actually strong and comparable to those typical for very active SERS molecules such as dyes and aromatic compounds.

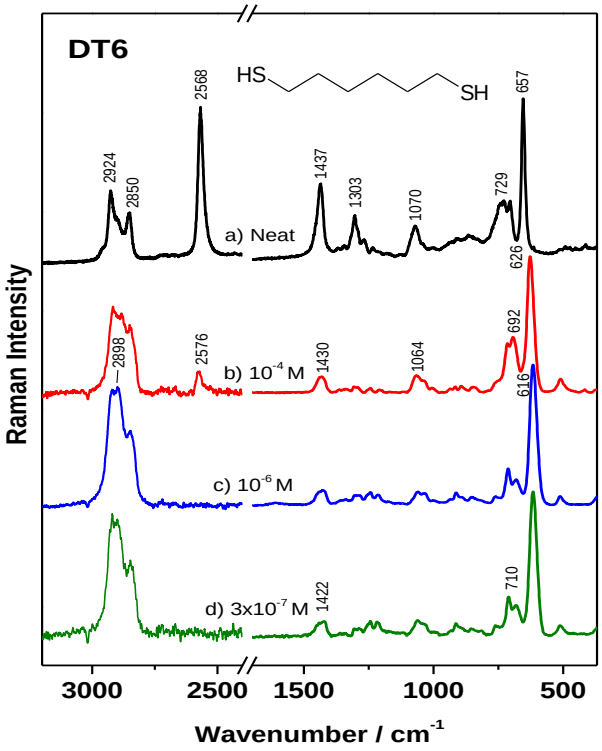

Fig. 13 – Raman spectrum of neat liquid DT6 (a) and SERS spectra of this dithiol on AgH at different concentrations: (b) 10^{-4}, (c) 10^{-6} and (d) $3x10^{-7}$ M. All spectra were obtained by using the 785 nm excitation line.

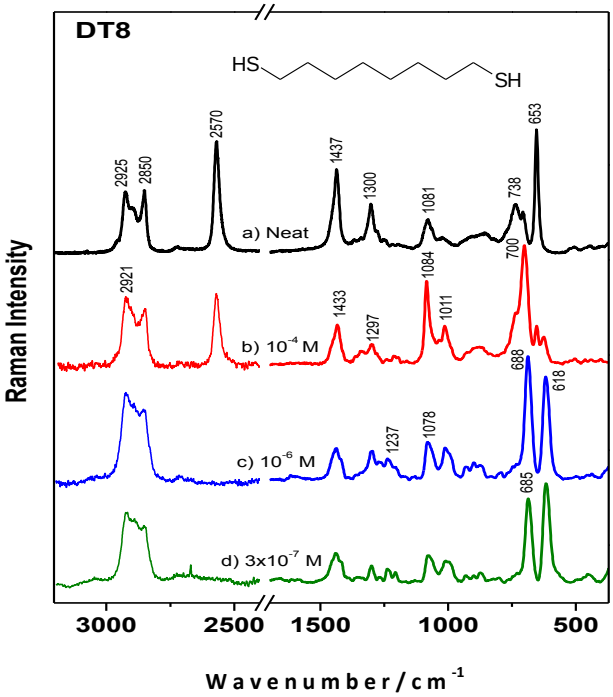

Fig. 14 – Raman spectrum of neat liquid DT8 (a) and SERS spectra of this dithiol on AgH at different concentrations: (b) 10^{-4}, (c) 10^{-6} and (d) $3x10^{-7}$ M. All spectra were obtained by using the 785 nm excitation line.

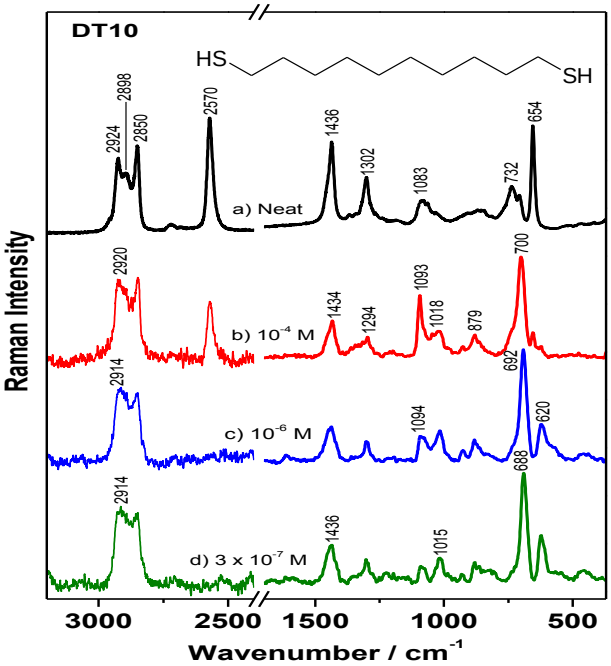

Fig. 15 – Raman spectrum of neat liquid DT10 (a) and SERS spectra of this dithiol on AgH at different concentrations: (b) 10^{-4}, (c) 10^{-6} and (d) $3x10^{-7}$ M. All spectra were obtained by using the 785 nm excitation line.

	Wavenumbers (cm^{-1}) of Raman spectra		Assignments[a]
Neat Liquid Sample	**SERS on AgC**	**SERS on AuC**	
2925*m*	2920*m*	2902*m*	ν_{as}(CH)/FR
2898*sh*	2889*sh*		ν_{as}(CH)
2850*m*	2856*m*	2845*m*	ν_{s}(CH)
2570*s*		2570*w*	ν(SH)
1437*s*	1437*m*	1436*s*	$\delta(CH_2)$
	1416*sh*		$\delta(CH_2)$
1300*m*	1297*m*	1297*s*	$\omega(CH_2)$
1247*vw*	1237*w*		$\tau(CH_2)$
	1200*sh*	1181*w*	$\tau(CH_2)$
	1078*m*	1081*s*	ν_{T}(CC)
1081*m*			ν_{G}(CC)
1022*w*	1009*m*	1008*w*	ν_{T}(CC)
	929*w*	906*sh*	$\rho(CH_2)$
	897*w*	875*w*	$\rho(CH_2)$
858*m*	868*w*		$\rho(CH_2)$
738*m*			ν_{T}(CS)
	688*vs*	703*w*	ν_{T}(CS)
705*sh*			ν_{T}(CS)
653*s*		640*m*	ν_{G}(CS)
	618*s*		ν_{G}(CS)
		280*vs*	ν(Au-S)
	220*vs*		ν(Ag-S)
		170*w*	ν(Au-S)

[a](ν): stretching, (δ): bending, (ω): wagging, (τ): twisting, (ρ): rocking, (vs): very strong, (s): strong, (m): medium, (w): weak, (sh): shoulder

Tab. 2 – Main experimental wavenumbers (cm^{-1}) and assignments of the bands observed in the Raman spectrum of neat liquid sample and the SERS spectra of DT8 adsorbed on AgC (10^{-6} M) and Au ($8x10^{-6}$ M) NPs. The assignments of the main bands are also presented.

The assignment of the vibrational bands of the adsorbed dithiols was made on the basis of the data found in the literature (Tab. 2) [Sandhyarani, N. & Pradeep, T. 1998; Anderson, D.J. & Moskovits, M. 2006]. SERS spectra reveal that dithiols interact strongly with plasmonic metals via the formation of a covalent bond through both S

atoms and the formation of alkanedithiolate species. This is deduced from the disappearance of the strong S–H stretching band at 2570 cm^{-1} seen in neat liquid dithiols (Fig. 13a, 14a and 15a). Alkane monothiols also show a similar behaviour when adsorbed on metals [Dubois, L.H. & Nuzzo, R.G. 1992]. SERS spectra provide an additional hint of this interaction from the appearance of the bands at 220 cm^{-1}, in the case of AgH (Fig. 16d), and at 280 and 170 cm^{-1} for AuC (Fig. 16c). These bands can be assigned to stretching vibrations of the Ag–S and Au–S bonds formed upon dithiol adsorption on the metal surface [Kato, H.S. *et al.* 2002; Cho, S.I. *et al.* 1999; Kluth, G.J. *et al.* 1999]. The presence of two Au–S bands indicates that the thiol groups are interacting with the metal surface through two different coordination mechanisms. Miao *et al.* reported the existence of three adsorption sites on Au: top, bridge and hollow [Miao, L. & Seminario, J. M. 2007]. Therefore, we suggest that the appearance of these two Au–S bands is due to the existence of two coordination mechanisms of the adsorbed molecules on the gold surface as also reported by Kato *et al.* [Kato, H.S. *et al.* 2002]. In fact, the relative intensity of the higher wavenumber component rises upon increasing the concentration of dithiols, due to the increasing importance of the on-top coordination mechanism under high coverage conditions. The presence of only one Ag–S band at 220 cm^{-1} may indicate that the coordination of sulfur atom with Ag occurs through only one coordination mechanism.

The complete disappearance of the band corresponding to the SH bond indicates that both SH groups interact with the metal and consequently the SERS signal corresponds mainly to dithiol molecules linked to NPs and placed in nanogaps. This is expected to be valid predominantly at low surface coverage. Molecules localized out of these gaps could also contribute to the SERS spectra undergoing a much lower intensification as deduced from the absence of free SH bands. Nevertheless, this effect could be also related to the possible lying-down (LD) orientation of dithiols on the metal surface [Carro, P. *et al.* 2010] as shown in Fig. 17A.

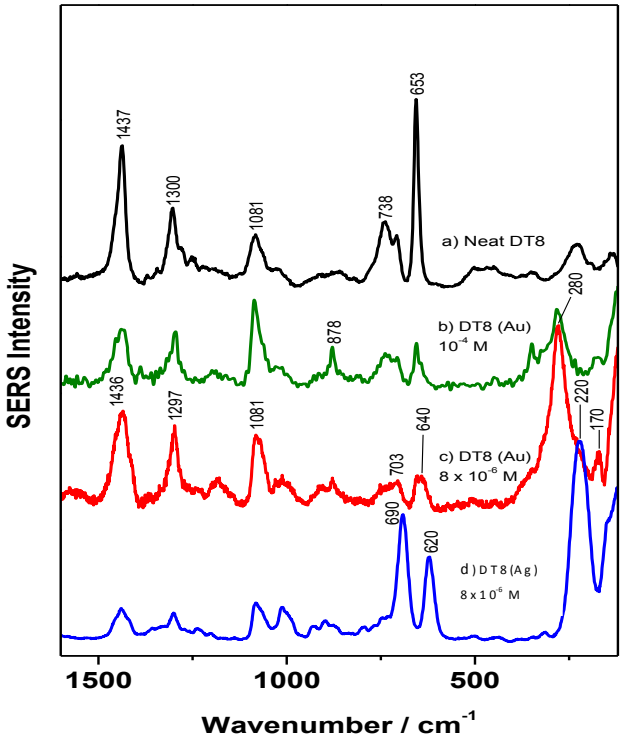

Fig. 16 – SERS of DT8 on AuC and AgH: (a) Raman spectrum of neat liquid DT8, (b) SERS spectrum of DT8 ($8x10^{-6}$ M) on AuC, (c) SERS spectrum of DT8 (10^{-4} M) on AuC, and (d) SERS spectrum of DT8 ($8x10^{-6}$ M) on AgH. All spectra were obtained by using the 785 nm excitation line.

5.1.2.1 SERS of dithiols on AgNPs

In the liquid state of DTX, a strong ν_G(C–S) band appearing at 660-650 cm^{-1} in the Raman spectra indicates a high molecular disorder of DTX molecules (Fig. 13a, 14a and 15a). When dithiols are adsorbed onto the metal surface, two SERS bands appear at approximately 700 and 630 cm^{-1}, corresponding to the ν_T(C–S) (T = trans) and ν_G(C–S) (G = gauche) bands, respectively [Joo, T.H. *et al.* 1987; Izquierdo-Lorenzo, I. *et al.* 2013]. Comparing the Raman spectra of neat liquid dithiols with the SERS ones (Fig. 13-15), a relative intensification of the ν(C–S) bands is observed in comparison with the bands corresponding to the ν(CH) and δ(CH_2) vibrations of the aliphatic central moiety. This effect is more evident for DT6 (Fig. 13), where less CH_2 groups are present in the aliphatic chain. Additionally, the degree of structural order in the aliphatic chain or crystallinity of dithiol molecules [Bryant, M.A. & Pemberton, J.E. 1991; Izquierdo-Lorenzo, I. *et al.* 2013] can be followed by analyzing the ratio $R_{CS} = I_{CST}/I_{CSG}$ of ν(C–S)

bands. Fig. 18A shows the R_{CS} values determined when varying the chain length and the surface coverage related to the different molecular self-assembly. While DT6 exhibits a highly disordered structure on the surface at all the studied concentrations, DT10 shows a more ordered structure in comparison to the liquid sample. It is worth noting that the DT10 displays a remarkable increase of the R_{CS} value at concentrations above $8x10^{-6}$ M. Finally, DT8 displays an intermediate behavior with a significant increase of R_{CS} at concentrations above 10^{-5} M, but with R_{CS} values closer to DT6 at very low concentrations ($<10^{-7}$ M). These data indicate that the conformational order of the methylene groups close to the CS group in DTX increases at high surface coverage due to a tighter molecular packing.

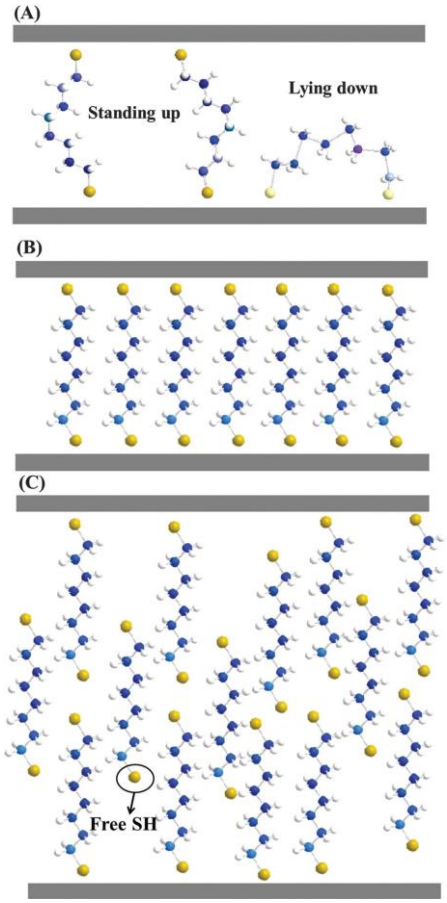

Fig. 17 – Different adsorption configurations deduced for DTX (specifically DT8) in nanogaps between two NPs at low surface coverage (A), where two possible adsorption patterns are possible (standing-up and lying-down); under the conditions of self-assembled monolayer (SAM) (B), and at high metal surface coverage giving rise to the formation of multilayers (C), where free SH groups appear. The last configuration appears above a threshold concentration of 1 μM.

To monitor the influence of the linker concentration on the interparticle distance, we have measured the distance between nanoparticles from the TEM images. The resulting measured distances are plotted in Fig. 19 for the specific case of DT8 at three different concentrations. As can be seen, interparticle distances below 1 nm tend to disappear when increasing dithiol concentration, in concordance with a lower G/T conformation ratio at increasing coverage. Moreover, distances over 3 nm are markedly increased at a concentration 10^{-4} M, corresponding to a multilayered adsorption scheme (Fig. 17C). In general, all concentrations show maxima between 1 and 2 nm, which correspond to the end-to-end distance of DT8.

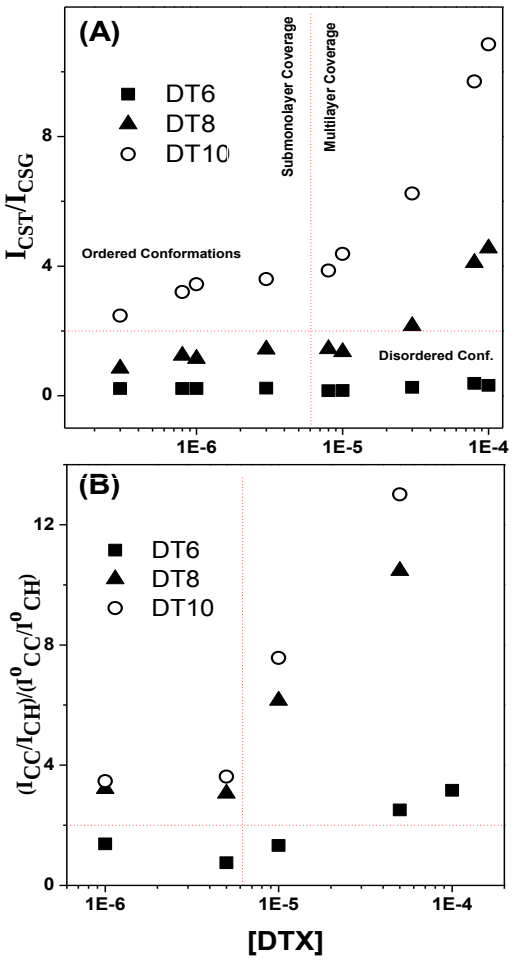

Fig.18 – Plot of the $R_{CS} = I_{CST}/I_{CSG}$ (A) and $R = (I_{CC}/I_{CH})/(I^0_{CC}/I^0_{CH})$ (B) ratios as a function of the dithiol concentration.

The adsorption of dithiols on the metal surface also induces a strong downshift of ν(C–S) wavenumber in relation to the position of the same band in neat liquid samples. This effect was also observed by Bryant *et al.* in the case of monothiols, and was attributed to the strong withdrawal of electrons from the C–S bond in the interaction with the metal [Bryant, M.A. & Pemberton, J.E. 1991]. The extent of the downshift depends on the surface coverage and the nature of the metal, being more pronounced at low coverage and when dithiols are adsorbed on Ag. It was reported that the extent of this shift increases with the number of metal atoms involved in the bond [Cho, S.I. *et al.* 1999], due to the fact that the coordination via hollow sites involves a higher π contribution, which is in turn antibonding with respect to the S–C bond [Sellers, H. *et al.* 1993]. Thus, the large downshift observed for dithiols adsorbed on Ag NPs suggests that the coordination of the thiolate group to the Ag surface takes place through hollow sites, and that coordination is related to the appearance of the ν(Ag–S) band at 220 cm^{-1}. This coordination was also proposed by Cho *et al.* for the adsorption of thiols on Ag electrodes [Cho, S.I. *et al.* 1999].

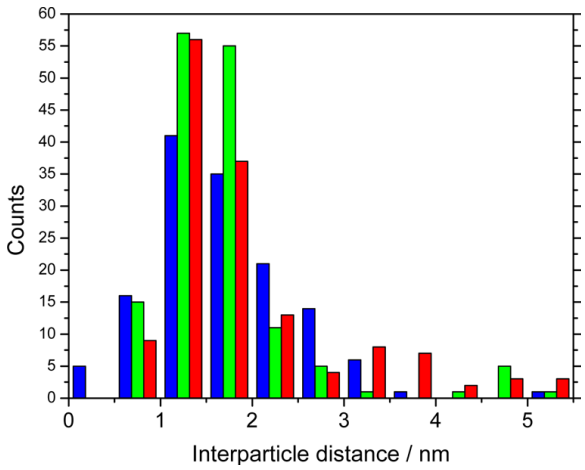

Fig. 19 – Interparticle distance distribution of AgNP in the presence of various concentrations of DT8, as measured by TEM. Blue bars, 10^{-6} M; green, 10^{-5} M; red, 10^{-4} M. The total number of analyzed distances was 140–150 for each concentration.

As the concentration of DTX is increased, the probability of interaction of these molecules with one or two metal atoms (on-top and bridge coordination) increases,

and this accounts for the lower red shift of the ν(C–S) frequency at higher coverage. Furthermore, another factor that can influence the position of the C–S stretching is the strong withdrawing capacity of residual chloride ions, coming from the preparation process of AgH, that are still adsorbed onto the metal surface at low dithiol concentrations, as revealed by the presence of an intense band at 235 cm^{-1} attributed to ν(Ag–Cl) (result not shown).

The conformational changes occurring on varying the surface coverage are also manifested in the C–H stretching region. In liquid dithiols two main bands in this region appear at ca. 2925 and 2850 cm^{-1} (Fig. 13a, 14a and 15a). The first one can be attributed to an overtone of CH_2 bending in Fermi resonance with $\nu_{as}(CH_2)$ vibration, while the latter band is attributed to $\nu_s(CH_2)$ [Abbate, S. *et al.* 1982]. In addition, a shoulder can be seen at 2898 cm^{-1} and this is assigned to the $\nu_{as}(CH_2)$ vibration. This spectral profile is typical for melted polymethylene chains, where the chain adopts a highly disordered structure [Abbate, S. *et al.* 1984]. The ratio R_{CH} (I_{2930}/ I_{2850}) is connected to the content of G conformers relative to the T ones in polymethylene chains [Abbate, S. *et al.* 1982]. In dithiols, the absence of terminal CH_3 groups facilitates the study of the order based on the R_{CH} ratio as no overlapping from the $\nu_s(CH_3)$ vibration is expected in this case in contrast to what happens in monothiols [Snyder, R.G. *et al.* 1982; Snyder, R.G. 1982]. In neat liquids, R_{CH} decreases from DT6 to DT10 indicating an increase of the chain order. In this context, the intensity increase of the band at 2898 cm^{-1} in dithiols of longer chain has been attributed to an increase of the lateral packing according to Wong *et al.* [Wong, P.T.T. & Mantsch, H.H. 1985].

The adsorption of DTX on Ag surface leads to important changes in the C–H stretching region as compared to neat liquid samples. On the one hand, an intensity decrease of the νC–H bands in relation to the νCC/νCS bands is observed, thus suggesting a dominant perpendicular orientation of the main molecular axis of dithiols on the surface. On the other hand, an increase of the molecular packing upon adsorption can be deduced from the relative enhancement of the $\nu_{as}(CH_2)$ band at 2898 cm^{-1}, mainy seen in DT6 (Fig. 13), and as also reported previously by other authors [Wong, P.T.T. & Mantsch, H.H. 1985; Snyder, R.G. *et al.* 1978; Gaber, B.P. *et al.* 1978]. The intensification of the 2898 cm^{-1} band avoids a proper analysis of the R_{CH}

ratio due to its overlapping with the other two CH bands. However, the high intermolecular interaction derived from the tight molecular packing seems to induce an increase of the conformational order and the molecular packing of aliphatic chains, as deduced from the downward shift of the 2925 cm^{-1} band, suggesting an increase of T conformers in the chain [Abbate, S. *et al.* 1984; Bunow, M.R. & Levin, I.W. 1977]. This deduction suggests a well organised self-assembled monolayer (SAM) of dithiols on the surface, involving a more ordered structure [Hamoudi, H. *et al.* 2008]. The 2850 cm^{-1} band is enhanced when the surface coverage is high and as the length of the polymethylene is increased, indicating that the conformational order also increases under the latter conditions due to the existence of better conditions for the establishment of a well organized SAM as depicted in Fig. 17B.

The analysis of the C–C stretching region (1150-1000 cm^{-1}) also reveals important information concerning the conformational order of the aliphatic chain in dithiols. As in the case of the C–S stretching, the bands corresponding to both T and G conformers can be found in the Raman spectra (ν_T(C–C) and ν_G(C–C)). The Raman spectra of liquid DTX display a medium intensity band at 1085-1070 cm^{-1} which can be attributed to ν_G(C–C) [Bryant, M.A. & Pemberton, J.E. 1991]. The adsorption of dithiols on Ag leads to changes in this region depending on the aliphatic chain length and the concentration. The SERS spectral profile of DT6 does not change significantly in comparison to the Raman spectrum of this dithiol in the neat sample (Fig. 13). This suggests the formation of a rather disordered layer of DT6 on the Ag surface, which is in agreement with the analysis of the ν(C–S) bands. In the case of DT8, the intensification of two narrow ν(C–C) bands at 1084 and 1011 cm^{-1} is observed at high concentration (above $5x10^{-5}$ M, Fig. 14b), which is related to the increase of the chain conformational order. These two bands may correspond to the ν_T(C–C) bands appearing at 1113/1090 and 1050 cm^{-1} in octadecanethiol adsorbed onto Ag [Anderson, D.J. & Moskovits, M. 2006; Bryant, M.A. & Pemberton, J.E. 1991]. The fact that these two bands are shifted toward lower wavenumber values is probably due to the simultaneous linking of the dithiol with two Ag surfaces, which may induce a change in the vibration frequency of C–C bonds placed between two Ag nanoparticles.

The orientation of the main molecular axis of DTX related to the metal surface can be estimated from SERS spectra by considering the SERS propensity selection rules, which predict a higher intensification of vibrational modes perpendicular to the surface [Moskovits, M. 1982; Creighton, J.A. 1988]. The stretching vibrations of DTX can be used to carry out the orientation study because they imply variations of the tensor component along the axis of a vibration. In addition, ν(C–S) and ν(C–C) modes are orthogonal to the ν(C–H) ones, and will be differently enhanced when the molecule is adsorbed on a surface in comparison to the relative intensities of Raman bands of neat liquid samples [Bryant, M.A. & Pemberton, J.E. 1991]. Thus, the ν(C–S)/ν(C–H) or ν(C–C)/ν(C–H) ratios (I_{CS}/I_{CH} and I_{CC}/I_{CH}), where I_{CS}, I_{CH} and I_{CC} represent the integrated intensity of all the bands of the same type, can be used to estimate the orientation of the main axis of dithiols on the surface [Bryant, M.A. & Pemberton, J.E. 1991]. We have used the (I_{CC}/I_{CH}) ratio to monitor the molecular orientation of dithiols, by normalizing this parameter to the same ratio of the neat liquid sample (I^0_{CC}/I^0_{CH}). This ratio represents in a better way the orientation of the molecular chain in contrast to the I_{CS}/I_{CH} one, which is rather related to the CS environment. To accomplish this procedure we have employed the spectra recorded with an excitation line at 532 nm, since a higher signal-to-noise ratio was obtained in the CH stretching region at this excitation. Fig. 18B shows the plot of the $[(I_{CC}/I_{CH})/(I^0_{CC}/I^0_{CH})]$ ratio (R) calculated from SERS and Raman spectra of DTX at different concentrations. As can be seen, R increases significantly at concentrations above a threshold concentration of $5x10^{-6}$ M reaching a value of 13 and 10,5 in the case of DT10 and DT8, respectively, meaning that the orientation of DTX on Ag surface is predominantly perpendicular at concentrations above this threshold value. This finding indicates that these dithiols adopt a standing-up orientation above the threshold concentration. The decrease of this ratio at lower concentrations is rather attributable to a lowering of the conformational order of the aliphatic chain which can eventually give rise to lying-down structures. From the values of R obtained at high surface coverage (above 10^{-5} M), a predominant perpendicular orientation of the aliphatic chain is deduced in contrast to the results obtained for monothiols [Dubois, L.H. & Nuzzo, R.G. 1992]. The differences found between dithiols and monothiols can be attributed to the existence

of two terminal thiol groups in DTX molecules, which are responsible for the behaviour regarding the tilt angle and the interchain packing.

In the case of DT6 a less perpendicular orientation was deduced, but this is again associated to a lower conformational order in the aliphatic chain of DT6. This lower order also induces an enhancement of the bands attributed to the twisting vibrational modes of CH_2 appearing in the 1250-1150 cm^{-1} region. However, in the case of DT8 the enhancement of twisting bands and the ν_G(C–S) band is mainly observed at submonolayer concentration (<10^{-7} M), thus suggesting that a lying-down orientation is possible at low surface coverage (Fig. 17A). This orientation is also highly probable in DT6, even at concentrations above the SAM conditions, as the structural order is very low for this dithiol at all the investigated concentrations.

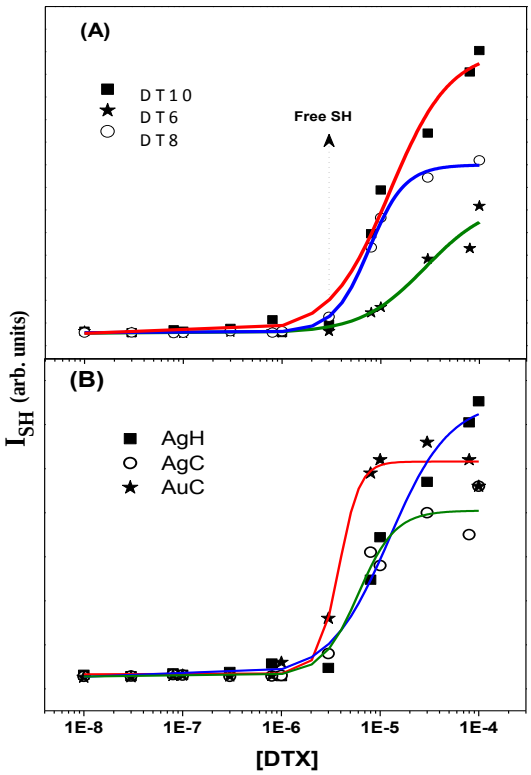

Fig. 20 – (A) Intensity of the free SH band (I_{SH}) determined from the SERS spectra of DT6, DT8 and DT10 on AgH colloid at different concentrations and normalized to the νCH band of the corresponding dithiol. (B) Intensity of the free ν(SH) band corresponding to DT8 at different concentrations and using different SERS substrates.

At a high surface coverage, a band corresponding to the vibration of free S–H groups appears at ca. 2570 cm^{-1} (Fig. 13b, 14b and 15b). The appearance of this band suggests that DTX molecules start to self-assemble inside nanogaps, forming multilayered structures where the free S–H groups may be present (Fig. 17C). Fig. 20A displays the relative intensity of the ν(S–H) band (I_{SH}) (normalized to the ν(CH) band) *vs*. the dithiol concentration for the three studied dithiol molecules on AgH NPs. The intensity of the ν(S–H) band increases substantially at concentrations above 1 μM, due to the saturation of the metal surface inside interparticle spaces and the formation of multilayers. The SERS intensity of the free ν(S–H) band measured at a fixed dithiol concentration is higher as the alkylic chain of DTX is longer. This observation is attributed to the stronger intermolecular interaction existing in the longer chains, i.e. DT8 and DT10, that are more suitable to form multi-layered structures adsorbed onto Ag. The appearance of the free S–H band is also associated to the presence of ν(C–S) bands corresponding to free C–SH groups, observed at the same wavenumber values as in the liquid dithiol.

The ν(S–H) band in SERS spectra of dithiols was used to study the adsorption of these adsorbates onto different metallic platforms. The concentration dependence of the intensity of the ν(S–H) band of DT8 adsorbed on the different substrates employed in this work, AgH, AgC, and AuC, is shown in Fig. 20B. In all cases an increase of the intensity of this band is observed above a concentration 1 μM, but the growth is steeper in the case of Au in relation to Ag nanoparticles. This fact can be explained by two different effects: (i) the lower available surface existing in Au NPs as compared to that of Ag NPs [Izquierdo-Lorenzo, I. *et al.* 2012], while AgH and AgC show a similar available adsorption surface, and (ii) the different adsorption and coordination mechanism of dithiols on Au in comparison with Ag nanoparticles.

5.1.2.2 SERS of dithiols on Au colloid

SERS spectra of DTX on AuC were also recorded at different concentrations. As an example we show the SERS spectra of DT8 registered at two concentrations: $8x10^{-6}$ M and 10^{-4} M (Fig. 16b, c). The lower downshift undergone by the ν(C–S) bands on this metal in comparison to Ag NPs suggests a weaker interaction of DTX with Au

surface. Shifts from 737 to 703 cm^{-1} and from 655 to 640 cm^{-1} for ν_T(C–S) and ν_G(C–S), respectively, were observed in the SERS spectra on Au NPs. The weaker interaction is also related to the appearance of the ν(Au–S) band at 280 cm^{-1}, which is attributed to the on-top coordination of S atoms on Au surface, provided that this coordination mechanism is energetically less favourable than the three-fold hollow or two-fold bridge coordinations [Olmos-Asar, J.A. *et al.* 2011]. This kind of coordination was reported to occur in the adsorption of aliphatic thiols on Au [Cho, S.I. *et al.* 1999]. On the other hand, the weak band at 220 cm^{-1} is attributed to the ν(Au–S) of dithiol linked to bridge or hollow sites.

The SERS of DT8 on AuC at low concentrations (Fig. 16b) resembles the Raman spectrum of this dithiol in the liquid state (Fig. 16a), except for the ν(C–S) bands, which are weaker, and the bands at 1300 cm^{-1} (attributed to ω(CH_2)) and those appearing in the 910-875 cm^{-1} region attributed to ρ(CH_2), which are relatively strong in the SERS spectrum. At concentrations higher than 1 μM, which represents the concentration needed for the saturation of the metal surface covered by dithiols, the bands corresponding to free SH groups are stronger than in Ag colloids. The appearance ofthe free SH band is also accompanied by an intensity increase of ν_T(C–S) and ν_G(C–S) bands of free CSH groups at 737 and 655 cm^{-1}, respectively, at 10^{-4} M concentration.

The high similarity between the SERS spectrum of dithiols adsorbed on Au and the Raman spectrum of the neat liquid sample points out the existence of a more disordered structure of DTX on Au than on Ag NPs. Indeed, this conclusion is also supported by the appearance of a strong band at 1081 cm^{-1} corresponding to ν_G(C–C) [Bryant, M.A. & Pemberton, J.E. 1991].

Regarding the orientation of dithiols on AuC, the lower intensity of ν(C–S) bands in relation to the SERS spectrum of DT8 on Ag at the same concentration (Fig. 16d) suggests a less perpendicular orientation of the C–S bond with respect to the Au surface than in the case of Ag. A similar result was reported by Bryant *et al.* [Bryant, M.A. & Pemberton, J.E. 1991] for monothiols. This orientation seems to be related to the coordination of DTX through on-top sites, since this mechanism implies a more tilted orientation associated to the sp^3 hybridization of the S atom [Sellers, H. *et al.* 1993].

As in the case of Ag NPs, the intensification of the bands corresponding to ν(C–C) and ν(C–S) vibrations with increasing dithiol concentration indicates that the aliphatic chains re-orientate towards a more perpendicular orientation.

In this part of thesis we have shown that SERS spectroscopy is a very useful tool in the study of the adsorption of dithiols on plasmonic NPs. The analysis of the vibrations of metal-DTX bond at low wavenumber values demonstrate that the coordination of dithiols is essentially different on the studied metals, being the bond with Ag more stable due to the formation of a bridged bond in contrast to Au where an on-top bond seems to be formed.

The conformation and molecular packing of adsorbed dithiols is highly determined by the surface coverage on plasmonic nanoparticles. The spectral changes are not continuous and there is a threshold concentration at which drastic variations in the adsorption and the structure are observed. This critical dithiol concentration is ca. 1 μM. The structural markers deduced from the SERS spectra (SH, CC, CS and CH stretching band) suggest that there are three main pictures that emerge from the analysis of the adsorption of these molecules. At concentrations below this threshold both thiol groups are attached to the metal surface forming nanogaps where the SERS intensificaction should be very high. At concentrations in the range of the critical value (1-5 μM) the full surface coverage lead to the formation of a dithiol SAM characterized by a significant increase of the order in the particular case of DT10 and DT8 dithiols. Above the latter concentrations dithiols are organized in multi-layered structure giving rise to a nanoparticle separation which is detected in the plasmon spectra. The study of the order/disorder indicates that the adsorbed DT6 bears a very disordered structure for all the studied concentrations, whereas DT10 is highly ordered due to the longer aliphatic chain, which favors the formation of intermolecular interactions for all the studied concentrations. DT8 undergoes an intermediate behavior showing a transition from a disordered structure at concentrations below 1 μM to an ordered one at above this threshold concentration. However, the adsorption of dithiols on Au leads to a more disordered structure in relation to Ag.

The orientation of the aliphatic chains is almost perpendicular at high concentrations, in contrast to the results obtained from monothiols. This difference is attributed to the bifunctional character of dithiols, which behaviour differs from that

of monothiols regarding the tilt angle and the interchain packing. The orientation on Au is not perpendicular as demonstrated the low intensity of CS stretching vibrations. These findings together with the different coordination deduced for dithiols on Ag and Au surfaces demonstrate that a significant difference exists between these plasmonic metals in the interaction with thiols. This effect must indeed be considered in functionalization processes where these molecules are employed.

5.2 Adsorption of aromatic dithiols on plasmonic nanoparticles

5.2.1 UV-VIS study of NPs aggregation and polymerization of aromatic dithiols

The adsorption of aromatic dithiols, 1,4-benzendithiol (BDT) and biphenyl-4,4-dithiol (BPDT) on plasmonic metal NPs was investigated by UV-visible absorption spectroscopy.

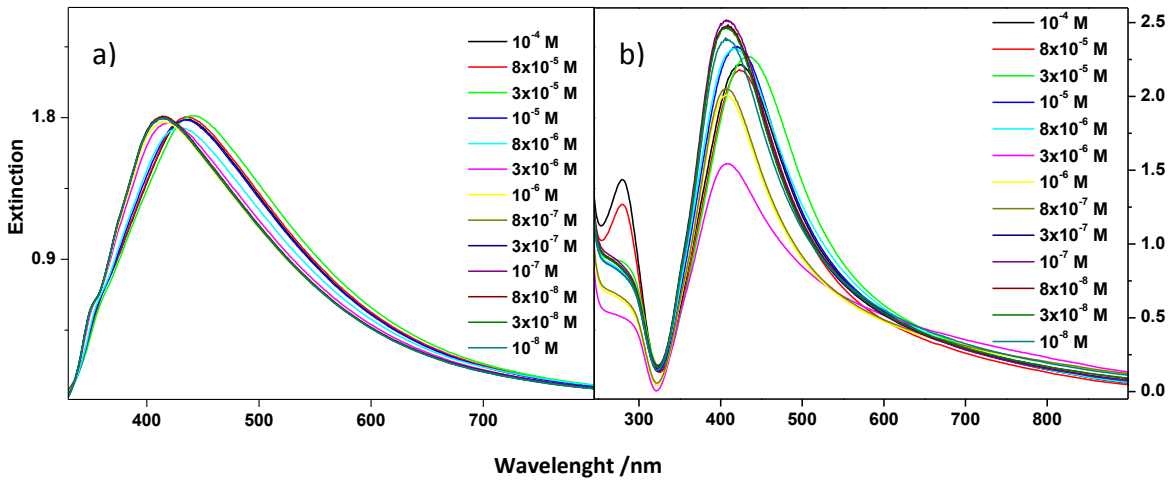

Fig. 21 – Plasmon extinction spectra of (a) AgC and (b) AgH colloid in the presence of BDT at different concentrations (10^{-4} – 10^{-8} M).

Fig. 21a shows the plasmon extinction spectra of AgC colloid in the presence of BDT at various concentrations (10^{-4} – 10^{-8} M). BDT induces a red-shift of the extinction maxima of AgC, which is clearly evident mainly at concentrations in the range 10^{-6} – 10^{-5} M. For these concentrations, plasmon resonance band red-shifts of 15-20 nm are observed. The extinction spectra of AgC do not contain the bands corresponding to the association of NPs into dimers or higher aggregates [Li, W.Y. *et al.*

2009], thus indicating that the adsorption of BDT does not induce any aggregation or NPs linking to form dimers of linear aggregates as in the case of the aliphatic dithiols. In addition, the large red-shift in the extinction peaks observed above $8x10^{-6}$ M concentration can be attributed to the adsorption of a broad layer of BDT molecules on individual Ag NPs monomers. This large layer inhibits the aggregation of NPs because prevents their approach.

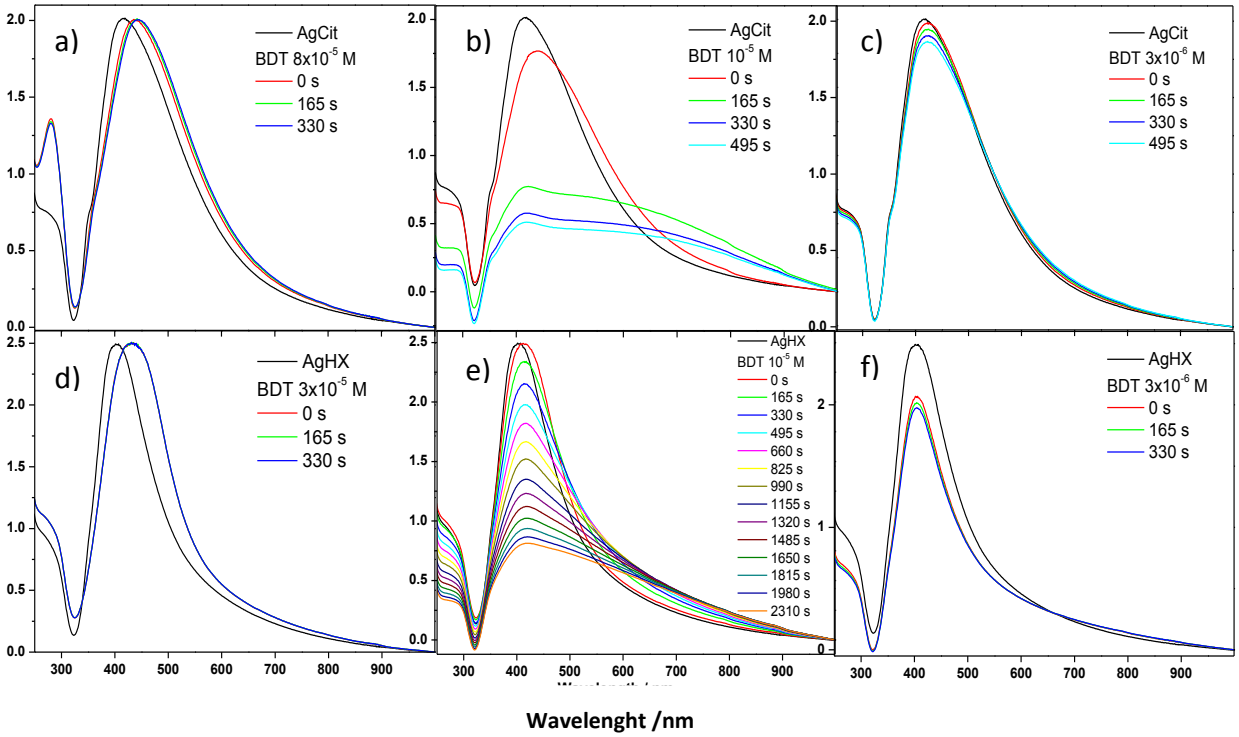

Fig. 22 – Effect of time on the extinction spectra of AgC and AgH colloids in the presence of different concentrations of BDT: (a) $8x10^{-5}$ M, (b) 10^{-5} M and (c) $3x10^{-6}$ M, and in AgH (d) $3x10^{-5}$ M, (e) 10^{-5} M and (f) $3x10^{-6}$ M.

The effect of the time on the extinction spectra of AgC and AgH in the presence of BDT is shown in Fig. 22. At low ($3x10^{-6}$ M) and at high concentrations ($8x10^{-5}$ M), the colloidal suspension shows a high stability, since a negligible aggregation is seen in the extinction spectra (Fig. 22a and 22c). On the contrary, at the intermediate concentration of 10^{-5} M, a substantial aggregation is observed with the rising time (Fig. 22b). At low concentrations, there is a low amount of adsorbed dithiol molecules on NPs, thus only a slight change is observed in the plasmon spectrum of these NPs. What

is quite unexpected is the behavior of the studied system at relatively high concentrations. Under this condition, the adsorption of a large amount of BDT molecule on NPs should induce a large aggregation. However, a large adsorption of BDT on NPs leads probably to a polymerization of this molecule on metal surface.

The large aggregation of NPs observed at 10^{-5} M concentration of BDT is evident from the time evolution of the band at 420 nm, corresponding to the band of the unaggregated NPs (Fig. 22b). The main observed effect is the intensity decrease of this band and the appearance of a very wide band in the 600-700 nm region due to the formation of aggregates, supposedly dimers [Li, W.Y. *et al.* 2009]. The latter broad band appearing at longer wavelengths indicates the formation of small aggregates.

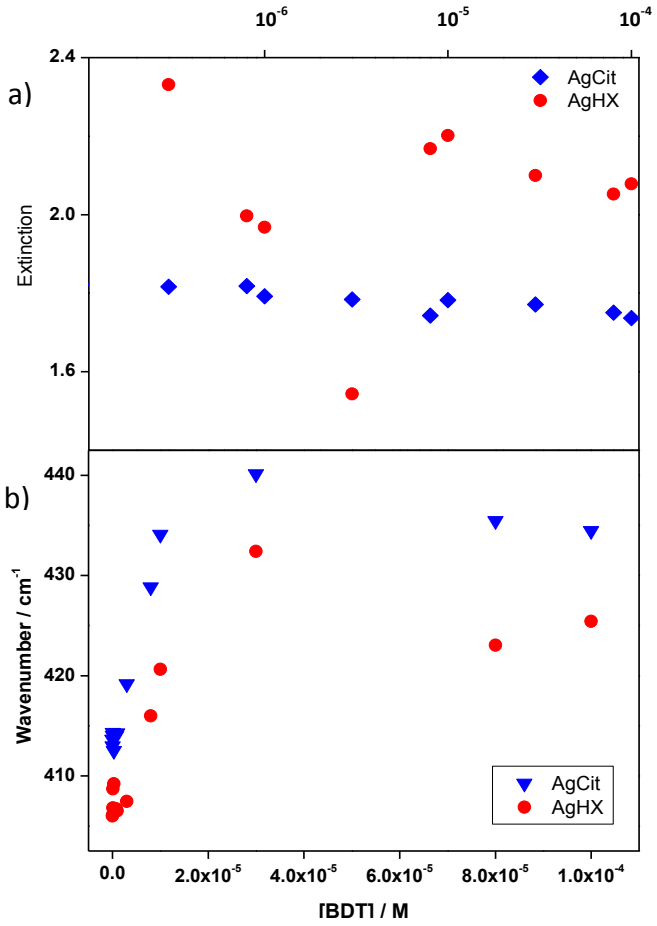

Fig. 23 – Effect of BDT concentration on (a) the intensity and (b) the position of the AgC plasmon resonance band.

A different behavior is observed upon adsorption of BDT on AgH NPs. In contrary to AgC colloid, we can observe in this case an immediate decrease of the

intensities of the absorption bands corresponding to the extinction of single NPs when increasing the concentration of BDT up to 10^{-5} M (Fig. 21b). Above this concentration, an opposite effect is observed, since the aggregation of NPs is prevented again and the maximum of the plasmon resonance undergoes a large shift to higher wavelengths (435 nm) (Fig. 22b). The result is associated to a significant adsorption of dithiol (BDT) on metal surface that prevents the NPs aggregation.

The changes in the extinction spectra of AgH colloid in the presence of BDT at various time after mixing are shown on Fig. 22d-f. As in the case of AgC colloid, a remarkable aggregation of NPs takes place in the 10^{-6}-10^{-5} M range of BDT concentration (Fig. 22e). However, above the concentration 10^{-5} M, the aggregation does not occur and only the above mentioned red-shift of the absorption peak is observed (Fig. 23d). The differences between properties of AgC and AgH nanoparticles are evident from Fig. 23. From this figure it is clear that AgH NPs display a higher sensitivity towards the aggregation by BDT (Fig. 24a) and lower red-shifts for the plasmon resonance band (Fig. 24b). The difference between these two types of colloids can be ascribed to the different chemical properties of the metal surface in these colloids. The special behaviour of AgH NPs is related to the presence of chloride ions on the surface of these NPs.

The extinction spectra of AgC and AgH colloids in the presence of BPDT do not exhibits the same behavior than in the presence of BDT. In Fig. 24, the extinction spectra of AgC colloid with BPDT adsorbed on the surface of NPs are shown at different concentrations of this dithiol. At concentrations above 10^{-7} M, the aggregation effect induced by BPDT is clear and the extinction spectra displays three different plasmon resonances. This behavior is similar to that found for the adsorption of aliphatic dithiols on metal NPs (Fig. 8). The band at 400 (AgC)/408 (AgH) nm corresponds to the non-aggregated NPs. When BPDT is adsorbed, this band undergoes a marked intensity decrease and a slight red-shift is also observed. The shoulder appearing at 500 nm is attributed to NPs dimers formed upon the linking of these nanoparticles by BPDT. Finally, the broad band centered at 800-1000 nm is attributed to the formation of aggregates of large size. A similar effect was found in the case of AgC colloid at different reaction time of BDT (spectra not shown). Therefore, the

absence of a large red shift in the monomer plasmon band, and the immediate aggregation of NPs in the presence of BPDT, indicates that this molecule presents a normal behavior regarding BDT, with a large formation of dimers due to the bifunctional character of BPDT.

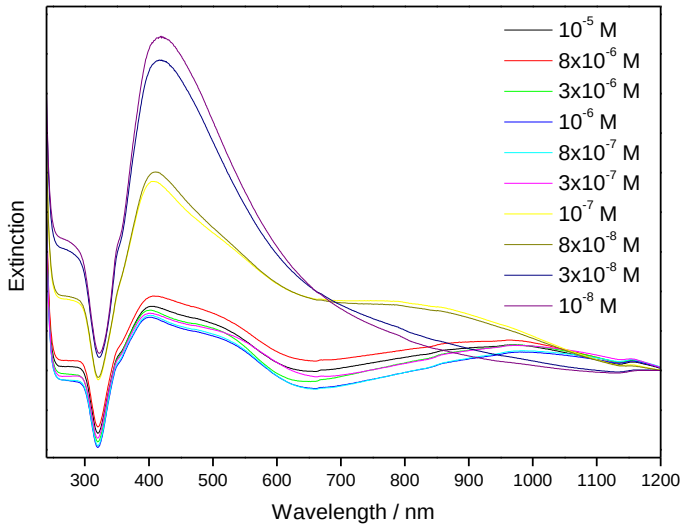

Fig. 24 – Plasmon extinction spectra of AgC colloid aggregated at different concentrations of BPDT (10^{-5} – 10^{-8} M).

5.2.2 SERS spectra of aromatic dithiols

A characterization of aromatic dithiols BDT and BPDT molecules by FT-Raman (1064 nm excitation) was done in order to consequently analyze the effect of the metal adsorption of these molecules on the vibrational properties of the dithiols. Fig. 25 shows the FT-Raman spectra of BDT and BPDT molecules in the solid state. The assignment of the vibrational bands of the studied aromatic dithiols was made on the basis of the data found in the literature [Joo, S.W. *et al.* 2001; Lee, Y.R. *et al.* 2013; Jung, H.Y *et al.* 2007]. Tab. 3 and Tab. 4 present the positions of the main bands observed in the FT-Raman spectra of these molecules as well as their assignments. The main difference between these compounds is the higher intensity of the bands corresponding to the thiol moiety in BDT (2556, 1094, 740 and 335 cm^{-1}), while BPDT displays more intense bands corresponding to the aromatic part of the molecule (1590, 1275 and 1117 cm^{-1}).

The SERS spectra of BDT and BPDT on different types of metal colloids are shown in Fig. 26 and 27. Although intense citrate bands are observed in the presence of AgC, the intense SERS bands of both dithiols can be seen even at low concentrations ($8x10^{-8}$ M for BDT and 10^{-7} M for BPDT). This high sensitivity indicates effectively formation of hot spots where the local field is highly enhanced leading to an enormous amplification of the Raman scattering signal from the studied molecules [Zhao, J. *et al.* 2008].

As in the case of the aliphatic dithiols, these aromatic molecules interact with the metal surface via the formation of a covalent bond through both S atoms and the formation of thiolate species. This is deduced from the disappearance of the strong S–H stretching band at 2556 cm^{-1} seen in their solid state and not present in SERS spectra (Fig. 25).

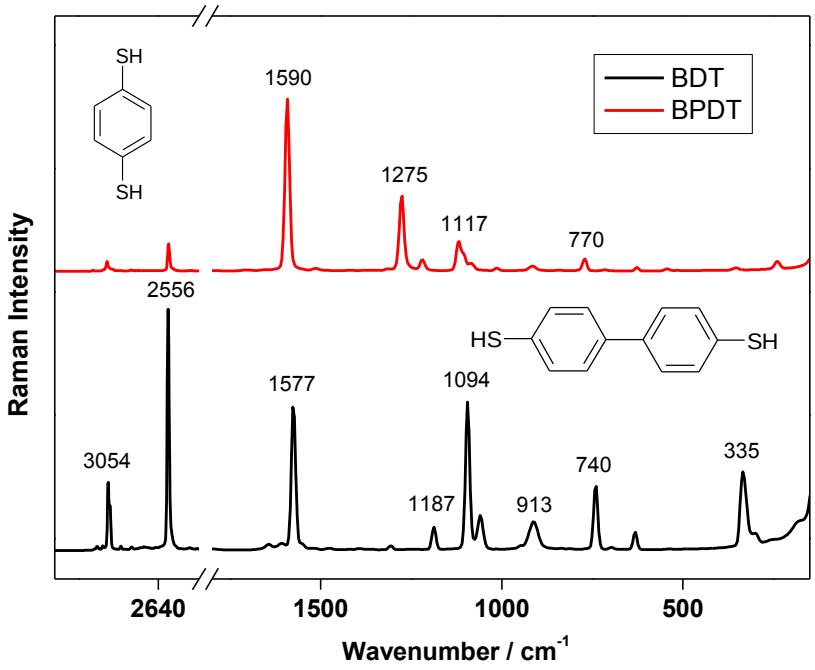

Fig. 25 – FT Raman spectra (excitation at 1064 nm) of BDT and BPDT in the solid state and the molecular structures of these dithiols.

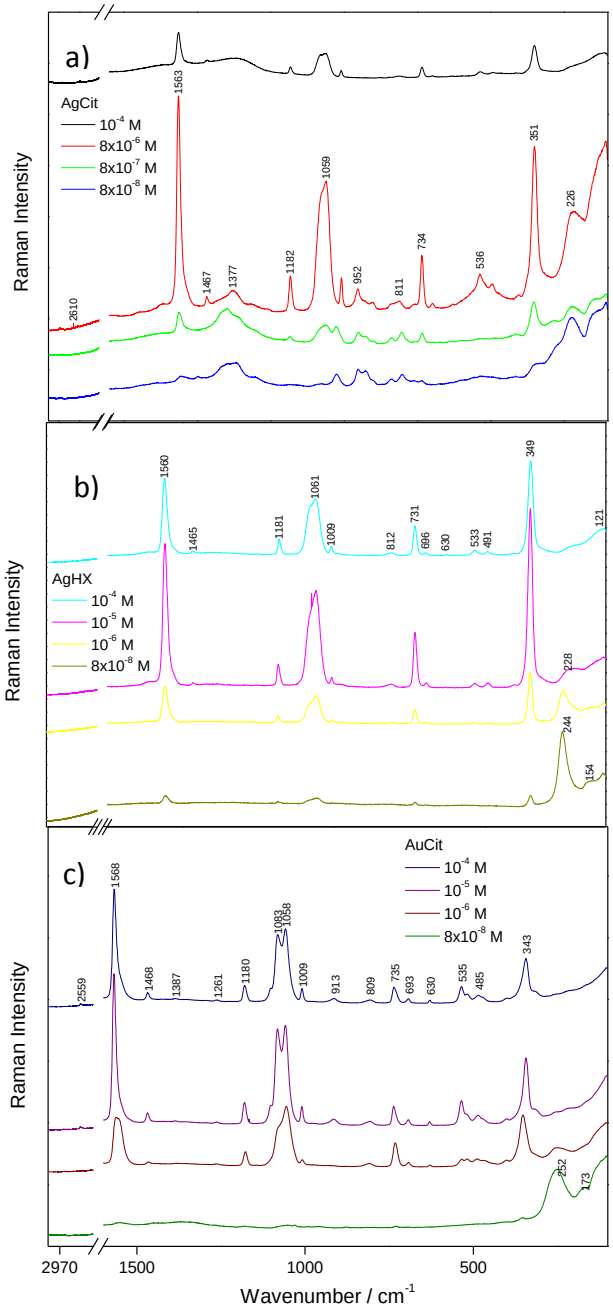

Fig. 26 – SERS spectra of BDT at various concentrations obtained on (a) AgC, (b) AgH and on (c) AuC. All spectra were obtained by using the 785 nm excitation line.

The disappearance of the band corresponding to the S–H bond (below 10^{-6} M dithiol concentration) indicates dissociative chemisorption of benzenedithiol onto Au by S–H breakdown. Consequently, the SERS signal corresponds mainly to dithiol molecules linked to NPs and placed in interparticle nanogaps. This is expected to be valid predominantly at low surface coverage by the analyzed molecules. Molecules

localized out of these gaps could also contribute to the SERS spectra, however, undergoing a much lower Raman signal intensification as deduced from the absence of free S–H bands [Kubackova, J. *et al.* 2014]. On increasing the dithiol concentration (>3x10^{-6} M), a weak band at 2559 cm^{-1} is observed indicating the appearance of free S–H group band. This observation points out that some of the BDT molecules do not interact with the surface of NPs. The spectral presence of free –SH group at the higher concentrations suggests the formation of multi-layered structures of this molecule, similarly as it was observed in the case of alkyl dithiols adsorbed on NPs.

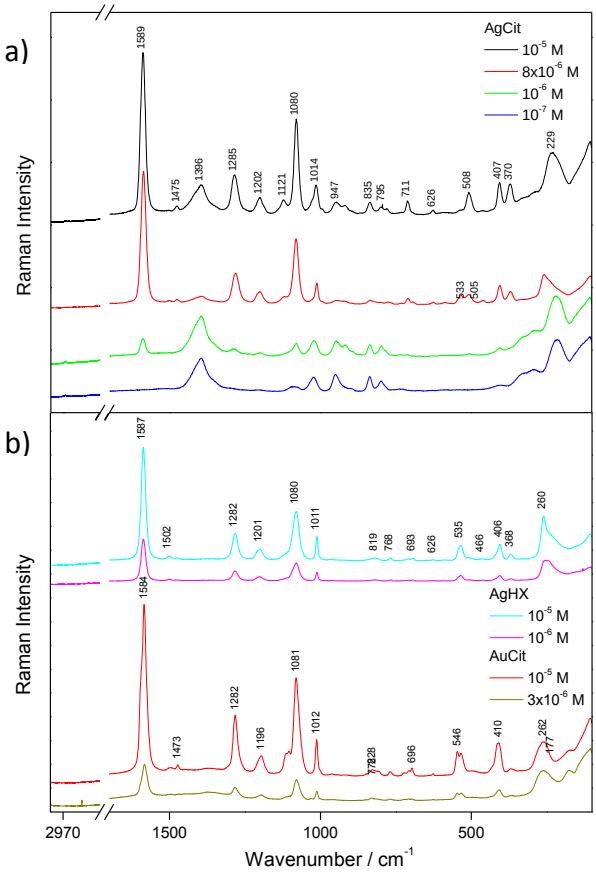

Fig. 27 – SERS spectra of BPDT at different concentrations obtained on (a) AgC and (b) AgH and AuC. Excitation line at 785 nm.

When increasing the concentration of aromatic dithiols, we observe a progressive intensification of a doublet at 530-490 cm^{-1}. This band is not seen in the Raman spectrum of the solid BDT (Fig. 29) and is attributed to the stretching vibration of S–S bonds formed upon BDT polymerization on the metalsurface (Fig. 28). This

polymerization process, which was not previously reported by any other author, probably accounts for the striking behaviour of the NPs extinction spectra observed in the presence of BDT (Fig. 21). The formation of a broad layer of polymer at high BDT concentrations seems to be responsible for the absence of NPs aggregation at these concentrations and for the large red shift of the plasmon resonance. Fig. 26 displays the SERS intensity of the ν(S-S) band as a function of the dithiol concentration in the presence of the different NPs used for SERS experiments. As can be seen, a higher BDT concentration leads to a higher intensity of the ν(S-S) band, suggesting that the polymerization the dithiol is increased. In addition, the polymerization is larger on Au NPs than on Ag NPs. This can be attributed to the higher catalytic activity of this metal. Furthermore, the AgC colloid displays a higher activity in the polymerization activity in comparison with the AgH one. The presence of chloride ions on the latter colloid can account for this observation, as halide ions are known to inhibit the catalytic activity of metals. Although a polymerization seems to take also a place in the case of BPDT, the higher effect of this molecule on the NPs aggregation suggests that this polymerization occurs in a lower extend for BPDT.

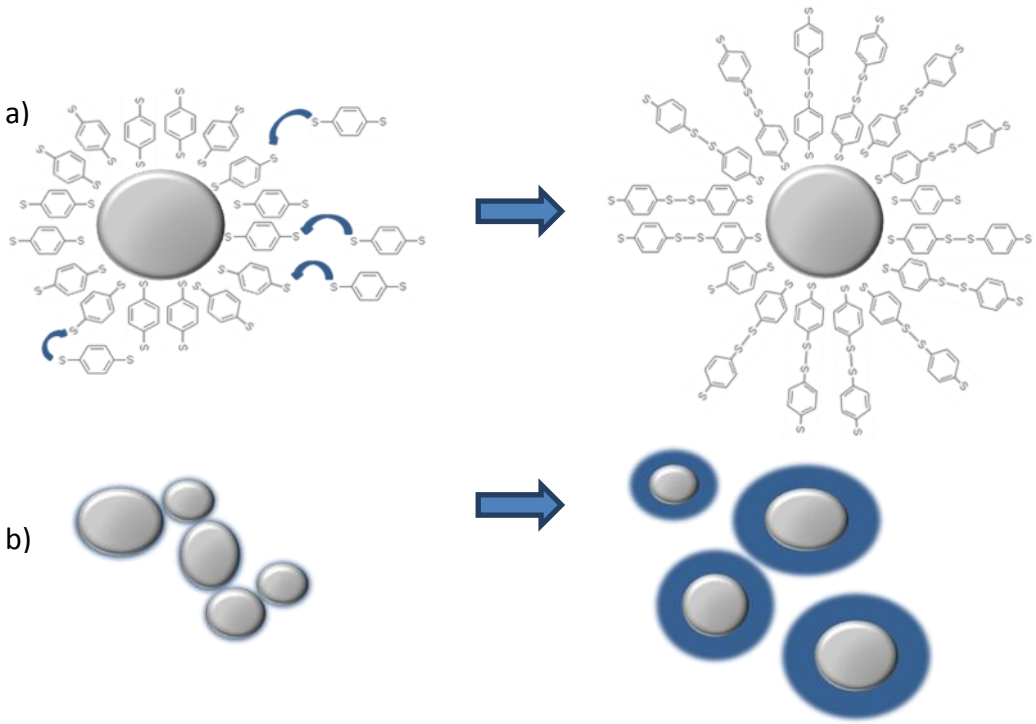

Fig. 28 – (a) Polymerization of BDT on silver surface of NPs and (b) formation of broad layers of BDT polymers around the metal that prevents the aggregation of NPs.

The SERS spectrum of BDT on Au NPs also show other changes that can be associated to the dithiol polymerization (Fig. 29): (i) the intensification of the band at 1083 cm^{-1}, (ii) the disappearance of the δ(CSH) band at 913 cm^{-1}, and (iii) the downshift of the band at 351 to 343 cm^{-1}. All these changes are also a consequence of the more intense polymerization process undergone by BDT on this metal.

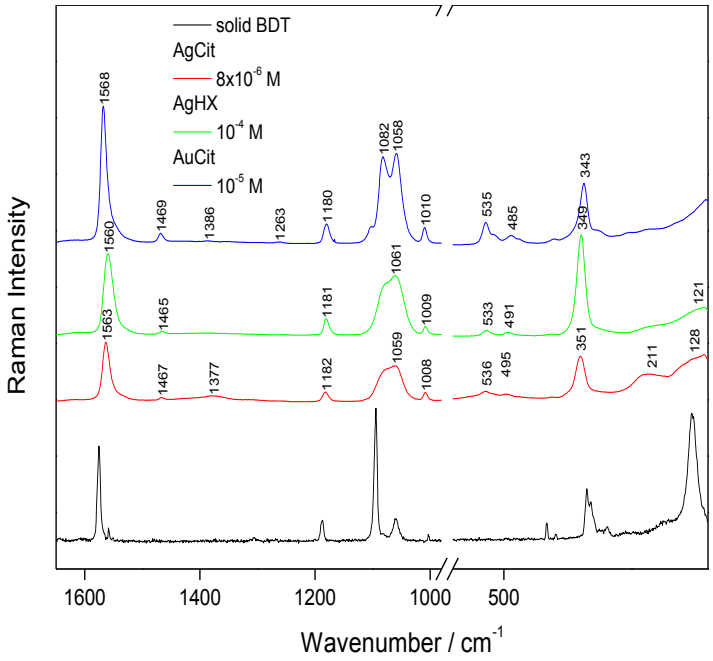

Fig. 29 – SERS spectra of BDT on Ag and Au colloids.Excitation line at 785 nm.

As in the case of aliphatic dithiols, the absorption of aromatic dithiols on the metal surface induces a strong downshift of the band corresponding to ν(C–S) in relation to the position of the same band in neat liquid samples [Bryant, M.A. & Pemberton, J.E. 1991]. The band corresponding to the aromatic ν(C–S) shows a change of the position and the intensity from 1094 cm^{-1} to 1081-1060 cm^{-1}. A similar downshift was observed for BPDT as well. The extent of the downshift depends on the surface coverage and the nature of the metal, being more pronounced at low coverage and when dithiols are adsorbed on Ag surface [Cho, S.I. *et al.* 1999; Sellers, H. *et al.* 1993]. We can observe a lower downshift of the aromatic ν(C–S) band at higher coverage of the surface, because we suppose that as the concentration of dithiols is increased, the probability of interaction of these molecules with one or two metal atoms (on-top and bridge coordination) also increases. Furthermore, another factor that can influence the

position ofthe C–S stretching is the strong withdrawing capacity of residual chloride ions, coming from the preparation process of AgH, that are still adsorbed onto the metal surface at low dithiol concentrations, as revealed by the presence of an intense band at 245 cm^{-1} attributed to ν(Ag–Cl) for BDT at concentrations below 10^{-5} M (Fig. 28b) [Kubackova, J. *et al.* 2014].

FT Raman	Raman	Wavenumbers (cm^{-1}) of Raman spectra			Assignments
		SERS on AgC	SERS AgH	SERS AuC	
130*s*	132*s*				
184*w*	188*w*				
300*w*	297*w*			316*w*	
335*s*	338*s*	351*s*	349*s*	343*s*	δ(CCS)
	398*w*			402*w*	Skeletal deformations
	416*m*				
		492*w*	491*w*	485*w*	
				518*w*	ν(S–S)
		536*w*	533*w*	535*m*	
632*m*	632*m*		630*w*	630*w*	Ring deformation
697*w*	699*w*	696*w*	696*w*	693*w*	
740*m*	741*m*	734*m*	731*s*	735*m*	ν(C–S)
809*w*	806*w*	813*w*	811*w*	807*w*	
836*w*	832*w*	845*w*			δ(C–H) *out-of-plane*
	844*w*				
	868*w*				
		879*w*			
913*m*	916*m*				δ(CSH) *in-plane*
	1003*w*	1009*w*	1009*w*	1009*m*	δ(CSH) *in-plane*
1060*m*	1061*m*	1060*s*	1061*s*	1058*s*	ν(C–S) *aromatic* Ring stretching deformation
		1063*s*		1081*s*	
1094*s*	1094*s*				
1187*m*	1187*m*	1182*w*	1181*m*	1180*m*	δ(C–H) *in-plane*
				1261*w*	
1307*w*	1306*w*				Ring stretching
1395*w*		1369*w*			
1476*w*		1466*w*	1465*w*	1468*m*	Ring stretching
1577*s*	1575*s*	1563*s*	1560*s*	1568*s*	ν(C–C) *aromatic ring*
	1559*w*				
1607*w*	1607*w*		1617*w*		
2556*s*	2557*s*				ν(S–H)
2861*w*	2876*m*				
2950*w*					
3054*s*	3057*w*				ν(=C–H)
3100*w*					
3146*w*	3145*w*				

[a](ν): stretching, (δ): bending, (ω): wagging, (τ): twisting, (ρ): rocking, (vs): very strong, (s): strong, (m): medium, (w): weak, (sh): shoulder

Tab. 3 – Experimental FT Raman, Raman and SERS bands cm^{-1} and the most probable band assignment of BDT on diffrente types of colloids.

FT Raman	Raman	Wavenumbers (cm^{-1}) of Raman spectra			Assignments
		SERS AgC	SERS AgH	SERS AuC	
111*m*	113*m*				
142*w*	140*w*				
				172*w*	
238*m*	239*m*	229*s*	260*s*	262*m*	
308*w*					
354*w*	355*w*	370*m*	368*w*	369*w*	δ(CCS)
408*w*					
		407*m*	410*m*	410*m*	δ(CCS)
		508*m*	507*w*	496*w*	ν(S–S)
516*w*	515*w*				Skeletal deformations
		539*w*	535*m*	534*w*	
543*w*	545*w*			546*m*	
628*w*	627*w*	626*w*	626*w*	627*w*	
			693*w*	696*w*	δ(C–H) *out-of-plane*
		711*m*	709*w*	707*w*	
716*w*	718*w*			723*w*	
770*m*	771*m*	779*w*	768*w*	770*w*	
		795*w*			Ring deformation
		800*w*		808*w*	
840*w*	839*w*	835*w*	819*w*	828*w*	δ(C–H) *out-of-plane*
913*m*	912*w*	918*w*			δ(CSH) *in-plane*
		993*w*			δ(CSH) *in-plane*
1013*w*	1014*w*	1014*m*	1011*m*	1012*m*	Ring in-plane deformation
	1043*w*				
1087*w*	1085*w*	1080*s*	1080*s*	1081*s*	ν(C–S)
	1105*m*			1104*m*	
1118*s*	1120*s*	1121*m*		1114*w*	
1218*m*	1220*m*	1202*m*	1201*m*	1196*m*	δ(C–H) *in-plane*
1276*s*	1276*s*	1285*s*	1282*s*	1282*s*	ν(C–C) *inter-ring*
1318*w*	1315*w*				
		1396*s*			
		1475*w*	1475*w*	1473*w*	ν(C–C) *aromatic ring*
1515*w*	1514*w*		1502*w*	1499*w*	ν(C=C) *aromatic ring*
1592*s*	1592*s*	1589*s*	1588*s*	1584*s*	ν(C=C) *aromatic ring*
1704*w*					
2552*m*	2554*w*				ν(–S–H)
3065*m*					ν(=C–H)

[a](ν): stretching, (δ): bending, (ω): wagging, (τ): twisting, (ρ): rocking, (vs): very strong, (s): strong, (m): medium, (w): weak, (sh): shoulder

Tab. 4 – Experimental FT Raman, Raman and SERS bands cm^{-1} and the most probable band assignment of BPDT on diffrente types of colloids.

5.3 Sensitive SERS detection of organochlorine pesticides by dithiolalkene-functionalized nanoparticles on selective plasmonic hot spots

5.3.1 Raman spectra of organochlorine pesticides in solid state

The Raman spectra of the solid state of organochlorine pesticides: aldrin, α-endosulfan, lindane and dieldrin, are shown on Fig. 30. The used excitation lines (785 and 1064 nm) have not significant influence on the relative intensities of the Raman bands of the pesticides. The tentative assignment of the vibrational bands of the studied pesticides was made on the basis of the data found in the literature [Mishra, S. *et al.* 2006; Guerrini, L. *et al.* 2008]. The Raman spectra are dominated by a group of bands appearing in the 400-300 cm^{-1} region, attributed to C-Cl stretching vibrations (ν(CCl)). These bands are the most intense in the Raman spectra, since the C-Cl stretching induces a large variation of the polarizability. Therefore, these bands can be employed as an actual fingerprint region to carry out the SERS detection of the studied organochlorine pesticides. The bands appearing below 300 cm^{-1} are attributed to bending vibrations (δ(CCCl), δ(ClCCl) and δ(CCC)). The Raman spectra of these pesticides also include weak C=C stretching bands in the case of the bicyclic pesticides (aldrin, α-endosulfan and dieldrin), appearing at 1599-1605 cm^{-1} and attributed to the stretching vibration of the Cl-C=C-Cl moiety. Aldrin also exhibits a second extra C=C band appearing at 1563 cm^{-1} corresponding to the C=C localized in the opposite molecular side (Fig. 30). Finally, the bands observed between the two above mentioned regions correspond to CC and CH and CH_2 bending of the aliphatic chain structure of these molecules.

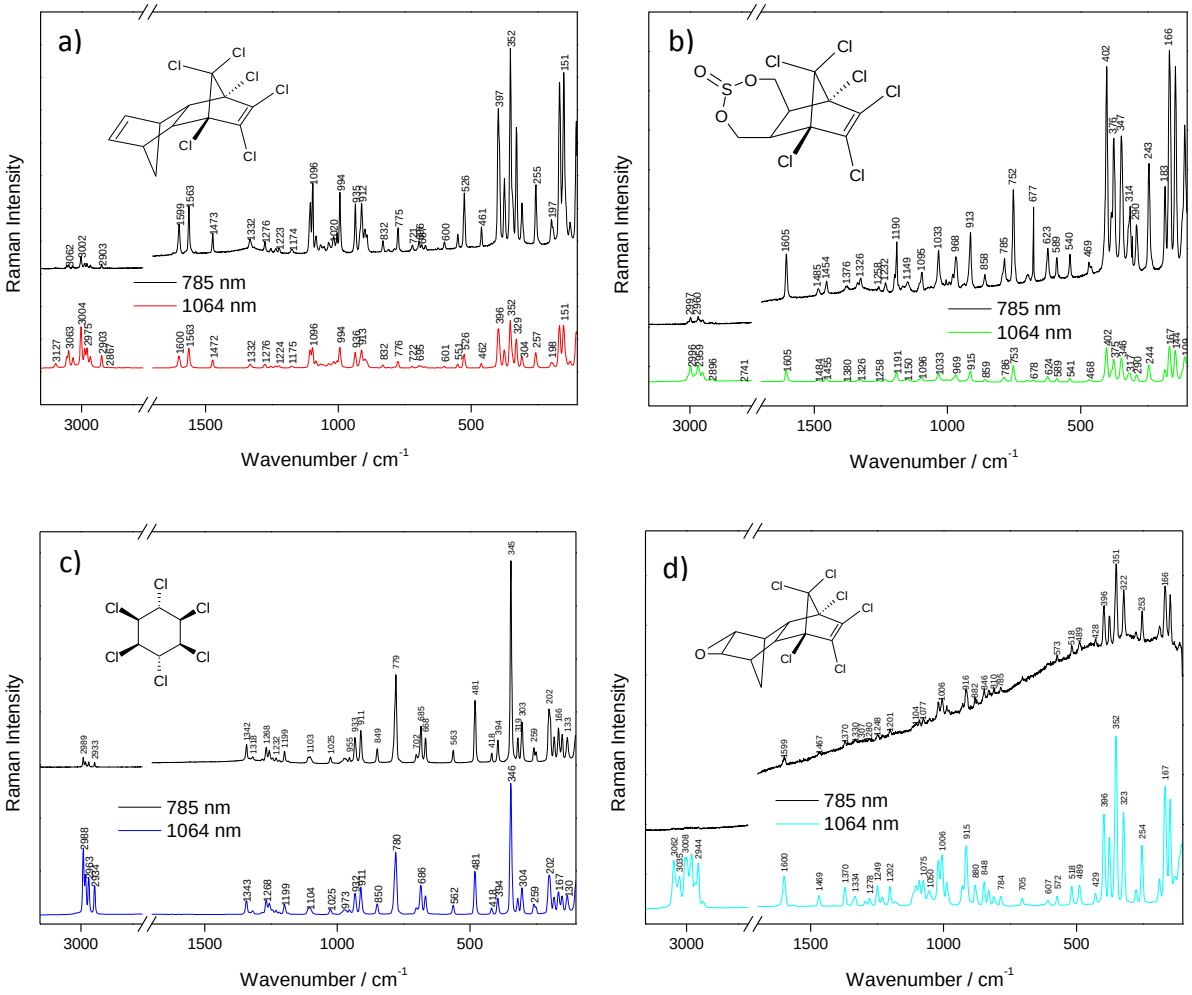

Fig. 30 – Raman (785 nm) and FT Raman (1064 nm) spectra of the solid state of the studied pesticides:(a) aldrin, (b) endosulfan, (c) lindane and (d) dieldrin.

5.3.2 SERS spectra of organochlorine pesticides

The analyzed organochlorine pesticides do not display any Raman band in the presence of metal NPs using either Ag or Au colloids, as can be seen in Fig. 31a for aldrin (10^{-5} M). This fact is due to the extremely low affinity of the analyzed pesticides to link the metal surface and to benefit from the EM field enhancement near this surface. To change this situation, we have modified the chemical properties of the metal surface by functionalizing the metal nanoparticles with molecular linkers, alkyl dithiols and aromatic dithiols. Aliphatic dithiols adsorbed on the Ag and Au NPs fulfill two different roles (see Fig. 32 for a schematic explanation): i) linking of NPs, as demonstrated in the previous chapters 5.1 and 5.2 and ii) functionalization of the hot

spots to attach the pollutant just to the gap between NPs, where the field is much more enhanced than in other parts of the surface (Fig. 32).

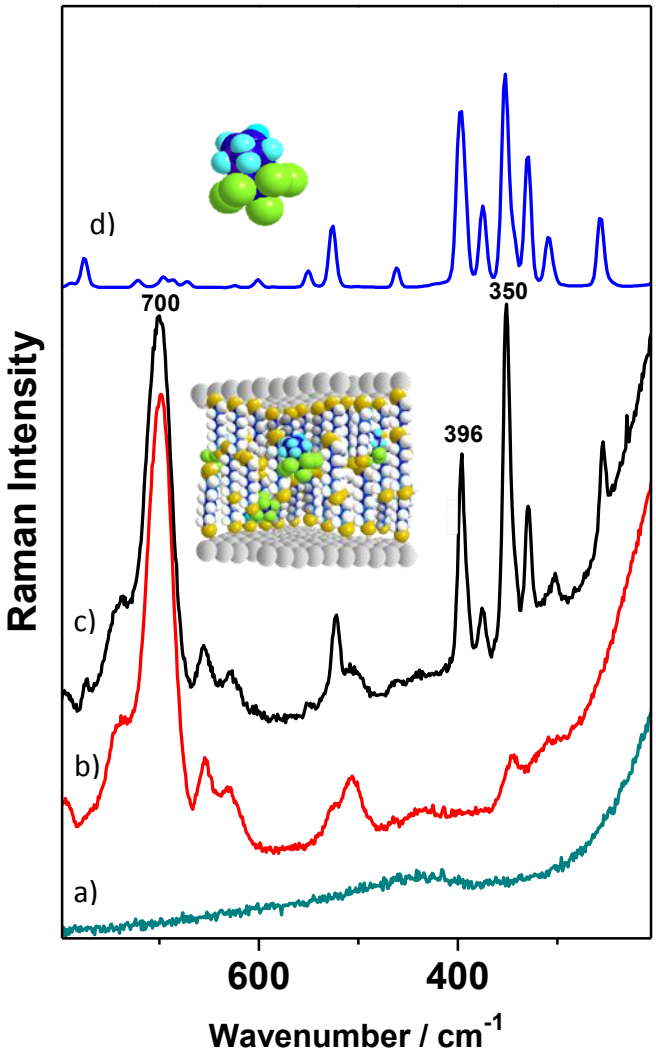

Fig. 31 – SERS spectra of aldrin (10^{-5} M) on AgC in the absence of dithiols (a), and on DT8-functionalized AgC (c). The latter spectrum shows the bands corresponding to DT8 that are seen in (b) for AgC functionalized with DT8 (10^{-5} M). Raman spectrum of the solid aldrin is presented as (d). All spectra were obtained at 785 nm excitation.

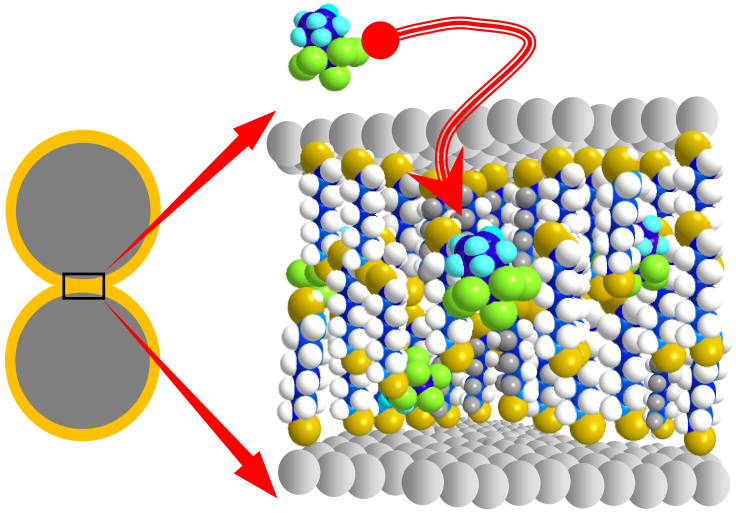

Fig. 32 – Scheme displaying the pesticide hosting (in this case for aldrin) in the dithiol layer organized in interparticle gaps.

The functionalization of the metal NPs with alkyl dithiols leads to a change of the chemical properties of the interface that allows the observation of the intense Raman bands of the pesticides in the 400-300 cm^{-1} region corresponding to the ν(CCl) bands. In Fig. 31c we show this effect for the particular case of aldrin. The observed SERS bands correlate very well with the Raman bands seen in the classical Raman spectrum (Fig. 31d), and are clearly distinguished from the dithiol bands in the 750-600 cm^{-1} region (Fig. 31b), which were employed as reference to calculate the relative intensities of the SERS bands of the analyzed pesticides.

A detailed analysis of the observed bands reveals that only slight changes are produced in the SERS spectra of either the dithiol or the pesticide molecule, indicating that the interaction between these molecules is not very strong, although it is strong enough to induce the inclusion of the pollutant into the aliphatic environment by van der Waals and/or hydrophobic interactions. These interactions also occur in the adipose tissue of mammals or in the plasmatic membranes where these substances can be accumulated. Small relative changes in the intensities of the Raman bands of the pesticides can be attributed to the specific orientation of these molecules inside the dithiol layer formed on the metal surface, as deduced from the propensity rules of SERS [Creighton, J.A. 1988].

5.3.3 Optimization of the detection of organochlorine pesticides by SERS

To optimize the functionalization of NPs by the adsorption of aliphatic dithiols we have carried out a study consisting in the variation of several key factors essential for the detection ability of these systems. These factors were: i) the structure of dithiols; ii) the chemical properties of the metal surface, iii) the aliphatic layer organization on the surface, and iv) the excitation wavelength. The structure was modified by using aliphatic or aromatic dithiols and by changing the length of the aliphatic chain in alkyl dithiols (6, 8 and 10 C atoms in DT6, DT8, DT10 dithiols, respectively). The chemical properties were modified by using plasmonic NPs prepared by different ways, i.e. by using hydroxylamine and citrate Ag NPs and citrate Au NPs. The layer organization around NPs was modified by varying the surface coverage of NPs at different dithiol concentrations.

An important step in the optimization process of the SERS detection of the pesticides was to find out the most suitable type of metal substrate. In order to carry out this study, we have employed the colloids: AgC, AgH and AuC. Fig. 33b shows the relative intensity of the most intense band seen in the SERS spectrum of aldrin at 10^{-5} M, which is the band appearing at 350 cm^{-1} (Fig. 31). The spectra were obtained in the presence of all the analyzed dithiols but we only show the results obtained on all the studied NPs systems covered by DT8. It is evident that the most intense bands appear in the SERS spectrum in the presence of AgC colloid, while utilization of Au NPs leads to a low SERS intensity of aldrine. In the presence of AgH colloid, the SERS spectrum of aldrin is also intense, however not such as in the case of AgC. The relative intensities of the aldrin bands in 400-300 cm^{-1} region are identical in both spectra obtained using AgC and AgH colloids. This observation suggests that the method of the preparation of silver colloids does not influence the orientation of the analyte inside the dithiol layer. The AgC was also found to be the best substrate for the other analyzed pesticides (results not shown). The reason to obtain a higher efficiency in the pesticide detection on AgC NPs in comparison with other SERS subtrates is difficult to assess, although two main reasons can be suggested: the different plasmonic activities of each substrate and the differences in the chemical properties of the exposed interfaces. The easy removal of the citrate ions existing in this substrate by the added dithiols can be the

reason to the better properties of AgC, since in the case of AgH, the chloride ions adsorbed on the surface are more strongly attached on the surface avoiding the adsorption of dithiols. Au NPs are less effective for SERS detection of the pesticides because the structure of dithiols adsorbed on this metal is more disordered as reported in the previous chapter 5.1. This fact prevents the formation of suitable sites for the incorporation of the pesticides inside nanoparticle gaps.

The employment of aromatic dithiols (BDT and BPDT) in the detection of the pesticides leads to negative results in all the cases. This result means that these molecules were not able to appriopriately link NPs and/or attract the pesticides into interparticle gaps.

Fig. 33 also shows the SERS intensity of the 350 cm^{-1} band in the specific case of aldrin (10^{-5} M), utilizing as SERS substrate the „optimal“ one (AgC NPs), in the presence of the three aliphatic dithiols bearing different chain length (DT6, DT8, DT10). In this experiment, DT8 was the linker giving rise to the most intense SERS bands of the analyzed pesticides. We can conclude that the length of DT8 is optimal for the creation of hot spots and/or an increase of the affinity of the studied pesticides towards metal surface and consequently for the detection of these molecules, as also found for the case of alkyl diamines [Guerrini, L. *et al.* 2010]. This is attributed to the better plasmonic properties of the nanogaps created between the linked NPs as displayed in Fig. 33a.

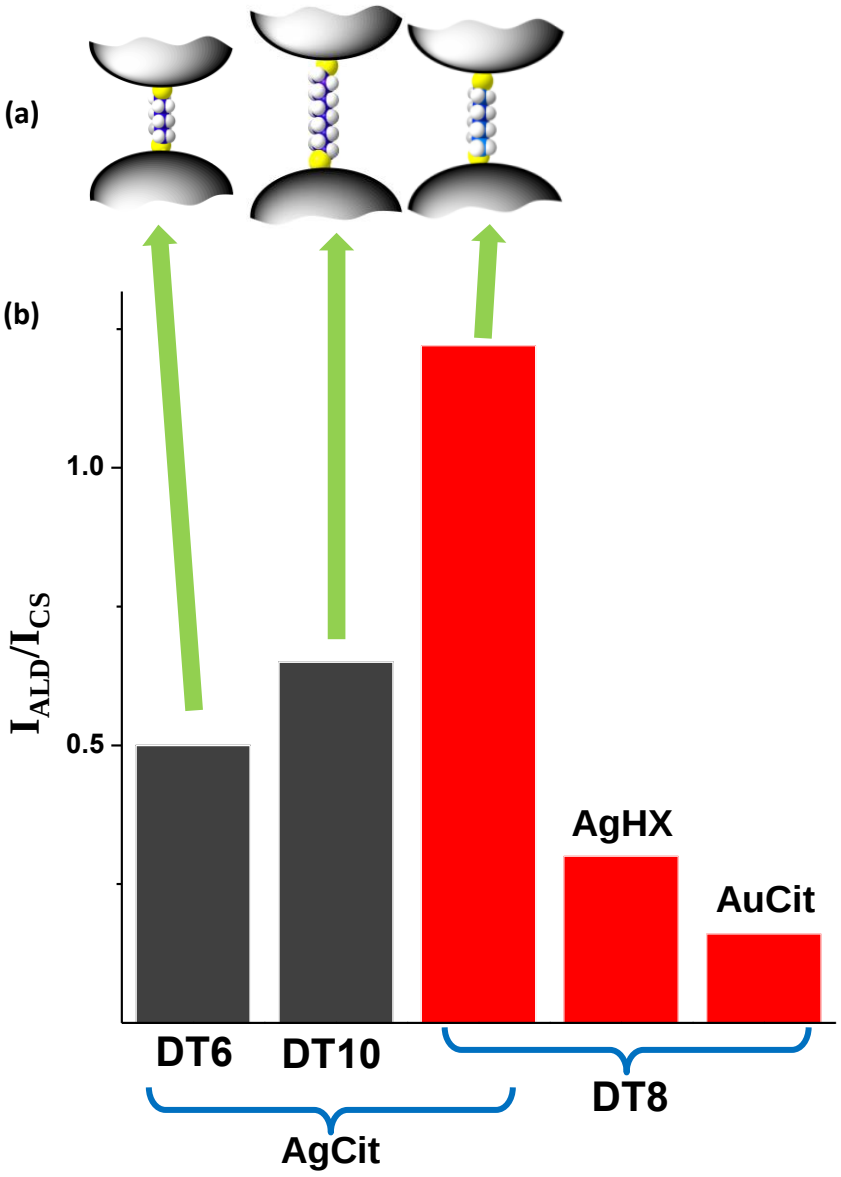

Fig. 33 – Optimization of the linker (DTX) and the plasmonic substrate in the detection of aldrin. The intensity of the 350 cm^{-1} band of aldrin is displayed here (b) as a function of different DTX-functionalized metal NPs. DT8 provided the most intense spectrum on AgC substrate due to the best plasmonic conditions of the interparticle gaps (a).

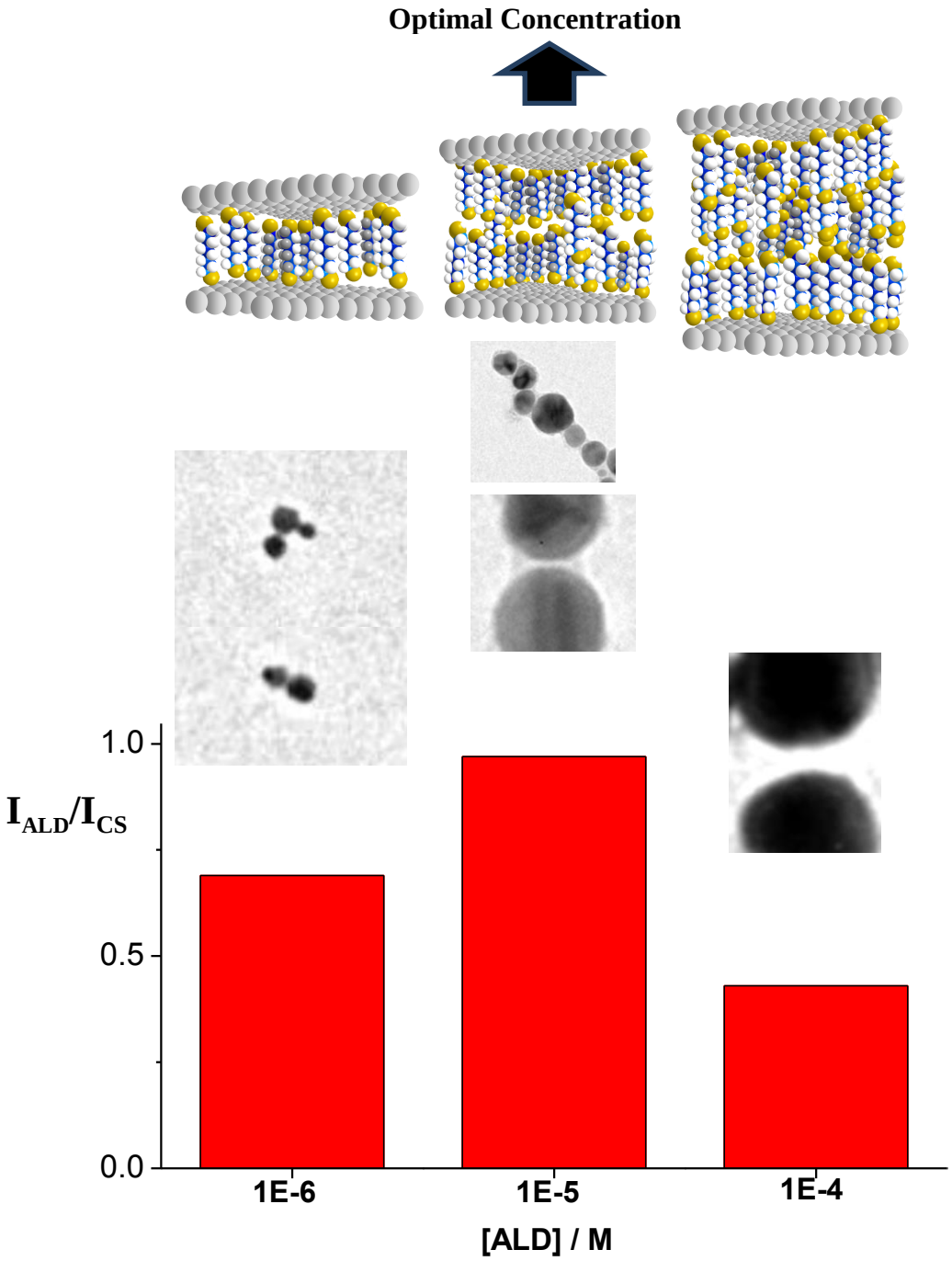

Fig. 34 – Relative SERS intensity of the 350 cm^{-1} band of aldrin recorded at different DT8 concentrations on AgC (Down). In the TEM images shown in the medium part, the nanogaps observed at different DT8 concentrations are observed displaying the different interparticle distance between NPs. The upper schemes show the layer organization suggested for the different concentrations of DT8.

The surface coverage of metal nanoparticles by dithiols is also an important factor that determine the layer organization of the aliphatic chains on the metal and in the interparticle cavity, and that may influence the ability of these system to detect organochlorine pesticides. To study this effect, several SERS spectra of the pesticides were obtained at different DT8 concentrations using the AgC colloid. The relative intensity of the aldrin band at 350 cm^{-1} at three various DT8 concentrations is shown in Fig. 34. As can be seen, the optimal concentration of DT8 is 10^{-5}M. In the chapter 5.1.2 we have demonstrated that at the latter concentration dithiols are organized in multi-layer structure on metal surface with an ordered structure of the aliphatic chains (Fig. 34, upper scheme). It seems that for the proper localization of the pesticides in interparticles gaps, a multilayer should be formed (this layers are formed above the concentration 1-5 μM [Kubackova, J. *et al.* 2014]. This is due to the increase of binding sites attained at this surface coverage. At lower concentration only a monolayer is formed (Fig. 34, upper scheme) and at very high concentrations (10^{-4} M), the distance between the two particles in the interparticle junction is too large and the electric field is not so intensified [Le Ru, E.C. *et al.* 2006].

Finally, the most intense SERS spectra of the organochlorine pesticides were obtained by using the line at 785 nm as excitation wavelength in all cases. This is due to the fact that the resulting aggregates, both in the case of Ag and Au, have plasmon resonance maximum close to this wavelength [Izquierdo-Lorenzo, I. *et al.* 2013].

5.3.4 Qualitative detection of organochlorine pesticides

Fig. 35 shows the SERS spectra of all the studied pesticides using the optimized SERS substrate determined above (AgC + DT8 (10^{-5} M)) and the excitation wavelength at 785 nm. All spectra possess characteristic bands in the fingerprint region at 400-300 cm^{-1} (corresponding to C-Cl stretching vibrations of all the pesticides). In addition, bands corresponding to DT8 are also identified (see the ν(C-S) band of DT8 in Fig. 35). There exist some changes in the relative intensities and positions of these bands as a function of the studied pesticide and its concentration. Regarding the dithiol bands, it is worth noting that the presence of the pesticide in the dithiol layer leads to an increase of the chain conformation to a higher chain ordering. However, to observe

this phenomenon it is necessary to low the dithiol concentration to get a surface coverage closer to the submonolayer or monolayer regime.

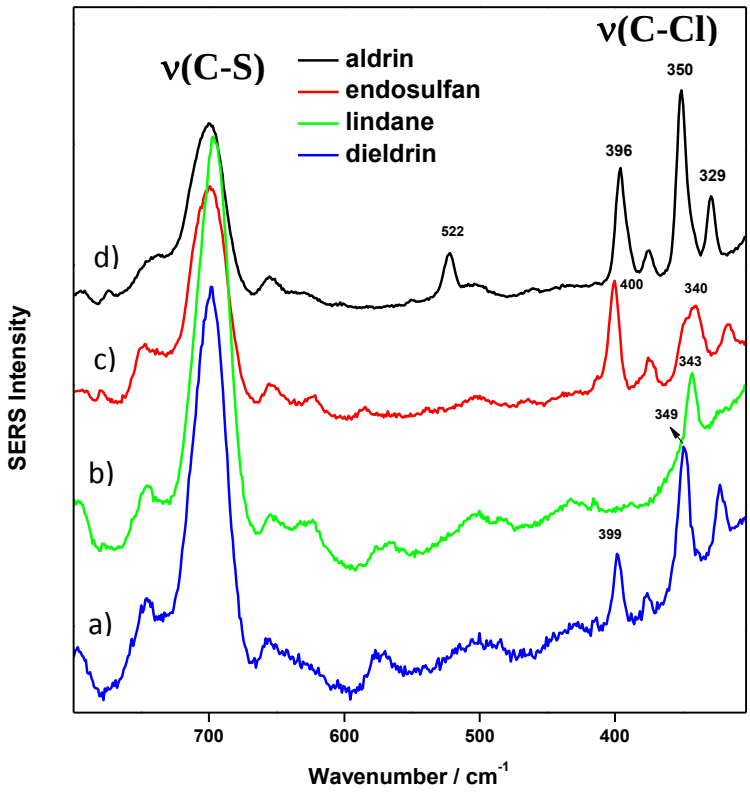

Fig. 35 – SERS spectra of the analyzed pesticides (10^{-5} M) on DT8-functionalized AgC NPs exciting at 785 nm, showing the C-Cl stretching bands of the fingerprint region (400-300 cm^{-1}) and the C-S stretching bands of DT8 in the deduced multilayer highly ordered conformation.

5.3.5 SERS determination of binding constants to NPs and limits of detection for organochlorine pesticides

SERS spectra of the organochlorine pesticides at various concentrations were recorded in order to determine the adsorption parameters related to the adsorption and interactions of the pesticides with the optimized Ag NPs. Marker bands of the individual pesticides were chosen from the ν(C-Cl) fingerprint region (400-300 cm^{-1}) in order to obtain the corresponding adsorption isotherm. These bands were those positioned at 350, 400, 343 and 349 cm^{-1}, for aldrin, α-endosulfan, lindane and dieldrin, respectively. Relative intensities of the above bands were determined by

normalizing with the band of DT8 at 700-695 cm^{-1}. The position of these bands did not change as the concentration of the studied pesticide molecules increases.

Fig. 36 (upper panel) shows the concentration dependence of the marker band intensity for each studied organochloride pesticide. It is evident that the adsorption of the organochlorine pesticides on the AgC surface follows a Langmuir model, indicating a direct interaction of the pesticides with the modified metal surface and a negligible intermolecular interaction. The adsorption constant (K_{ad}) related to the interaction between surface and adsorbate can be deduced from the Langmuir adsorption model according to the expression:

$$R_c = I/I_o = K_{ad}[A]/(1+K_{ad}[A])) \quad (20)$$

where $\mathbf{R_c}$ is the relative coverage of the Ag surface by pesticides and **[A]** represents concentration of an adsorbate. Since the SERS intensity depends on the number of molecules adsorbed on a plasmonic surface, R_c ratio can be related to the SERS intensities I/I_o, where **I** is the SERS intensity at concentration [A] and $\mathbf{I_o}$ is the SERS intensity at saturation of the surface coverage. Therefore fitting the SERS intensity of the marker band *vs.* the pesticide concentration leads to the direct determination of binding constant K_{ad}.

At very low concentration, the Eq. 20 can be expressed as:

$$I = K_{ad} I_o [A] \quad (21)$$

The limit of detection (LOD) can then be deduced from the linear dependence of Eqn. 21 by considering the concentration $[A]_{LOD}$ at which a relative intensity $I'=3\sigma$ is obtained, being σ the standard deviation of the blank measurement. This linear dependence is shown in Fig. 36 (lower panel) for the analyzed pesticides.

The parameters K_{ad} and LOD for each studied organochlorine pesticides are listed in Tab. 5. As can be seen, the affinity of the pesticides to the metal surface covered by DT8 varies as follows: dieldrin>aldrin>α-endosulfan>lindane. The different

affinity constants are probably associated with the variable liposolubility of the analyzed substances into the aliphatic multilayer created by the adsorption of DT8 on Ag NPs. In fact the affinity is higher for the more liposoluble pesticides (dieldrin and aldrin), while it is lower for the pesticides including polar groups in their structure like endosulfan. Other pesticides analyzed by this method could not be detected (linuron, atrazine and quintozene) due to their lower affinity towards the dithiol-functionalized NPs platforms prepared by the method reported here.

Furthermore, the different affinities of the pesticides towards the optimized silver substrate are also related to the different values of LOD for the individual compounds (Tab. 5). The lowest detection limit is obtained for aldrin (45 μg/l (ppb)). This value is comparable with those obtained for the detection of these substances by means of other techniques (GC + MS) [EFSA 2005].

The method reported here based on the detection by SERS presents the great advantage, regarding conventional methods, of the direct analysis without a pretreatment process of the sample that usually consists of pre-concentration and/orextraction of the pesticide by using organic solvents [WHO 2003; Brandenberger, H. & Maes, R.A. 1997].

	LOD (ng/ml)	**$K_{ad}(M^{-1})$**
aldrin	45	$5,3x10^5$
endosulfan	170	$1,4x10^5$
lindane	1029	$3,3x10^4$
dieldrin	316	$7,9x10^5$

Tab. 5 – Limit of detection and K_{ad} values calculated for aldrin, endosulfan, lindane and dieldrin.

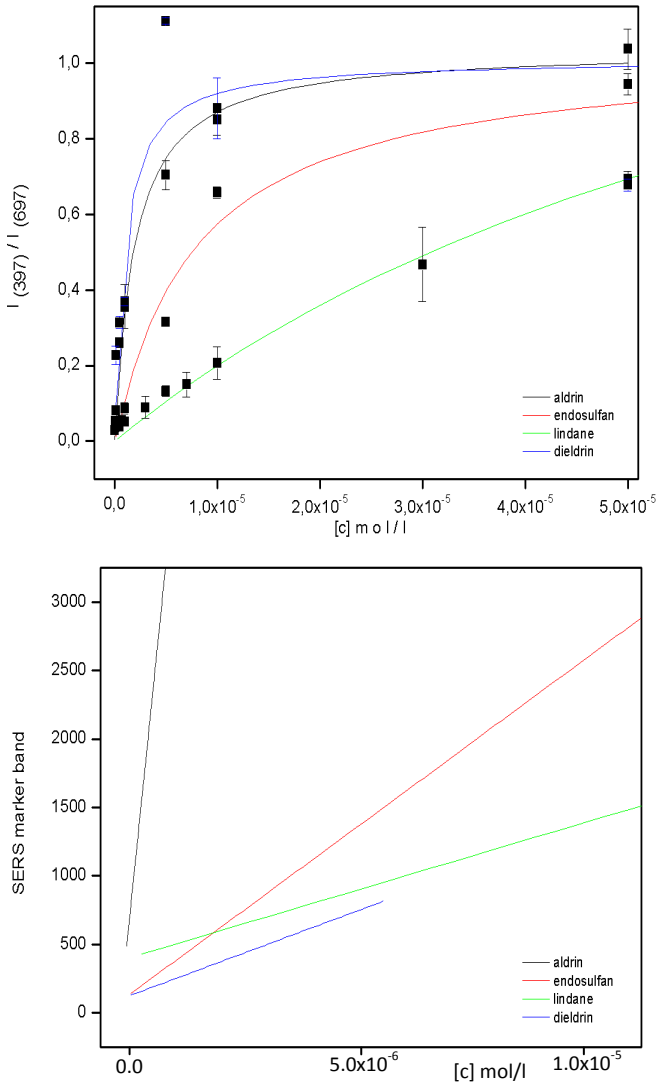

Fig. 36 – Adsorption isotherms obtained for the analyzed pesticides from the relative intensity of the marker bands (ν(C-Cl)/ν(C-S)) (upper panel). Calibration line fitted in the region of linear dependence of the relative intensity with the pesticide concentration showing the different sensitivity of the plasmonic substrate towards each pesticide (lower panel).

In conclusion, we have shown that SERS spectroscopy is capable to detect low concentrations of the organochlorine pesticides aldrin, α-endosulfan, lindane and dieldrin. This is possible thanks to the functionalization of metal nanoparticles with aliphatic α,ω-dithiols as bifunctional linkers. These substances played two different roles: i) the nanoparticle assembly to create 1-2 nm gaps where a large intensification of the EM field can take place, and ii) the modification of the chemical properties of the surface to make these hot spots attractive to the pollutant. By means of this method, strong molecular marker bands (in the 300-400 cm^{-1} region) can be detected

that constituted an actual fingerprint of the pesticides. The preparation of the substrate consisting of nanoparticle plus the dithiol was optimized. The maximum detection efficiency is obtained for those substrates using AgC nanoparticles linked with DT8 at a concentration of 10^{-5} M. At these conditions the alkylic chains are organized in multilayers providing a maximum number of binding sites just at the formed hot spots localized in the gaps between nanoparticles. The affinity constant and the limit of detection were determined from the calibration curves obtained at different concentrations, which represent the adsorption isotherms of the process. These isotherms fitted a Langmuir curve indicating that the pesticide is inserted in the dithiol multilayer with a negligible pesticide-pesticide intermolecular interaction. The calculated limit of detection is comparable to those determined by other techniques, with the advantage of no sample pre-treatment required by other techniques.

6 Conclusions

- Aliphatic dithiols can act as linkers between metal nanoparticles and induce the formation of nanogaps with a controllable interparticle distance depending on the dithiol length and the concentration.
- The interaction through both thiol groups makes the adsorption of dithiols on metal surface substantially different from that of monothiols, in particular the orientation of dithiols is perpendicular, while monothiols adopt a tilted orientation. The nanogaps thus formed are able to produce hot spots exhibiting a large intensification of electromagnetic field in these points.
- Dithiol-functionalized nanoparticles were successfully employed in the SERS detection of trace concentrations of chemicals which can be trapped in these gaps by an increase of the adsorption affinity induced by the presence of the polymethylene chain between two nanoparticles.
- The most suitable substrate for SERS detection of the organochlorine pesticides (aldrin, α-endosulfan, lindane and dieldrin) was determined to be citrate silver colloid particles covered by 1,8-octanedithiol (10^{-5} M).
- Functionalization of the metal surface by aromatic dithiols does not lead to a SERS substrate suitable for the detection of the organochlorine pesticides. This observation is attributed to different adsorption properties of aromatic dithiols on metal surface in comparison with aliphatic dithiols.
- The fingerprint region (300–400 cm^{-1}) for the SERS detection of the organochlorine pesticides was determined. The pesticides follow a Langmuir adsorption model from which the adsorption constant and the limit of detection for individual pesticides were determined. The obtained results confirm the high sensitivity of SERS for the detection of low quantities (~10^{-8}M) of these pesticides which provide solid basis for the construction of suitable nano-sensors for the identification and quantitative analysis of this type of chemicals.

References

- **Abbate**, S.; Wunder, S.L.; Zerbi, G. *Journal of Physical Chemistry* **1984**, 88, 593-600
- **Abbate**, S.; Zerbi, G.; Wunder, S.L. *Journal of Physical Chemistry* **1982**, 86, 3140-3149
- **Agency for Toxic Substances and Disease Registry** (ATSDR) *Endosulfan* **1995**
- **Agency for Toxic Substances and Disease Registry** (ATSDR)*Toxicological profile for Aldrin/Dieldrin* **2002**, 1-3
- **Agency for Toxic Substances and Disease Registry** (ATSDR) *Toxicological Profile for Alpha-, Beta-, Gamma-, and Delta-Hexachlorocyclohexane* **2005**, 29-113
- **Agency for Toxic Substances and Disease Registry** (ATSDR) *Toxicological profile for endosulfan* **2013**, 10-128; 209-212
- **Aktar**, W.; Sengupta, D.; Chowdhury, A. *Journal of Interdisciplinary Toxicology* **2009**, 2, 1-12
- **Albrecht**, M.G.; Creighton, J.A. *Journal of the American Chemical Society* **1977**, 99, 5215-5217
- **Alford-Stevens**, A.L.; Bellar, T.A.; Eichelberger, J.W.; Budde, W.L. *Journal of Analytical Chemistry* **1986**, 58, 2022-2029
- **Alonzo-Gonzáles**, P.; Albella, P.; Schnell, M.; Chen, J.; Huth, F.; García-Etxarri, A.; Casanova, F.; Golmar, F.; Arzubiaga, L.; Hueso, L.E.; Aizpurua, J.; Hillenbrand, R. *Nature Communications* **2012**, 3, 684-690
- **Anderson**, D.J.; Moskovits, M. *Journal of Physical Chemistry B* **2006**, 110, 13722-13727
- **Aroca**, R. *Surface-Enhanced Vibrational Spectroscopy* **2006**, John Wiley & Sons
- **Aroca**, R.F.; Alvarez-Puebla, R.A.; Pieczonka, N.; Sanchez-Cortez, S.; Garcia-Ramos, J.V. *Advances inColloid and Interface Science* **2005,** 116, 45-61
- **Ashcroft**, N.W. & Mermin, N.D. *Solid State Physics* **1976,** Brooks Cole
- **Bantz**, K.C.; Nelson, H.D.; Haynes, C.L. *Journal of Physical Chemistry C* **2012**, 116, 3585-3593

- **Barcarolo**, R.; Tealdo, E.; Tutta, C. *Journal of High Resolution Chromatography* **1988**, 11, 539-541
- **Barro**, R.; Regueiro, J.; Llompart, M.; Garcia-Jares, C. *Journal of Chromatography A* **2009**, 1216, 540-566
- **Barron**, L.D. *Molecular Light Scattering and Optical Activity* **2004**, Cambridge University Press
- **Bennett**, D.A.; Chung, A.C.; Lee, S.M. *Journal of AOAC International* **1997**, 80, 1065-1077
- **Brandenberger**, H.; Maes, R.A. *Analytical Toxicology* for *Clinical*, *Forensic* and *Pharmaceutical Chemists* **1997,** Ed. Walter de Gruyter, Berlin
- **Brasil**, A.M.; Farias, T.L.; Carvalho, M.G.; Koylu, U.O. *Journal of Aerosol Science* **2001**, 32, 489-508
- **Bryant**, M.A. & Pemberton, J.E. *Journal of the American Chemical Society* **1991,** 113, 3629-3637
- **Bryant**, M.A. & Pemberton, J.E. *Journal of the American Chemical Society* **1991**, 113, 8284-8293
- **Bunow**, M.R. & Levin, I.W. *Biochimica et Biophysica Acta* **1977**, 487, 388-394
- **Camargo**, P.H.C.; Rycenga, M.; Au, L.; Xia, Y.N. *Angewandte Chemie-International Edition* **2009**, 48, 2180-2184
- **Campion**, A. and Kambhampati, P. *Chemical Society Reviews* **1988**, 27, 241-250
- **Cañamares**, M.V.; Garcia-Ramos, J.V.; Gomez-Varga, J.D.; Domingo, C.; Sanchez-Cortes, S. *Langmuir* **2005**, 21, 8546-8553
- **Cao**, Y.C.; Jin, R.; Mirkin, C.A. *Science* **2002**, 297, 1536-1540
- **Carro**, P.; Creus, A.H.; Munoz, A.; Salvarezza, R.C. *Langmuir* **2010**, 26, 9589-9595
- **Centers for Disease Control and Prevention** (CDC) *Fourth National Report on Human Exposure to Environmental Chemicals* **2009**, 77-80
- **Cerrillo**, I.; Granada, A.; Lopez-Espinosa, M.J.; Olmos, B.; Jimenez, M.; Cano, A.; Olea, N.; Olea-Serrano, M.F. *Environmental Research* **2005**, 98, 233-239
- **Cinta-Pinzaru**, S.; Pavel, I.; Leopold, N.; Kiefer, W. *Journal of Raman Spectroscopy* **2004**, 35, 338-346

- **Creighton**, J.A. *Spectroscopy of Surfaces* **1988**, Clark, R.J.H. and Hester, R.E. Eds., John Wiley & Sons
- **Damgaard**, I.N.; Skakkebaek, N.E.; Toppari, J.; Virtanen, H.E.; Shen, H.; Schramm, K.W.; Petersen, J.H.; Jensen, T.K.; Main, K.M.; Nordic Cryptorchidism Study Group *Environmental Health Perspectives* **2006** 114, 1133-1138
- **Domingo**, C.; Garcia-Ramos, J.V.; Sanchez-Cortes, S.; Aznarez, J.A. *Journal of Molecular Structure* **2003**, 661, 419-427
- **Domingo**, C.; Guerrini, L.; Leyton, P.; Campos-Vallette, M.; Garcia-Ramos, J.V.; Sanchez-Cortes, S. *ACS Symposium Series* (eds Kneipp, K.; Aroca, R.; Kneipp, H.; Wentrup-Byrne, E.) **2007**, 963, 138-151
- **Du**, C.L.; Yang, M.X.; You, Y.M.; Chen, T.; Chen, H.Y.; Shen, Z.X. *Chemical Physics Letters* **2009**, 473, 317-320
- **Dubois**, L.H. & Nuzzo, R.G. *Annual Review of Physical Chemistry* **1992**, 43, 437-463
- **European Food Safety Authority** Journal (EFSA) **2005**, 1-43, 285
- **Etchegoin**, P.G. & Le Ru, E.C. *Annual Review of Physical Chemistry* **2012**, 63, 65-87
- **Fernandez**, M.F.; Olmos, B.; Granada, A.; Lopez-Espinosa, M.J.; Molina-Molina, J.M.; Fernandez, J.M.; Cruz, M.; Olea-Serrano, M.F.; Olea, N. *Environmental Health Perspectives* **2007**, 115, 8-14
- **Fleischman**, M.; Hendra, P.J. and McQuillan, A.J. *Chemical Physics Letters* **1974**, 26, 163-166
- **Food and Agriculture Organization** (FAO)**/World Health Organization** (WHO) *Pesticide residues in food – 1994. Report of the Joint Meeting of the FAO Panel of Experts on Pesticide Residues in Food and the Environment and WHO Toxicological and Environmental Core Assessment Groups* **1995**
- **Futamata**, M. *Faraday Discussions* **2006**, 132, 45-61
- **Gaber**, B.P.; Yager, P.; Peticolas, W.L. *Biophysical Journal* **1978**, 21, 161-176
- **Gardiner**, D.J. *Practical Raman spectroscopy* **1989**, Springer-Verlag
- **Giannini**, V.; Fernández-Domínguez, A.I.; Heck, S.C.; Maier, S.A. *Chemical Reviews* **2011**, 111, 3888-3912

- **Gilden**, R.C.; Huffling, K.; Sattler, B. *Journal of Obstetric, Gynecologic and Neonatal Nursing* **2010**, 39, 103-110
- **Gonçalves**, M.R.; Enderle, F.; Marti, O. *Journal of Nanotechnology* **2012**, 2012, 173273-173288
- **Grubisha**, D.S.; Lipert, R.J.; Park, H.Y.; Driskell, J.D.; Porter, M. *Analytical Chemistry* **2003**, 75, 5936-5943
- **Guardino**, X.; Serra, C.; Obiols, J.; Rosell, M.G.; Berenguer, M.J.; López, F.; Brosa, J. *Journal of Chromatography A* **1996**, 719, 141-147
- **Guerrini**, L.; Aliaga, A.E.; Carcamo, J.; Gomez-Jeria, J.S.; Sanchez-Cortes, S.; Campos-Vallette, M.; Garcia-Ramos, J.V. *AnalyticalChimica Acta* **2008**, 624, 286-293
- **Guerrini**, L.; Garcia-Ramos, J.V.; Domingo, C.; Sanchez-Cortes, S. *Analytical Chemistry* **2009**, 81, 953-960
- **Guerrini**, L.; Garcia-Ramos, J.V.; Domingo, C.; Sanchez-Cortes, S. *Journal of PhysicalChemistry C* **2008**, 112, 7527-7530
- **Guerrini**, L.; Garcia-Ramos, J.V.; Domingo, C.; Sanchez-Cortes, S. *Langmuir* **2006**, 22, 10924-10926
- **Guerrini**, L.; Izquierdo-Lorenzo, I.; Garcia-Ramos, J.V.; Domingo, C.; Sanchez-Cortes, S. *Physical Chemistry Chemical Physics* **2009**, 11, 7363-7371
- **Guerrini**, L.; Izquierdo-Lorenzo, I.; Rodriguez-Oliveros, R.; Sanchez-Gil, J.A.; Sanchez-Cortes, S.; Garcia-Ramos J.V.; Domingo, C. *Plasmonics* **2010**, 5, 273-286
- **Guerrini**, L.; Jurasekova, Z.; Domingo, C.; Perez-Mendez, M.; Leyton, P.; Campos-Vallette, M.; Garcia-Ramos, J.V.; Sanchez-Cortes, S. *Plasmonics* **2007**, 2, 147-156
- **Halas**, N.J.; Lal, S.; Chang, W-S.; Link, S.; Nordlander, P. *Chemical Reviews* **2011**, 111, 3913-3961
- **Halsall**, C.J.; Barrie, L.A.; Fellin ,P.; Muir, D.C.G.; Billeck, B.; Lockhart, L.; Rovinsky, F.; Kononov, E.; Pastukhov, B. *Environmental & Science Technology* **1997**, 31, 3593-3599

- **Hamoudi**, H.; Guo, Z.; Prato, M.; Dablemont, C.; Zheng, W.Q.; Bourguignon, B.; Canepa, M.; Esaulov, V.A. *Physical Chemistry Chemical Physics* **2008**, 10, 6836-6841
- **Harvey**, R.G. *Polycyclic Aromatic Hydrocarbons* **1997,** Wiley-VCH
- **Hayes**, W.J.Jr. *Pesticides studied in man* **1982**, Williams & Wilkins
- **Hendra**, P. *International Journal Vibrational Spectroscopy* **1998**, 1, 6-16
- **Huh**, Y.S.; Chung, A.J.; Erickson, D. *MicrofluidNanofluid* **2009**, 6, 285-297
- **Chemicals Regulation Directorate** (CRD) *Banned and Non-Authorised Pesticides in the United Kingdom* **2009**
- **Cho**, E.C.; Choi, S.W.; Camargo, P.H.C.; Xia, Y. *Langmuir* **2010**, 26, 10005-10012
- **Cho**, S.I.; Park, E.S.; Kim, K.; Kim, M.S. *Journal ofMolecular Structure* **1999**, 479, 83-92
- **Indian Chemical Council** (ICC) *Form for submission of information specified in Annex E* **2009**
- **Izquierdo-Lorenzo**, I.; Alda, I.; Sanchez-Cortes, S.; Garcia-Ramos, J.V. *Langmuir* **2012**, 28, 8891-8901
- **Izquierdo-Lorenzo**, I.; Kubackova, J.; Manchon, D.; Mosset, A.; Cottancin, E.; Sanchez-Cortes, S. *Journal of Physical Chemistry C* **2013**, 117, 16203-16212
- **Jeanmarie**, D.L. & Van Duyne, R.P. *Journal of Electroanalytical Chemistry* **1977**, 84, 1-20
- **Jensen**, T.R.; Malinsky, M.D.; Haynes, C.L.; Van Duyne, R.P. *Journal of Physical Chemistry B* **2000**, 104, 10549-10556
- **Jimenez**, M.; Rivas, A.; Olea, F.; Olea, N. *Ecosistemas* **2004**, 13, 45-50
- **Joo**, S.W.; Han, S.W.; Kim, K. *Journal of Colloidal and Interface Science* **2001**, 240, 391-399
- **Joo**, T.H.; Kim, K.; Kim, M.S. *Journal of Molecular Structure* **1987**, 158, 265-274
- **Jung**, H.Y.; Park, Y.K.; Park, S.; Kim, S.K. *Analytica Chimica Acta* **2007**, 602, 236-243
- **Kato**, H.S.; Noh, J.; Hara, M.; Kawai, M. *Journal of Physical Chemistry B* **2002**, 106, 9655-9658

- **Kluth**, G.J.; Carraro, C.; Maboudian, R. *Physical Review B: Condensed Matter and Materials Physics* **1999**, 59, 10449-10452
- **Kneipp**, J.; Kneipp, H.; Rice, W.L.; Kneipp, K. *Analytical Chemistry* **2005**, 77, 2381-2385
- **Kneipp**, K.; Moskovits, M.; Kneipp, H. *Surface-Enhanced Raman Scattering-Physics and Applications* **2006**, Springer
- **Kneipp**, K.; Wang, Y.; Kneipp, H.; Perlman, L.T.; Itzkan, I.; Dasari, R.R.; Feld, M.S. *Physical Review Letters* **1997**, 78, 1667-1670
- **Kobayashi**, H.; Sato, K.; Matano, O.; Goto, S.*Journal of Pest Science* **1983**, 8, 105-110
- **Kubackova**, J.; Izquierdo-Lorenzo, I.; Jancura, D.; Miskovsky, P.; Sanchez-Cortes, S. *Physical Chemistry Chemical Physics* **2014**, 16, 11461-11470
- **Landsberg**, G.; Mandelstam, L.A. *Naturwissenschaften* **1928**, 16, 557-559
- **Langhammer**, Ch.; Yuan, Z.; Zorić, I.; Kasemo, B. *Nano Letters* **2006**, 6,833-838
- **Lee**, P.C. & Meisel, D. *Journal of Physical Chemistry* **1982**, 86, 3391-3395
- **Lee**, Y.R.; Kim, M.S.; Kwon, C.H. *Bulletin of the Korean Chemical Society* **2013**, 34, 470-474
- **Lee Ru**, E.C.; Etchegoin, P.G.; Meyer, M. *Journal of Chemical Physics* **2006**, 125, 204701-204713
- **Leopold**, N. & Lendl, B. *Journal of Physical Chemistry B* **2003**, 107, 5723-5727
- **Leyton**, P.; Sanchez-Cortes, S.; Garcia-Ramos, J.V.; Domingo, C.; Campos-Vallette, M.; Saitz, C.; Clavijo, R.E. *Journal of Physical Chemistry B* **2004**, 108, 17484-17490
- **Li**, W.Y.; Camargo, P.H.C.; Lu, X.M.; Xia, Y.N. *Nano Letters* **2009**, 9, 485-490
- **Lin**, M.Y.; Lindsay, H.M.; Weitz, D.A.; Ball, R.C.; Klein, R.; Meakin, P. *Nature* **1989**, 339, 360-362
- **Lombardi**, J.R.; Birke, R.L. *Journal of Physical Chemistry C* **2008**, 112, 5605-5617
- **Lombardi**, J.R.; Birke, R.L.; Lu, T.; Xu, J. *The Journal of Chemical Physics* **1986**, 84, 4174-4180
- **Lorenz**, E. S. *Ag Communications and Marketing* **2009,** 1-8

- **Lyandres**, O.; Shah, N.C.; Yonzon, C.R.; Walsh, J.T., Jr.; Gluckberg, M.R.; Van Duyne, R.P. *Analytical Chemistry* **2005**, 77, 6134-6139
- **Mariani**, G.; Benfenati, E.; Fanelli, R. *International Journal of Environmental Analytical Chemistry* **1995**, 58, 67-72
- **Martin**, P. A. & Rothen, F. *Many-Body Problems and Quantum Field Theory* **2004**, Springer-Verlag Berlin Heidelberg, Germany
- **Metcalf**, R.L. *Insect Control* in *Ullmann's Encyclopedia of Industrial Chemistry* **2002,** Wiley-VCH
- **Miao**, L. & Seminario, J. M. *Journal of Chemical Physics* **2007**, 126, 184706
- **Mishra**, S.; Vallet, V.; Poluyanov, L.V.; Domcke, W. *Journal of Chemical Physics* **2006**, 125, 164327-8
- **Moskovits**, M. *Journal of Chemical Physics* **1982**, 77, 4408-4416
- **Moskovits**, M. *Reviews of Modern Physics* **1985**, 57, 783-826
- **Moskovits**, M.; Jeong, D.H. *Chemical Physics Letters* **2004**, 397, 91-95
- **Naidu**, N.V. and Yakubu, M.A. *The Explorer Magazine* **2013**, 1, 13-15
- **Nam**, J.M.; Stoeva, S.I.; Mirkin, C.A. *Journal of the American Chemical Society* **2004**, 126, 5932-5933
- **Nie**, S.; Emory, S.R. *Science* **1997**, 257, 1102-1106
- **Olmos-Asar**, J.A.; Rapallo, A.; Mariscal, M.M. *Physical Chemistry Chemical Physics* **2011**, 13, 6500-6506
- **Olson**, L.G.; Uibel, R.H.; Harris, J.M. *Applied Spectroscopy* **2004**, 58, 1394-1400
- **Otto**, A.; Mrozek, I.; Grabhorn, H. and Akemann, W. *Journal of Physics*: *Condensed Matter* **1992**, 4, 1142-1212
- **Placzek**, G. *Hdb. der Radiologie* **1934**, 6, 209-374
- **Polman**, A.& Atwater, H.A. *Materials Today* **2005**, 8, 56
- **Premasiri**, W.R.; Moir, D.T.; Klempner, M.S.; Krieger, N.; Jones, G.; Ziegler, L.D. *Journal of Physical Chemistry B* **2005**, 109, 312-320
- **Raman**, C.V. &Krishnan, K.S. *Nature* **1928**, 121, 501-503
- **Richardson**, A. and Robinson, J. *Xenobiotica* **1971**, 1, 213-219
- **Ritchie**, R.H. *Physical Review* **1957**, 106, 874-881

- **Report on Carcinogens** (12th edition*) Lindane, Hexachlorocyclohexane (Technical Grade), and Other Hexachlorocyclohexane Isomers* **2011**
- **Rosa**, R.; RodriguezFarre, E.; Sanfeliu, C. *Journal of Pharmacology and Experimental Therapeutics* **1996**, 278, 163-169
- **Rycenga**, M.; Camargo, P.H.C.; Xia, Y.N. *SoftMatter* **2009**, 5, 1129-1136
- **Sandhyarani**, N.& Pradeep, T. *Vacuum* **1998**, 49, 279-284
- **Sanchez-Cortes**, S.; Garcia-Ramos, J.V.; Morcillo, G. *Journal of Colloid and Interface Science* **1994**, 167, 428-436
- **Sanchez-Cortes**, S.; Garcia-Ramos, J.V.; Morcillo, G.; Tinti, A. *Journal of Colloid and Interface Science* **1995**, 175, 358-368
- **Sanchez-Cortes**, S.; Guerrini, L.; Garcia-Ramos, J.V.; Domingo, C. *Optica Pura y Aplicada* **2007**, 40, 235-242
- **Sellers**, H.; Ulman, A.; Shnidman, Y.; Eilers, J.E. *Journal of the American Chemical Society* **1993**, 115, 9389-9401
- **Shafer-Peltier**, K.E.; Haynes, C.L.; Glucksberg, M.R.; Van Duyne, R.P. *Journal of the American Chemical Society* **2003**, 125, 588-593
- **Schlücker**, S. *Surface enhanced Raman spectroscopy* **2011,** Wiley-VCH
- **Silambarasan**, S. and Abraham, J. *PLOS ONE* **2013**, 8, 1-10
- **Siiman**, O. & Feilchenfeld, H. *Journal of Physical Chemistry* **1988**, 92, 453-464
- **Smith**, W.E. and Dent, G. *Modern Raman Spectroscopy – A Practical Approach* **2005,** John Wiley & Sons
- **Smith**, W.E.; McNay, G.; Eustace, D.; McInroy, A.; Fitchett, K. *Innovations in Pharmaceutical Technology* **2010**, 52-56
- **Snyder**, R.G. *Journal of Chemical Physics* **1982**, 76, 3342-3343
- **Snyder**, R.G.; Hsu, S.L.; Krimm, S. *Spectrochimica Acta, Part A* **1978**, 34, 395-406
- **Snyder**, R.G.; Strauss, H.L.; Elliger, C.A. *Journal of Physical Chemistry* **1982**, 86, 5145-5150
- **Strutt**, J.W.*Philosophical Magazine* **1871**, 4, 41, 107-120; 274-279
- **Strutt**, J.W. *Philosophical Magazine* **1871**, 4, 41, 447-454
- **Strutt**, J.W. *Philosophical Magazine* **1881**, 5, 12, 81-101
- **Strutt**, J.W. *Philosophical Magazine* **1899**, 5, 47, 375-394

- **Sutherland**, W.S.; Winefordner, J.D. *Journal of Colloidal and Interface Science* **1992**, 148, 129-141
- **The Daily Green** *EPA Bans Pesticide Found on Cucumbers, Zucchini, Green Beans and Other Vegetables* **2010**
- **The Hindu** *Endosulfan: Supreme Court to hear seeking ban on Monday* **2011** Chennai, India
- **United States Environmental Protection Agency** (US EPA) *Ambient water quality criteria for polychlorinated biphenyl*s **1980**
- **United States Environmental Protection Agency** (US EPA) *Basic Information about Lindane in Drinking Water* **2014**
- **United States Environmental Protection Agency** (US EPA) *EPA Action to Terminate Endosulfan* **2010**
- **United States Environmental Protection Agency** (US EPA) *Technical support document for water quality-based toxics control* **1990b**
- **Vlckova**, B.; Moskovits, M.; Pavel, I.; Siskova, K.; Sladkova, M.; Slouf, M. *Chemical Physics Letters* **2008**, 455, 131-134
- **Walker**, A.I.T.; Stevenson, D.E.; Robinson, J.; Thorpe, E.; Roberts, M. *Toxicologyand Applied Pharmacology* **1969**, 15, 345-373
- **Wan**, M.T.; Kuo, J.N.; Buday, C.; Schroeder, G.; Van Aggelen, G.; Pasternak, J. *Environmental Toxicologyand Chemistry* **2005**, 24, 1146-1154
- **Weekly Times** *Australia should ban endosulfan: Greens* **2009**
- **Williams**, A.C. *Practical Spectroscopy Series* **2001,** Marcel Dekker, New York, USA
- **Wokaun**, A. *Molecular Physics* **1985**, 56, 1-33
- **Wong**, P.T.T. & Mantsch, H.H. *Biochemistry* **1985**, 24, 4091-4096
- **World Health Organization** (WHO) *Aldrin and dieldrin in drinking-water. Background document for preparation of WHO Guidelines for drinking-water quality* **2003**
- **Worthing**, C.R. and Walker, S.B. *The pesticide manual: A world compendium* **1983,** The British Crop Protection Council, Croydon, UK

- **Wu**, D.Y.; Li, J.F.; Ren, B.; Tian, Z.Q. *Chemical Society Reviews* **2008**, 37, 1025-1041
- **Xu**, M.M.; Wang, M.; Yao, J.L.; Zou, W.J.; Ling, L.; Gu, R.A. *Spectroscopy and Spectral Analysis* **2009**, 29, 1289-1291
- **Zeng**, S.; Baillargeat, D.; Ho, H.P.; Yong, K.T. *Chemical Society Reviews* **2014**, 43, 3426-3452
- **Zhao**, J.; Pinchuk, A.O.; McMahon, J.M.; Li, S.; Ausman, L.K.; Atkinson, A.L.; Schatz, G.C. *Accounts of Chemical Research* **2008**, 41, 1710-1720
- **Zuloaga**, J.; Prodan, E.; Nordlander, P. *Nano Letters* **2009**, 9, 887-891

List of publications

Current contents publications

- Kubackova, J.; Izquierdo-Lorenzo, I.; Jancura, D.; Miskovsky, P.; Sanchez-Cortes, S. Adsorption of linear aliphatic α,ω-dithiols on plasmonic metal nanoparticles: a structural study based on surface-enhanced Raman spectra *Physical Chemistry Chemical Physics* 2014, 16, 11461-11470
- Izquierdo-Lorenzo, I.; Kubackova, J.; Manchon, D.; Mosset, A.; Cottancin, E.; Sanchez-Cortes, S. Linking Ag Nanoparticles by Aliphatic α,ω-Dithiols: A Study of the Aggregation and Formation of Interparticle Hot Spots *Journal of Physical Chemistry C* 2013, 117, 16203-16212
- Kubackova, J.; Fabriciova, G.; Miskovsky, P.; Jancura, D.; Sanchez-Cortes, S. Sensitive detection of organochlorine pesticides by dithiolalkene-functionalized nanoparticles on selective plasmonic hot spots. *Analytical Chemistry* 2014 – submitted
- Sanchez-Cortes, S.; Garcia-Ramos, J.V.; Izquierdo-Lorenzo, I.; Garcia-Leis, A.; Kubackova, J. Plasmonic Nanoparticles: Nanofabrication and Controlled Assembly for High Surface-Enhanced Raman Scattering Performance and Molecular Detection *Handbook of Nanoparticles* (ed. Dr. Aliofkhazraei) – in press

Conference contributions: oral presentations

- Kubackova, J.; Miskovsky, P.; Jancura, D.; Sanchez-Cortes, S. Application of surface-enhanced Raman spectroscopy for the detection of trace amounts of chemical compounds (flame retardants, pesticides); *Week of Doctoral Studies 2012*, 21-25 May (2012), Novy Smokovec, Slovakia
- Kubackova, J. Application of dithiol-functionalized nanoparticles in the detection of organochlorine pesticides *Summer School on Biospectroscopy*, 24-27 June (2014), Jaca (Aragon), Spain

Conference contributions: poster presentations

- Kubackova, J.; Miskovsky, P.; Jancura, D.; Sanchez-Cortes, S. Application of surface-enhanced Raman spectroscopy for the detection of trace amounts of chemical compounds (flame retardants, pesticides); *XXIII Reunión Nacional – VII Congresso Ibérico*, 17-20 September (2012), Cordoba, Spain
- Kubackova, J.; Miskovsky, P.; Fabriciova, G.; Sanchez-Cortes, S.; Jancura, D. Application of surface-enhanced Raman spectroscopy for the detection of trace quantity of pesticides aldrin, α-endosulfan, and lindane; *15th European Conference on the Spectroscopy of Biological Molecules 2013*, 25-30 August (2013), Oxford, United Kingdom
- Kubackova, J.; Miskovsky, P.; Fabriciova, G.; Sanchez-Cortes, S.; Jancura, D. Application of surface-enhanced Raman spectroscopy for the detection of trace quantity of pesticides aldrin, α-endosulfan, and lindane; *8th International Conference Structure and Stability of Biomacromolecules SSB 2013*, 10-13 September (2013), Kosice, Slovakia
- Kubackova, J.; Miskovsky, P.; Fabriciova, G.; Sanchez-Cortes, S.; Jancura, D. Application of surface-enhanced Raman spectroscopy for the detection of trace quantity of pesticides aldrin, α-endosulfan, and lindane; *Regional Biophysics Conference RBC 2014*, 15-20 May (2014), Smolenice Castle, Slovakia

Grants and financial supports

This work has been supported by the Agency of the Ministry of Education of Slovak Republic for the Structural funds of the European Union, Operational program Education (Doctorand, ITMS code: 26110230013 and KVARK, ITMS code: 26110230084) and Operational program Research and Development (NanoBioSens (ITMS code: 26220220107) and CEVA II (ITMS code: 26220120040)), by the Slovak Research and Development Agency under the contract APVV-0242-11, by the project CELIM (316310) funded by 7FP EU, by the Spanish *Ministerio de Economía y Competitividad* (MINECO, grant FIS2010-15405) and *Comunidad de Madrid* through MICROSERES II network (grant S2009/TIC-1476),

Anex 1

- Izquierdo-Lorenzo, I.; Kubackova, J.; Manchon, D.; Mosset, A.; Cottancin, E.; Sanchez-Cortes, S. Linking Ag Nanoparticles by Aliphatic α,ω-Dithiols: A Study of the Aggregation and Formation of Interparticle Hot Spots *Journal of Physical Chemistry C* 2013, 117, 16203-16212

Anex 2

- Kubackova, J.; Izquierdo-Lorenzo, I.; Jancura, D.; Miskovsky, P.; Sanchez-Cortes, S. Adsorption of linear aliphatic α,ω-dithiols on plasmonic metal nanoparticles: a structural study based on surface-enhanced Raman spectra *Physical Chemistry Chemical Physics* 2014, 16, 11461-11470